SYNTHESIS OF ECO-FRIENDLY ADSORBENTS
FOR THE REMOVAL OF CONTAMINANTS
IN WASTEWATER

廃水中の汚染物質除去のための低環境負荷型吸着剤の合成

March 2019

HO HONG QUYEN

SYNTHESIS OF ECO-FRIENDLY ADSORBENTS FOR THE REMOVAL OF CONTAMINANTS IN WASTEWATER

廃水中の汚染物質除去のための低環境負荷型吸着剤の合成

HO HONG QUYEN

Doctoral dissertation

Life and Materials Systems Engineering

Graduate School of Advanced Technology and Science

Tokushima University

March 2019

Table of contents

Publications

Journal articles

1. <u>Quyen Hong Ho</u>, Maki Yoshioka, Masashi Kurashina, Mikito Yasuzawa and Thuy Thi Xuan Le, Eco-friendly removal of phosphate from aqueous solution using natural dietary fibers and minerals, *International Journal of Modern Physics B*, Vol.32, No.19, 1840075-1-1840075-5, 2018, Published

(DOI: 10.1142/S0217979218400751)

2. Thuy Thi Xuan Le, Suong Thi Le, Mai Thi Sao Nguyen, <u>Quyen Hong Ho</u> and Mikito Yasuzawa, Purification of groundwater contaminated with iron and manganese by effective cost filter materials for households in rural areas, *International Journal of Modern Physics B*, Vol.32, No.19, 1840079-1-1840079-6, 2018, Published

(DOI: 10.1142/S0217979218400799)

3. Thuy Thi Xuan Le, Mai Thi Sao Nguyen, <u>Quyen Hong Ho</u>, Mikito Yasuzawa and Vu Xuan Tran, Removal of Nickel from Plating Wastewater Using the Magnetic Flocculant PG-M, *Chemical Science International Journal*, Vol.22, No.1, 1-9, 2018, Published

(DOI: 10.9734/CSJI/2018/39902)

Conference

Poster presentation: Masashi Kurashina, Maki Yoshioka, <u>Ho Hong Quyen</u>, Mikito Yasuzawa, Adsorption/desorption and Recovery of Phosphate using Eco-friendly materials (環境親和型材料を用いたリン酸イオンの吸脱着と回収), *The 68th Annual Meeting of the Society of Sea Water Science, Japan (日本海水学会第68年会)*, Kyoto, 2017.

Oral presentation: <u>Ho Hong Quyen</u>, Maki Yoshioka, Le Thi Xuan Thuy, Masashi Kurashina and Mikito Yasuzawa, Eco-Friendly Removal of Phosphate from Aqueous Solution Using Natural Dietary Fibers and Minerals, *8th International Conference on Advanced Materials Development & Performance, India, 2017.*

Poster presentation: Purification of Groundwater Contaminated Iron and Manganese by Effective Cost Filter Materials for Households in Rural Areas, Le Thi Xuan Thuy, Le Thi Suong, Nguyen Thi Sao Mai, Le Phuoc Cuong, Pham Thi Kim Thoa, <u>Ho Hong Quyen</u> and Mikito Yasuzawa, *8th International Conference on Advanced Materials Development & Performance, India, 2017.*

Poster presentation: <u>Ho Hong Quyen</u>, Maki Yoshioka, Le Thi Xuan Thuy, Masashi Kurashina and Mikito Yasuzawa, Effective Phosphate Removal from Aqueous Solution Using Environmental-Friendly Adsorbent, *4th International Forum on Advanced Technologies March, 2018, Tokushima, Japan.*

Abbreviations and Symbols

P: phosphorus

EC: electrocoagulation

MWCO: molecular weight cut-off

EBPR: enhanced biological phosphorus removal

PAOs: phosphate accumulating organisms

VFAs: volatile fatty acids

PHAs: polyhydroxyalkanoates

M: Mannuronate

G: Guluronate

CaO: calcium hydroxide

$Ca(OH)_2$: calcium hydroxide

$Ca_{10}(PO_4)_6(OH)_2$: hydroxylapatite

XRD: X-ray powder diffraction

SEM: scanning electron microscope

CCRs: coal combustion residuals

FGD: flue gas desulfurization

ESP: electrostatic precipitator

SCR: selective catalytic reduction

USEPA: United States Environmental Protection Agency

WHO: World Health Organization

NMDG: *N*-methyl-D-glucamine

GMA: glycidyl methacrylate

MMA: methyl methacrylate

DVB: divinyl benzene

PEI: polyethylenimine

EGDE: ethylene glycol diglycidyl ether

VBC: 4-vinylbenzyl chloride

MC: magnetic chitosan microbeads

MCG: magnetic multi-hydroxyl microbeads

GL: D-(+)- glucono - 1,5 lactone

CH$_3$COOH: trifluoroacetic acid

ChNFs: chitosan nanofibers

GChs: gluconated chitosan

GChNFs: gluconated chitosan nanofibers

DD%: degree of deacetylated units

DG%: degree of gluconated units

^{1}H NMR: proton nuclear magnetic resonance

Cosy: correlation spectroscopy

ppm: parts per million

mg/L: milligrams per liter

mg/g: milligram per grams

%: percent

v,v%: volume/volume percent

ºC: degree Celsius

h: hour

min: minute

Summary

Water is an essential resource for maintaining the life of all living creatures on our planet. However, its shortage and pollution cause serious problems for millions of people in the world. Anthropogenic activities from the urbanization process, industry and agriculture are the main causes of pollution the water bodies such as ponds, lakes, rivers, groundwater and seawater. Polluted water has a remarkable effect on the disappearance of biodiversity in aquatic and degraded the quality of irrigation water for crops and drinking water for the human. The access of a wide variety of toxic and non-biodegradable chemicals via food chain leads to various diseases if these substances are difficult to remove by the excretory organs and accumulated by the human body in the long period. Therefore, the control of contaminants in wastewater in the permissive concentration before discharging to water sources is the struggle for water conservation.

In the process of treatment, the use of various hazardous reagents and solvents and the production of secondary pollutants can impact negatively on human health and the environment. Hence, the applications of sustainable and green chemistry in both products and process are the way to minimize environmental pollution.

In this study, the removal of phosphate and boron towards the approach of green chemistry was introduced. In the first part, the removal of phosphate from aqueous solution by using the main constituents in the shells, the solid waste from aquaculture with the support of eco-friendly flocculants was investigated. We expect to provide a simple method with eco-friendly materials for phosphate removal that can be applied in Viet Nam. In the second part, the synthesis of non-toxic adsorbent from chitosan and chitosan nanofibers in the simple process was conducted for the separation of boron.

Removal of phosphate from aqueous solution using natural dietary fibers and minerals (Chapter 1 to 2)

The excess of phosphate from domestic, industrial and agricultural wastewater is the cause of eutrophication, resulting in the negative effects on aquatic ecosystem. However, the decrease in the amount of phosphate ore relates to the scarcity of fertilizer, and food supply in the future. The recovery of phosphate from wastewater to produce fertilizer is the solution that can reduce water pollution as well as contribute to the solution of phosphate shortage in agriculture.

In **chapter 1**, the general introduction of problems due to phosphorus element and its removal methods were discussed.

Chapter 2 focused on the eco-friendly method for phosphate removal by using calcium oxide (CaO) and calcium hydroxide $Ca(OH)_2$, the dominant constituents in calcined shells (crab, scallop, mussel, oyster and egg). CaO and $Ca(OH)_2$ easily reacted with phosphate solution, and the precipitate formed after reaction could be applied as the fertilizer for plants. In the presence of the non-toxic flocculants of alginic acid, $NaHCO_3$ and $CaCl_2.2H_2O$, the alginate gel was generated which enhanced the phosphate removal rate and the efficient separation of precipitate by filtration.

Green synthesis and characterization of the novel multi-hydroxyl functionalized chitosan and chitosan nanofibers for removal of boron (Chapter 3 to 5)

The overdose and long-term accumulation of boron involve adverse effects on the quality and quantity of plants and human health. Boron-selective adsorbents have been applied for boron separation from aqueous solution because of the high efficiency, simple operation and capability of water and wastewater treatment with large volume. Due to the possession of *vis*-diols, the boron-selective sites for boron removal, these adsorbents offer an effective interaction with boron.

In **chapter 3**, the general introduction of properties of boron and its compounds, applications and environmental problems of boron and the review of boron-selective adsorbents were discussed.

In **chapter 4**, gluconated chitosan (GChs) particles were synthesized in the facile process. Chitosan was selected as the substrate and functionalized with D-(+)- glucono - 1,5 lactone (GL) to provide *vis*-diols which is the boron-selective sections for boron removal. Adsorption isotherm of boron onto GChs was investigated in the range of initial boron concentration from 10 to 400 ppm at 115 $^{\circ}$C for 24 h in the shaking condition. The adsorption kinetics was conducted at certain periods (0.5 - 24 h) with 400 ppm of initial boron concentration at 25 $^{\circ}$C under shaking. The effect of initial pH was investigated from 5.6 to 9.8 at 115 $^{\circ}$C for 24 h under shaking. The effect of ionic strength was investigated in the range of NaCl between 0 and 1000 mmol/L with 400 ppm of initial boron concentration at 25 $^{\circ}$C for 24 h. The availability, abundance, biodegradability, non-toxicity and low cost of chitosan and non-toxicity of D-(+)-

glucono - 1,5 lactone were the approaches to sustainable and green chemistry in the use of friendly environmental materials.

In **Chapter 5**, in order to overcome the limitation of low porosity and surface area of chitosan flake, the novel of adsorbent, gluconated chitosan nanofibers (GChNFs) in the form of sponge were synthesized by grafting D-(+)- glucono - 1,5 lactone into chitosan nanofibers (ChNFs). Various parameters of reaction time, reaction temperature, pressure, the use of acid to dissolve ChNFs and the use of sodium hydroxide for neutralization were investigated in order to find the highest degree of gluconated units ($DG\%$). GChNFs sponge prepared in pressure condition at 115 ^{o}C for 12 h had the $DG\%$ determined by colloidal titration 3.5 times higher than GChs particles prepared from chitosan flake in reflux condition at 115 ^{o}C for 24 h. ChNFs was capable of reacting with GL in the absence of acid, and the products were obtained without using sodium hydroxide. SEM images displayed the fiber structure in GChNFs, providing the large surface for enhanced boron adsorption. The achievement of ChNFs in the increase in surface area of adsorbent, the reduction in reagents utilization and the simple synthesis process introduced a promising material for the development of an eco-friendly method for boron removal.

Chapter 1

General introduction of phosphorus and its removal processes

1.1. The effect of phosphorus element excess on ecosystem

Phosphorus (P) is a crucial element for the growth and reproduction of plants and is found in all living organisms. It is sorted as the main nutrient for crop production. P relates to a variety of principal functions in plants, including photosynthetic, energy transfer, storage and transportation of nutrient and genetic transfer [1]. However, the excess of P, nitrogen and other nutrients in water sources from agricultural activities, food and beverage factories and domestic wastewater accelerate the uptake of organic matters, especially algae. When the algae bloom happens, the level of dissolved oxygen is depleted, the photosynthetic process of biota in the bottom water layer is affected, and the poisons and bad odour are produced (Fig. 1.1) [2-4]. This phenomenon called eutrophication can break the ecosystem functions, leading to the death of various aquatic organisms as well as adverse effects on human health through the food chain. For this reason, the treatment of P element in the municipal wastewater treatment plants or in the wastewater of food industries before discharging to water bodies is the effort to protect water sources from pollution.
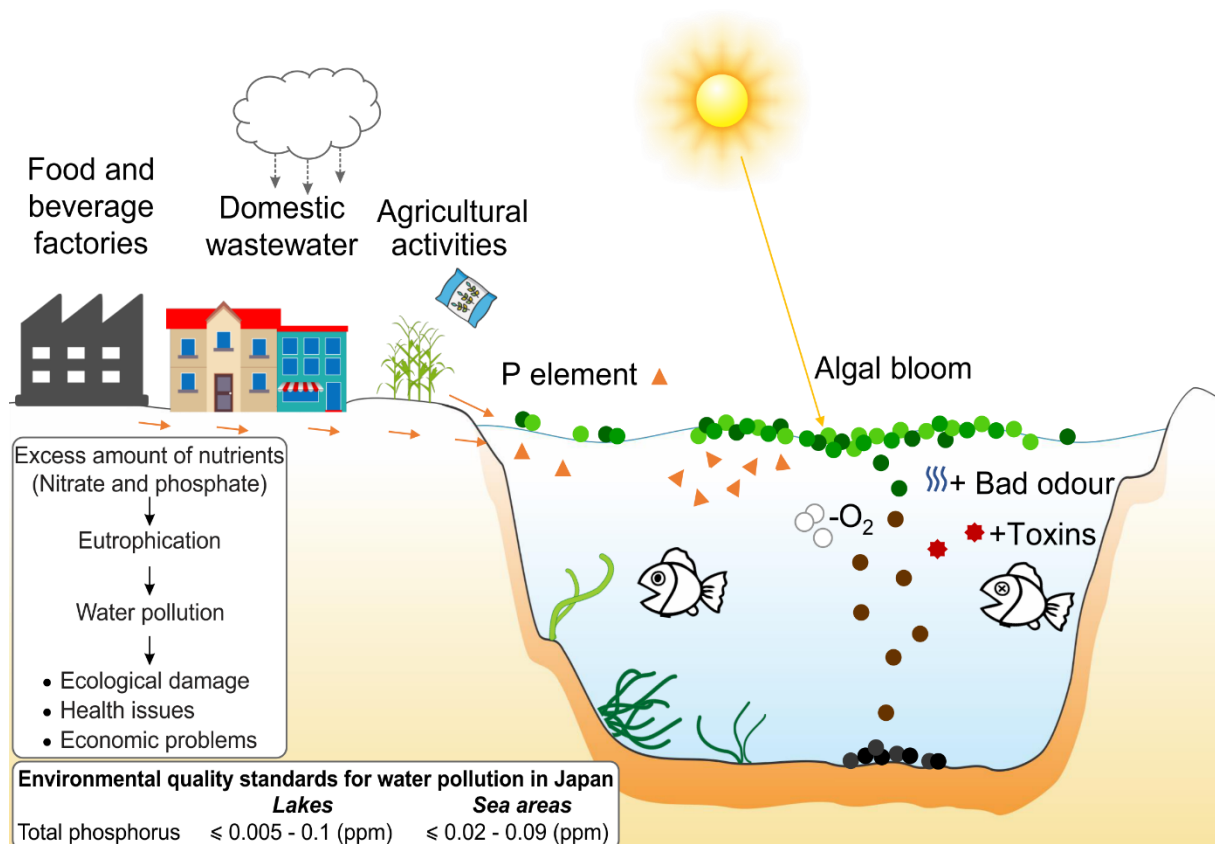
Fig. 1.1. The effect of excessive nutrients in water sources on the ecosystem.

1.2. The shortage of phosphorus resource

P is the important, limited and fixed resource which is decreased because of the development of P application and the decline in phosphate ore and rock reserves [5]. The scarcity of this element could result in a shortage in the fields of agriculture and food supply in the future. Thus, the focus of P recovery from wastewater and sludge for fertilizer production has received considerable research attention. The perspective of considering P in wastewater as the resource is the way to reach the sustainable P cycle. This solution helps to minimize the water pollution (eutrophication), recycle the waste (sludge) of wastewater treatment plants, decrease the disposal and treatment of the mass of sludge as well as supply the fertilizer resource for agriculture.
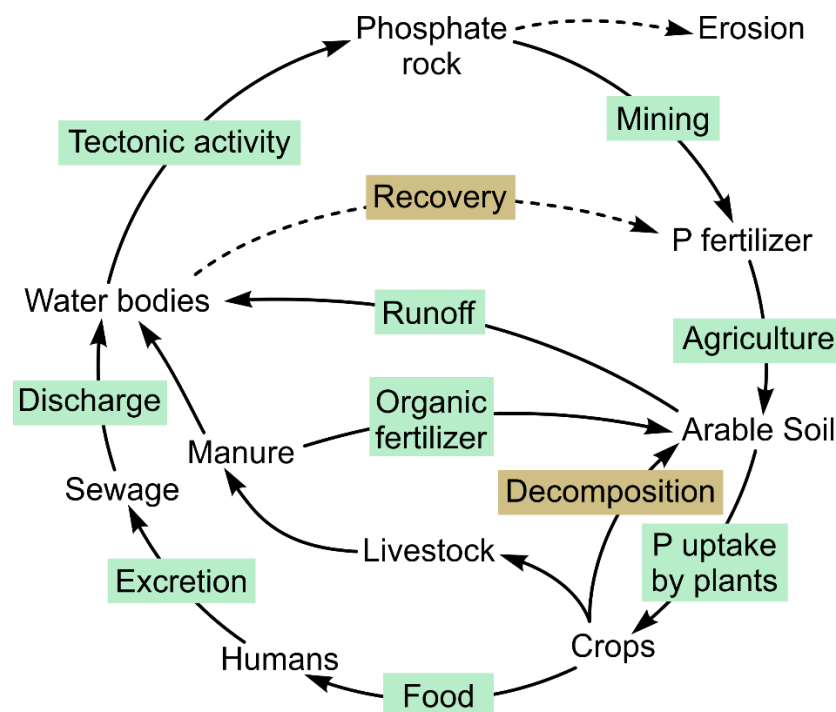
Fig. 1.2. Schematic diagram of the global phosphorus cycle.

(Reproduced from [6])

1.3. Methods for phosphorus removal

Removal of P from wastewater is the beginning of its recovery. The most popular technologies including chemical precipitation, electrocoagulation (EC), membrane filtration, biological method and adsorption have been applied for P removal. This part provides a review of the principles of P removal from these methods and their advantages and disadvantages.

3

1.3.1. Chemical precipitation

The addition of aluminium (Al) or iron (Fe) salts into the phosphate solution could transform the phosphate ions to the insoluble state through chemical precipitation. The formation of the precipitate is conducted by (1) generation of a core solid nuclei, (2) the storage of the precipitate and (3) the development of precipitate [7]. The reaction between the phosphate solution and the variety of salts was given as follows:

$$Al_2(SO_4)_3. 14H_2O + 2PO_4^{3-} \rightarrow 2AlPO_4\downarrow + 3SO_4^{2-} + 14H_2O \quad (1.1)$$

$$Fe_2(SO_4)_3. 9H_2O + 2PO_4^{3-} \rightarrow 2FePO_4\downarrow + 3SO_4^{2-} + 9H_2O \quad (1.2)$$

$$3FeSO_4. 7H_2O + 2PO_4^{3-} \rightarrow Fe_3(PO_4)_2\downarrow + 3SO_4^{2-} + 7H_2O \quad (1.3)$$

$$FeCl_3 + H_3PO_4 \rightarrow FePO_4\downarrow + 3HCl \quad (1.4)$$

The disadvantages of chemical precipitation method are the high energy consumption for operation, the large amount of chemicals and sludge management [8]. Moreover, the further application of sludge for fertilizer production is restricted because of containing various toxic metals for plants and vegetable [9].

1.3.2. Membrane filtration

MF: microfiltration   UF: ultrafiltration

NF: nanofiltration   RO: reverse osmosis
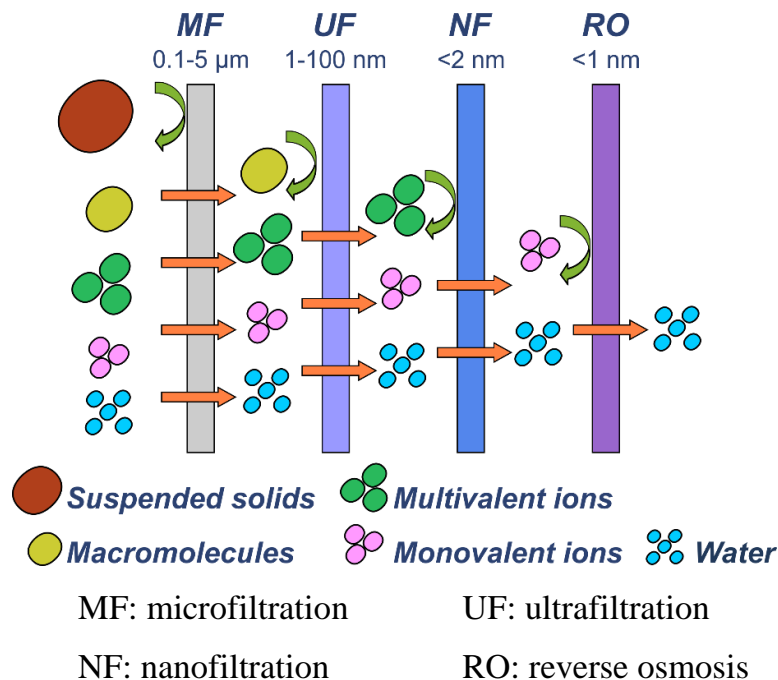
Fig. 1.3. Classification of membrane filtration.

The capture of P by membrane filtration can obtain by solid-liquid separation [10]. Based on the pore sizes or molecular weight cut-off (MWCO), this method can be

classified into nanomembrane filtration or reverse osmosis membrane filtration [11] (Fig. 1.3). Although these two kinds of filtration are the effective techniques for P separation, the process of operation has the high cost of energy, and the efficiency of phosphate removal significantly depends on the wastewater flux, the feed phosphorus concentration, pH and ionic strength [12].

1.3.3. Electrocoagulation (EC)

EC technology operates on the base of in situ formation of coagulants of dissolved P from an aqueous solution by moving an electric current to the submerged electrodes in order to release the metal cations in the solution [13]. These metal cations can neutralize PO_4^{3-} anions (negatively charged pollutant) to generate the polymeric metal hydroxides. The dispersed particles can agglomerate to create the coagulants. EC is considered to the green method for P removal due to the remarkable characteristics such as simple operation, short control time, less generation of sludge, negligible utilization of reagents which lead to the disappearance of secondary contaminants [14]. However, the efficacy of EC method is influenced by the kind of electrode, the size of electrode, the number of electrode, the material of electrode, the density of current and pH [15].
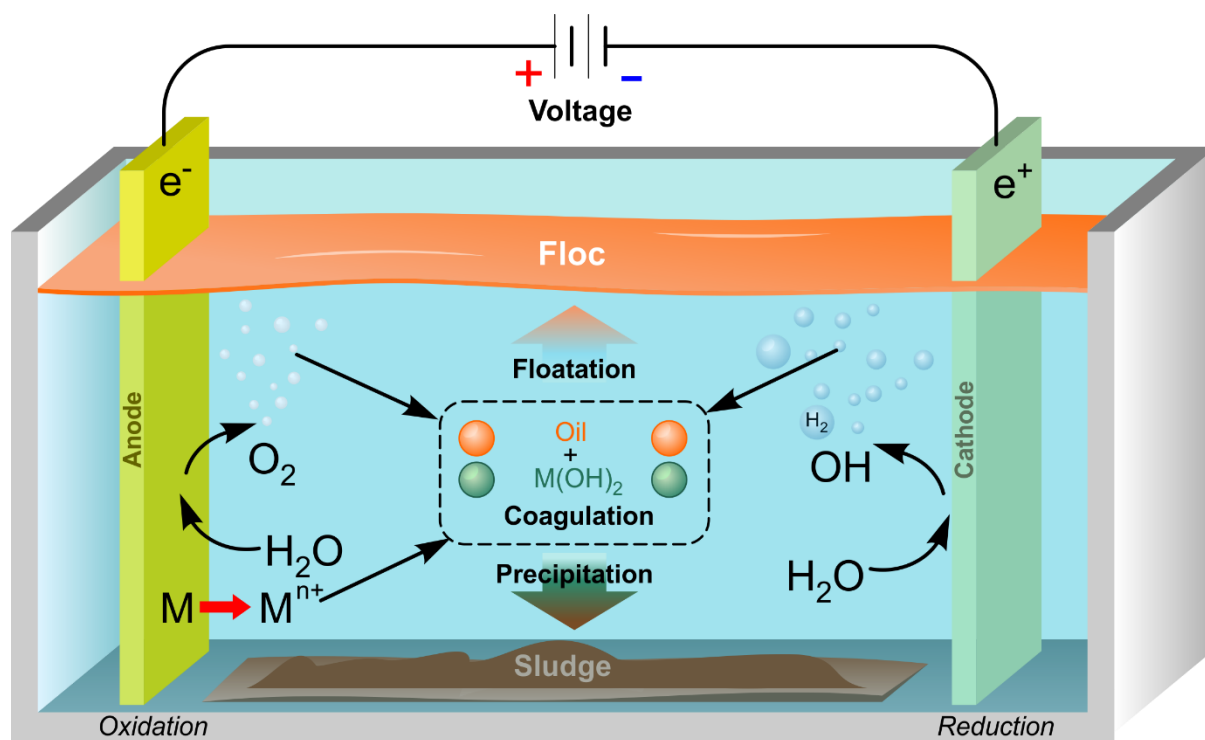
Fig. 1.4. The fundamental principle of EC process.

(Reproduced from [16])

1.3.4. Biological method

Biological process for P removal is influenced by the ability of algae, organisms (activated sludge) and plants accumulating, converting and storing an amount of P into the cell. The main research fields of biological method focus on the enhanced biological phosphorus removal (EBPR) process and constructed wetland process. EBPR technology used in municipal wastewater treatment is based on the activity of activated sludge containing organisms accumulating polyphosphate in their cells. In the anaerobic condition, phosphate accumulating organisms (PAOs) can decompose their poly-P and form adenosine triphosphate (ATP), use this compound to consume volatile fatty acids (VFAs) and store VFAs as polyhydroxyalkanoates (PHAs) in the organism cells [17]. EBPR is an effective method for P removal and extensively applied in full-scale wastewater treatment plants. Nonetheless, the process is limited by the high energy consumption to maintain the multi-conditions including aerobic, anaerobic and anoxic [18].
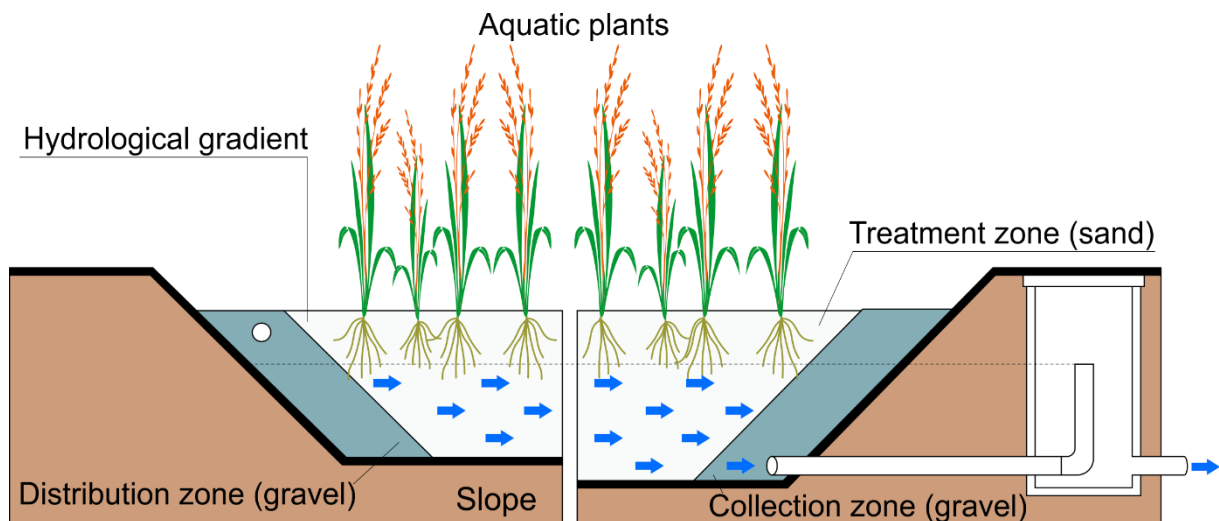
Fig. 1.5. The fundamental operation of constructed wetland.

(Reproduced from [19])

Another approach to drop P amount in wastewater is to apply constructed wetland. The designed system of vegetation as the biofilter, soil and gravel and other filter materials are indispensable constituents in the adsorption and filtration processes for separating nutrients (nitrogen and P), suspended solids, heavy metals, detergents and pesticides [20-23] (Fig. 1.5). The advantages of this method are bioenergy production, low technology and low cost of operation, maintenance and energy consumption [24-26]. Nevertheless, the low P retention capacity, the large area for operation, the

6

dependence of climate conditions for vegetation have limited the application of constructed wetland system [19, 27, 28].

1.3.5. Adsorption method

Adsorption technique has attracted more attention owing to the high performance, simple design, technical feasibility and inexpensive cost. Besides, phosphate-laden adsorbents can be used as the fertilizer for agricultural activities [29]. The numerous of adsorbents can categorized as (i) natural adsorbents such as calcite [30], apatite [31], bentonite [32], zeolite [33], sepiolite [34], pyrrhotite [35], peat [36] and shale [37], (ii) synthetic adsorbents including layered double hydroxides (LDHs) [38, 39], mesoporous materials [40], graphene supported materials and biopolymer materials [29] and (iii) wastes or by-products such as steelmaking slag [41], red mud [42], fly ash [43], and shells (crab, scallop, mussel, oyster and egg) [44-48].

1.4. Alginate and their ability of gel formation

Alginate is a polysaccharide consisting of mannuronic acid (mannuronate) (M) and guluronic acid (guluronate) (G) (Fig. 1.6). Alginate extracted from brown seaweeds as dietary fibers are used in medical and pharmaceutical application, food industry, cosmetic and water purification due to the non-toxicity and biodegradability [49-51]. When alginate is added to the solution containing divalent cations such as Ca^{2+}, Ba^{2+} or Mg^{2+}, sodium ions (Na^+) can exchange these cations, then the gel is formed through the physical crosslink between one Ca^{2+} ion with four guluronic monomers [52, 53]. This chain arrangement is often called the "egg-box" model (Fig. 1.7).

1.5. Conclusion

This chapter offered an overview of the importance of P in the food supply and agricultural activities as well as water pollution because of the excess of this element in water sources. Chemical precipitation, electrocoagulation EC, membrane filtration, biological method and adsorption have been applied for P removal. Each method has both advantages and disadvantages. The recovery of P in wastewater is the objective for applying suitable methods.

a

Mannuronate (M)

b

Guluronate (L)

c

M   M   M

G   G   G   G

M   G   M
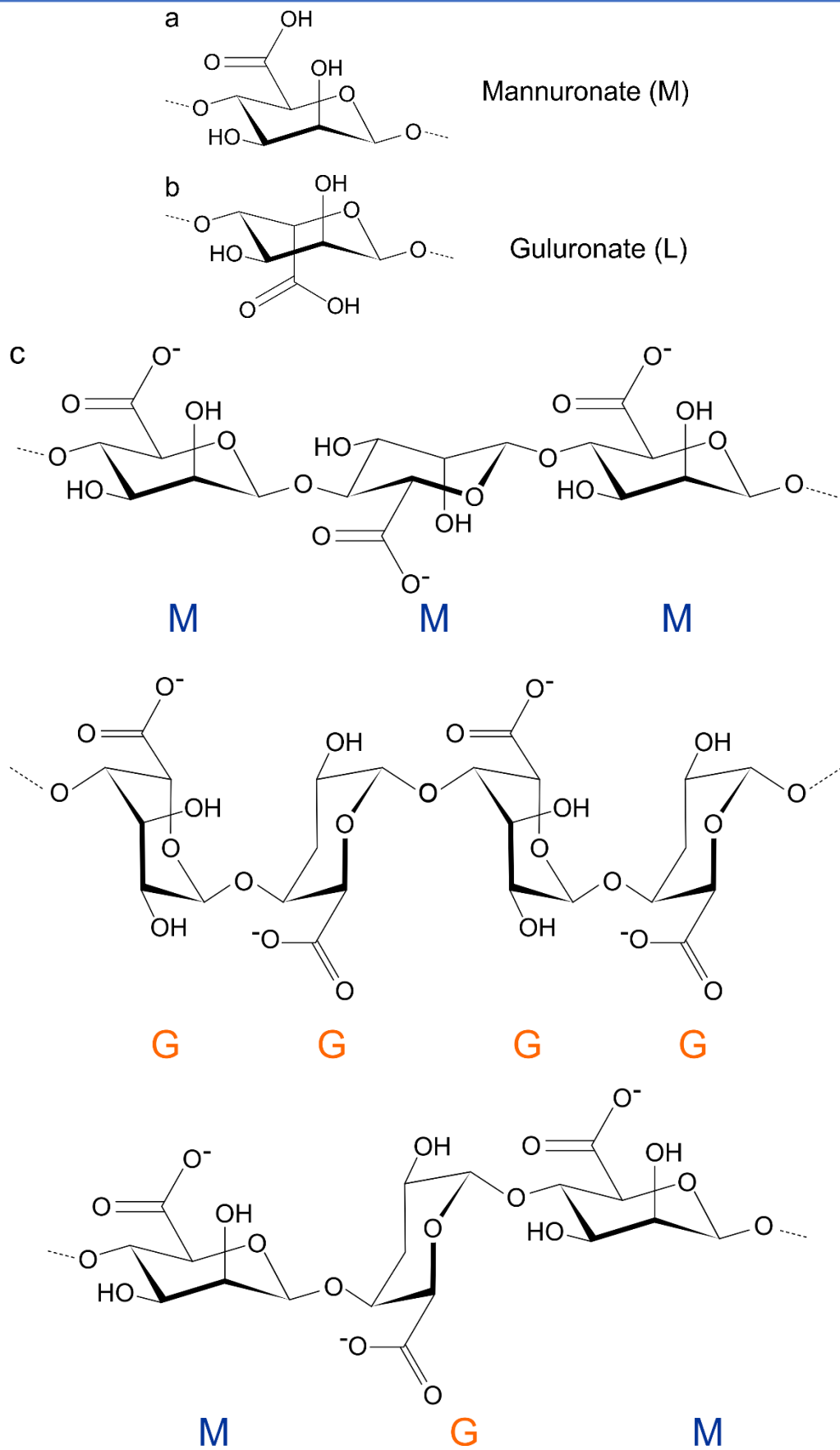
Fig. 1.6. The structure of mannuronate (M) (a) and guluronate (G) (b) and types of

alginate block (c).

(Reproduced from [54])
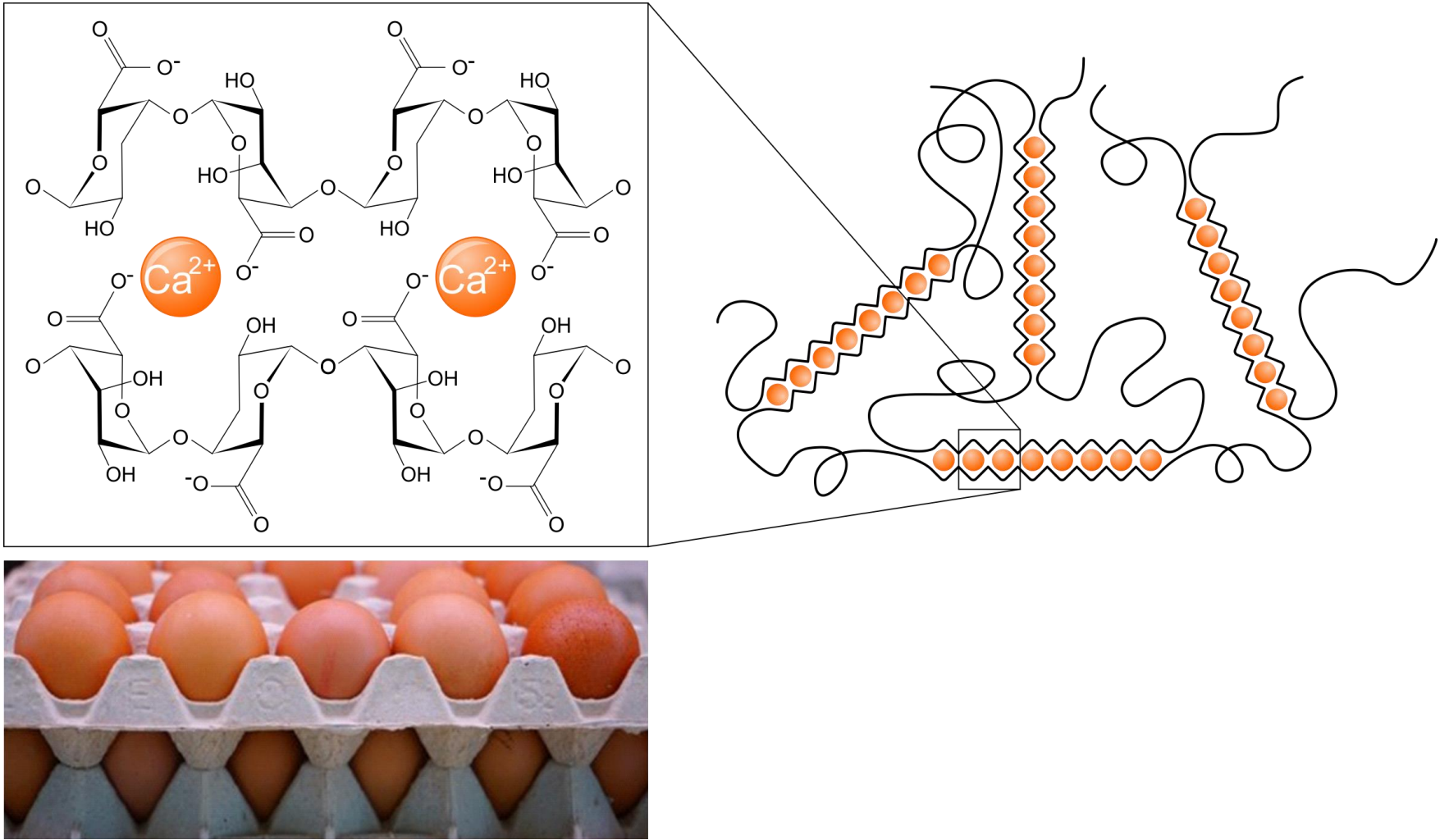
Fig. 1.7. The "egg box" model of alginate gel.

(Reproduced from [54])

Chapter 2

Eco-friendly removal of phosphate from aqueous solution using natural dietary fibers and minerals

Abstract

Excess of phosphate in water sources leads to the eutrophication which is the cause of water pollution, health issues and economic problems. In this study, we focused on the investigation of phosphate removal using calcium oxide (CaO) and calcium hydroxide $Ca(OH)_2$, the dominant compounds in calcined shells. Hydroxylapatite $Ca_{10}(PO_4)_6(OH)_2$, the component of industrial fertilizer, was formed after precipitation process following the XRD results. The phosphate removal rate of samples filtered through 2.7 μm particle retention filter paper increased from 20% to 97% with the aid of flocculants of alginic acid, $NaHCO_3$ and $CaCl_2 \cdot 2H_2O$ in the initial phosphate concentration as P 50 ppm, and this removal rate was roughly equivalent to the samples filtered through 0.2 μm membrane filter without flocculants (99%). This work provided the effectiveness of eco-friendly flocculants in the separation of precipitates by filtration in the range of phosphate concentration from 20 to 120 ppm.

Keywords: phosphate removal; eco-friendly treatment; calcined shell; alginate and flocculants.
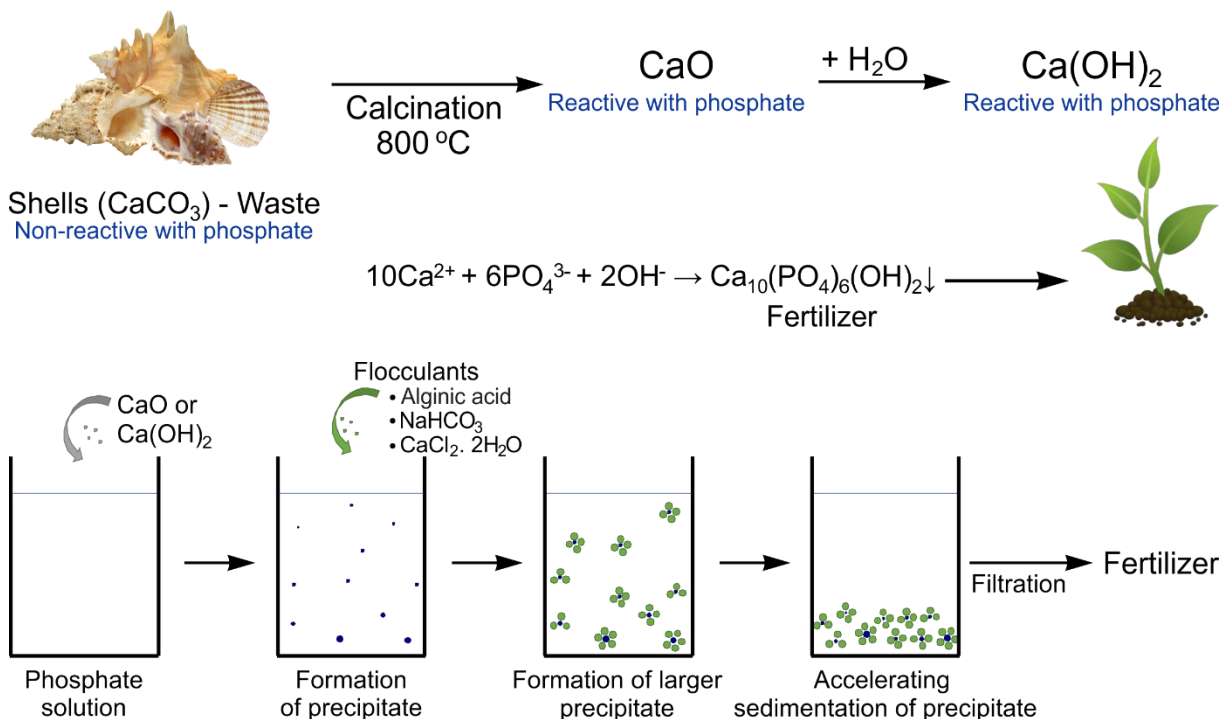
Fig. 2.1. Schematic diagram of phosphate removal using CaO and $Ca(OH)_2$ with the aid of flocculants.

2.1. Introduction

P plays a vital role in the growth and development of crops but the decrease in reserves of phosphate ore leads to the shortage of fertilizer and the problem of food security [55]. However, the enrichment of nutrients such as phosphate and nitrate from municipal, agricultural or industrial wastewater in water sources is the cause of eutrophication. This issue can threaten natural habitats, damage the biodiversity of the aquatic ecosystem and impact adversely on human health via the food chain [2, 56]. Hence, Environmental Quality Standard for water pollution (EQS) in Japan limits the total P lower than 0.1 ppm in rivers and lakes and lower than 0.02 - 0.09 ppm in coastal waters to control P concentration [57]. In order to preserve the quality of water sources, the management of P concentration in the limitation of standard is the challenges for wastewater treatment plants. The treatment of P by recycling this element in wastewater is regarded as a sustainable solution when the P from waste runoff turns to the products for agriculture and reduces the water pollution caused by eutrophication [58].

Numerous chemical, physical and biological methods have been developed for removal of P from aqueous solution [59]. The weakness of chemical precipitation is the large consumption of chemicals such as alum, lime and iron salts as well as the considerable production of sludge in the process of P removal [46]. Besides, the recycle of sludge for fertilizer is considered because the toxic elements are found in the sludge. The physical methods like membrane filtration, electrocoagulation have the high P removal rate, less use of chemicals and less production of sludge. However, high cost is the disadvantage of the large-scale application of these techniques [60]. The biological method using microorganism has a strict requirement of aerobic and anaerobic conditions. Hence, it is hard to maintain the stability of organism activities [61]. Adsorption technique with the natural adsorbents such as apatite, zeolite, bentonite or adsorbents from the waste such as steelmaking slag, red mud, fly ash, peat and shells (crab, scallop, mussel, oyster and egg) is getting more attention due to the high efficiency, simplicity, availability and low cost [62-64].

Previous researches have reported that the calcined shells have been highlighted as the promising materials for P adsorption. Calcium carbonate ($CaCO_3$) is the chief compound in the shells can be transformed into CaO by the thermal treatment [44]. In

addition, $Ca(OH)_2$ is easily formed by the reaction with moisture in the atmosphere. The reactions are described as:

$$\text{Shells (CaCO}_3) \xrightarrow{\text{heat}} CaO + CO_2 \qquad (2.1)$$

$$CaO + H_2O \rightarrow Ca(OH)_2 \qquad (2.2)$$
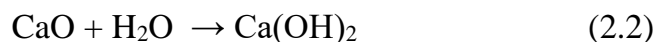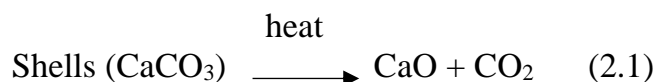
Indeed, CaO and $Ca(OH)_2$ are more active than $CaCO_3$ because the solubility of CaO and $Ca(OH)_2$ in solution is much higher than $CaCO_3$ [65]. More significantly, the products after the reaction between calcined shells and phosphate solution are appropriate to be applied as the fertilizer.

Alginate, also called alginic acid, is a block copolymer composed of mannuronic acid and guluronic acid. It is extracted from brown seaweeds and regarded as dietary fiber which [66]. Due to the non-toxic and biodegradable characteristics, alginate is used in food additives, toothpaste, cosmetics, medicines and water treatment [67]. In the presence of calcium, alginate will generate the gel via the crosslink between Ca^{2+} and guluronic monomers [68]. In particular, this characteristic of alginate has been applied in making the artificial fish egg [69].

In this work, capacity of phosphate removal using CaO and $Ca(OH)_2$, the major components of shells calcinated at high temperatures, was investigated. Next, the mixture of non-toxic flocculants including alginic acid, $NaHCO_3$ and $CaCl_2$ was added to the solution in order to improve the removal efficiency of phosphate and increase the effective separation of precipitates by filtration. The characterization of precipitates collected by filtration was conducted by SEM and XRD.

2.2. Experimental

2.2.1. Materials and reagents

All chemicals used were analytical grade and used without further treatment. The phosphate stock solution (PO_4^{3-}) containing different P concentration was prepared by potassium dihydrogen phosphate (KH_2PO_4) purchased from Kanto, Japan. CaO, $Ca(OH)_2$, sodium hydrogen carbonate ($NaHCO_3$) and calcium chloride dihydrate ($CaCl_2.2H_2O$) were obtained from Kanto, Japan. Alginic acid was supplied from Trademark, Japan. All aqueous solutions were prepared using Mili-Q water from Direct-Q UV3, Merck Millipore.

2.2.2. Precipitation studies

First of all, 0.1 g of CaO or Ca(OH)$_2$ was added to the polypropylene bottle (PP) containing 100 mL of phosphate solution with the different initial concentration of P 5, 10, 20, 50, 100, 200, 500, and 1000 ppm. After shaking at 25 ºC for 18 h in the water bath to reach the equilibrium state of the reaction, the samples were i, filtered through a Whatman 50 filter paper (2.7 µm particle retention) offered by International Ltd. Maidstone, England; ii, filtered through a 0.2 µm membrane filter (Omnipore hydrophilic PTFE) supplied by Merck Millipore Ltd, Ireland; iii, transferred to the beaker 200 mL. Next, the flocculants of alginic acid: NaHCO$_3$: CaCl$_2$.2H$_2$O following the weight ratio (1: 0.3: 0.02) were poured into the solution that was then magnetically stirred for 5 minutes, settled for 10 minutes, and the supernatant was filtered through the Whatman 50 filter paper, 2.7 µm particle retention (Fig. 2.2).

The phosphate concentration of the samples before and after precipitation experiment were examined by molybdenum blue method with ascorbic acid using UV/VIS/NIR Spectrophotometer V-570, Jasco, Japan [70]. The determination of phosphate concentration was conducted at 880 nm wavelength which corresponds to the maximum absorbance.

The removal efficiency of phosphate (*H*) and the mass of adsorbed P per unit mass of material (*q*$_e$) were determined by the following equation.

$$H = \frac{C_0 - C_e}{C_0}.100 \quad (\%) \qquad (2.3)$$

$$q_e = \frac{C_0 - C_e}{M}.V \quad (mg/g) \qquad (2.4)$$

Where *C*$_0$ and *C*$_e$ are the initial and equilibrium concentrations of phosphate (ppm), respectively, *M* is the mass of CaO or Ca(OH)$_2$ (g) and *V* is the volume of sample (L).
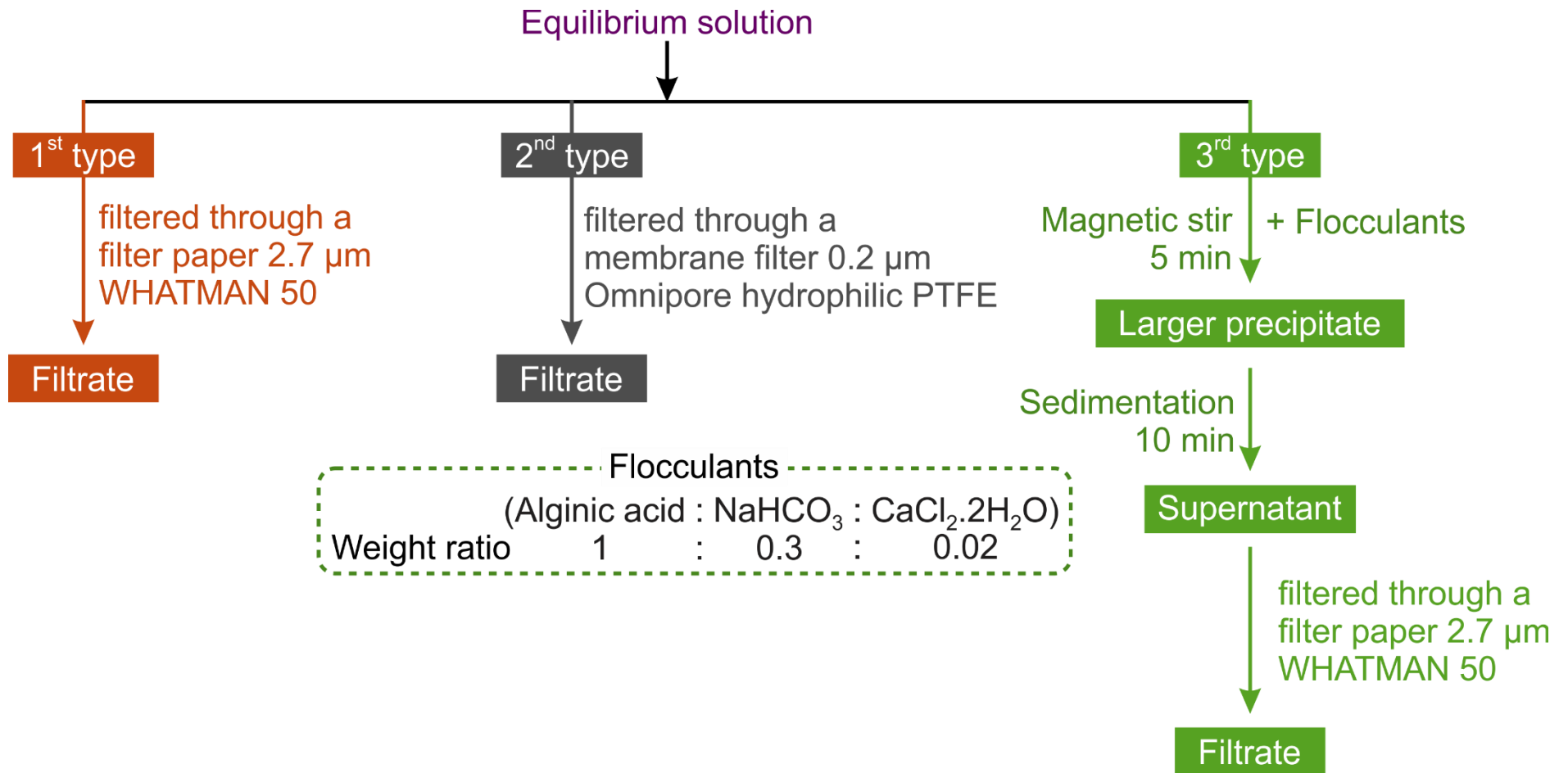
Fig. 2.2. Three kinds of filtration.
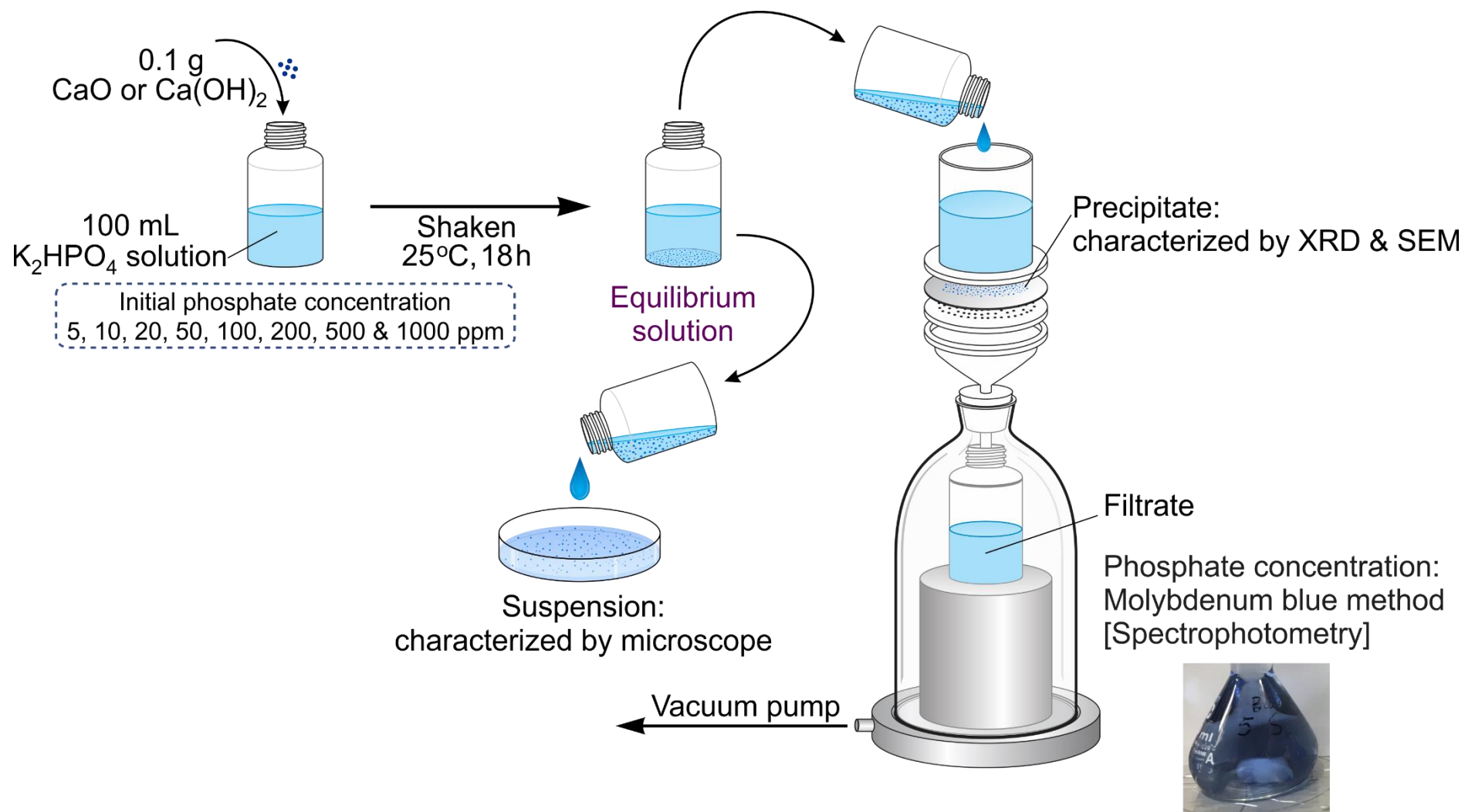
Fig. 2.3. The set-up of phosphate removal experiment and characterization of samples.
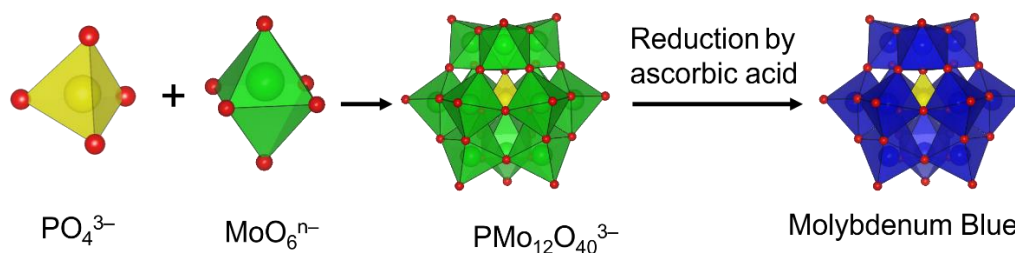
Fig. 2.4. The formation of molybdenum blue.

2.2.3. SEM analysis

SEM images of precipitates produced after the reaction between CaO or Ca(OH)$_2$ with phosphate solution at the different initial concentration were obtained by field emission scanning electron microscope (Hitachi S-4700 FE-SEM, Japan).

2.2.4. X-ray diffraction analysis

In order to identify the products formed by reaction between CaO or Ca(OH)$_2$ and phosphate solution, XRD measurement using SmartLab X-ray Diffractometer (Rigaku, Japan) was conducted with CuKα radiation of wavelength λ = 1.5418 Å. The X-ray generator worked at a power of 45 kV and the current of 200 mA. XRD patterns were collected in the 2θ range of 10 to 90° using a continuous scanning speed of 40° min^{-1}. The precipitates of samples after filtration was dried at room temperature, then was placed on the silicon sample holder for XRD analysis.

2.2.5. Microscope

The images of dispersion after precipitation process without filtration was captured by Keyence VHX-6000 Microscope, U.S.A.

2.3. Results and discussion

2.3.1. Capacity of phosphate removal using CaO and Ca(OH)$_2$ with and without flocculants

The removal rate of phosphate by CaO and Ca(OH)$_2$ is given in Fig. 2.5. There was a slight difference of phosphate removal rate between the filtration through 2.7 μm filter paper with flocculants (3rd type) and the filtration through 0.2 μm membrane filter without flocculants (2nd type), and the removal rate of both two these cases was much higher than the filtration through 2.7 μm filter paper without flocculants (1st type) in the range of initial phosphate concentration from 20 to 100 ppm. It was assumed that

generated products were trapped easily in the 0.2 µm membrane filter, and the small size precipitates could pass through the 2.7 µm filter paper. Indeed, the highest phosphate efficiency removal of CaO and $Ca(OH)_2$ by the filtration through 0.2 µm membrane filter (2nd type) and 2.7 µm filter paper with the addition of flocculants (3rd type) was 99% and 97% in the phosphate solution of 50 ppm, respectively.

The maximum phosphate removal capacity of CaO was 309 mg/g, whereas it made up 264 mg/g with $Ca(OH)_2$ when the samples with the flocculants were filtered through 2.7 µm filter paper (3rd type) at 500 ppm of initial phosphate concentration (Fig. 2.6). It was worth noting that the phosphate removal rate of CaO and $Ca(OH)_2$ samples without flocculants at 50 ppm made up 19 and 20 % (1st type) were lower than that of the samples with flocculants in the case of 2.7 µm filter paper (3rd type). All results indicated that flocculants played an important role to combine the suspended precipitates in the solution to create the bigger size products for easier separation.

2.3.2. Characterization of precipitates

Fig. 2.7 shows the SEM images of precipitates after precipitation experiment collected by filtration. It can be seen that crystallites were only found in the case of initial phosphate concentration of 10 ppm. In addition, the images of dispersion without filtration observed under the microscope (Fig. 2.8) displayed the precipitates at phosphate concentration of 200 ppm were a spherical shape (10-100 µm) and were substantially larger than the samples of 10 and 50 ppm which were not able to determine particle size. The analysis of SEM and microscope of precipitates revealed that the crystallites generated at the phosphate concentration lower than 20 ppm, and precipitate microsphere formed at phosphate concentration higher than 120 ppm were easily filtered through 2.7 µm filter paper which made the phosphate removal rate over 80%. However, precipitates could pass through 2.7 µm filter paper because of the tiny size of the particle in the range of phosphate concentration from 20 to 120 ppm, resulting in the dramatic decrease in phosphate removal rate (approximately 20%). These results further proved that the effectiveness of flocculants presence for phosphate removal from 20 to 120 ppm.
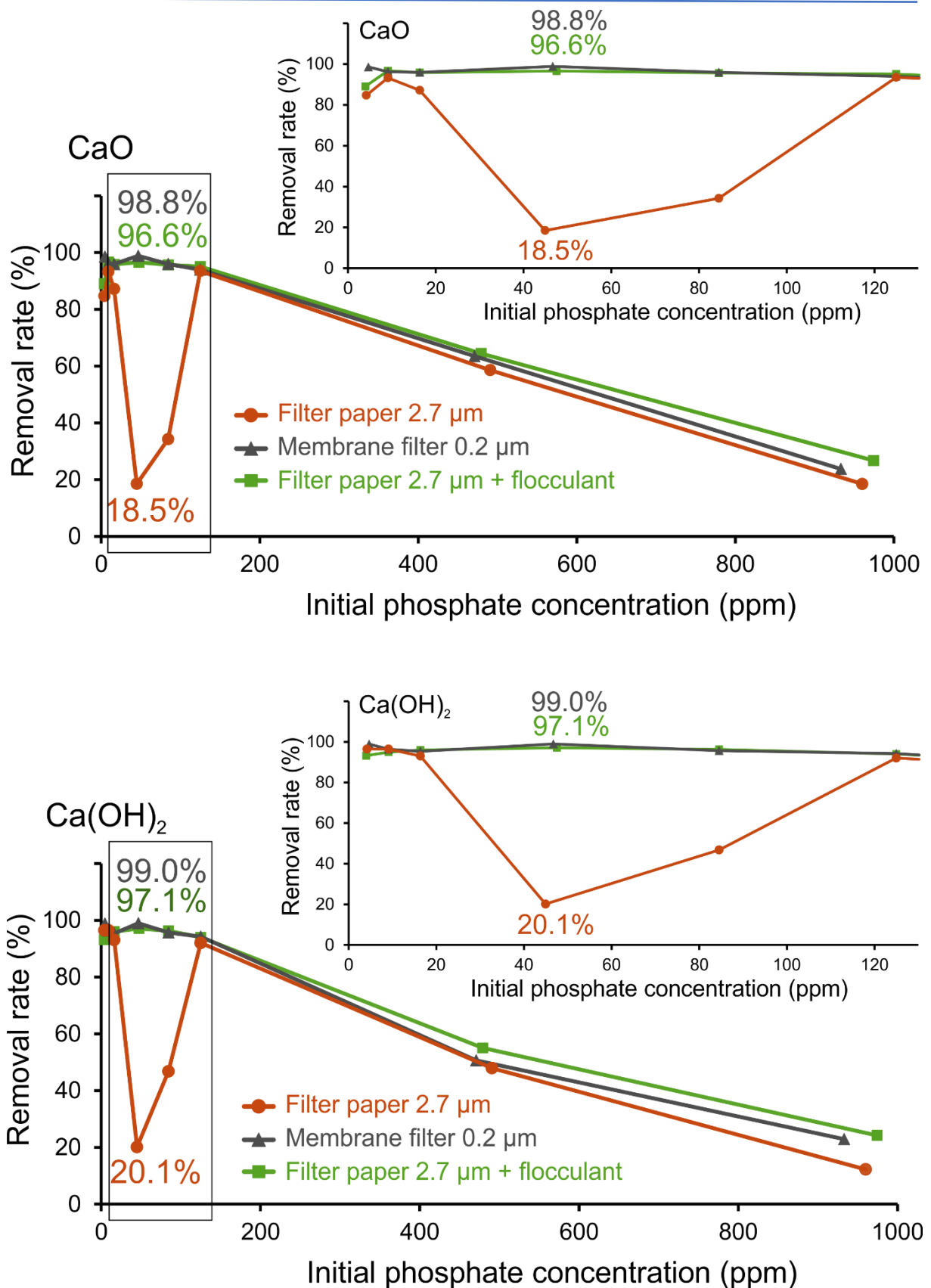
Fig. 2.5. The removal rate of phosphate by CaO (a) and Ca (OH)$_2$ (b) using different pore size of filter paper with and without flocculants.
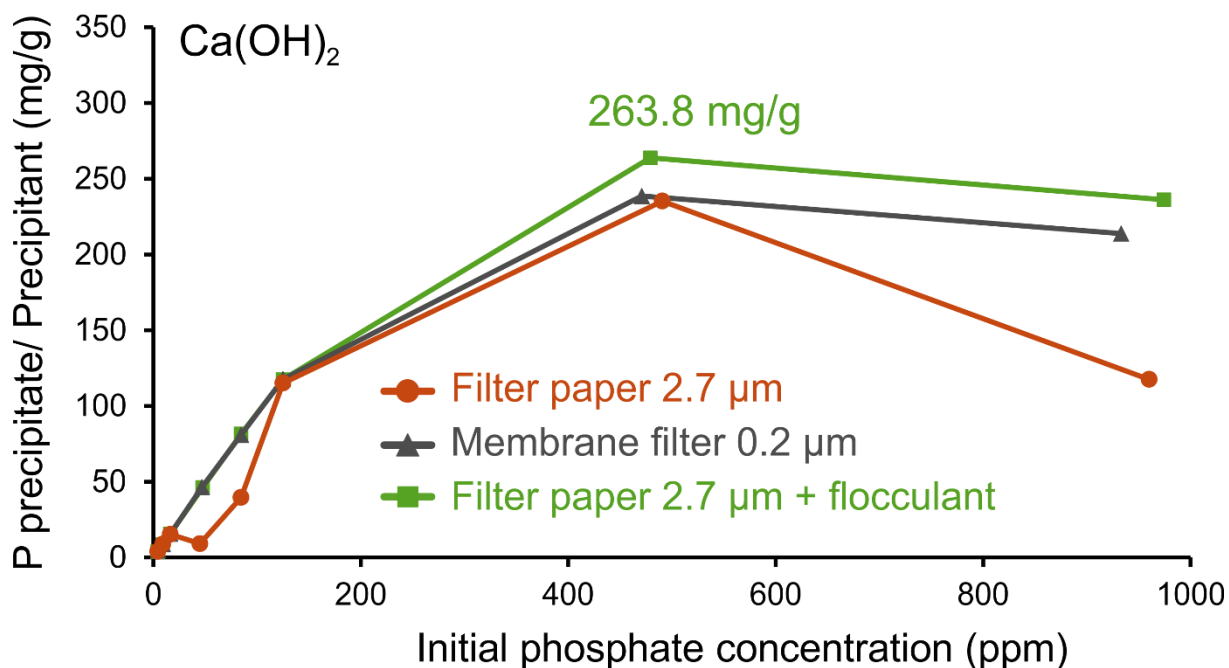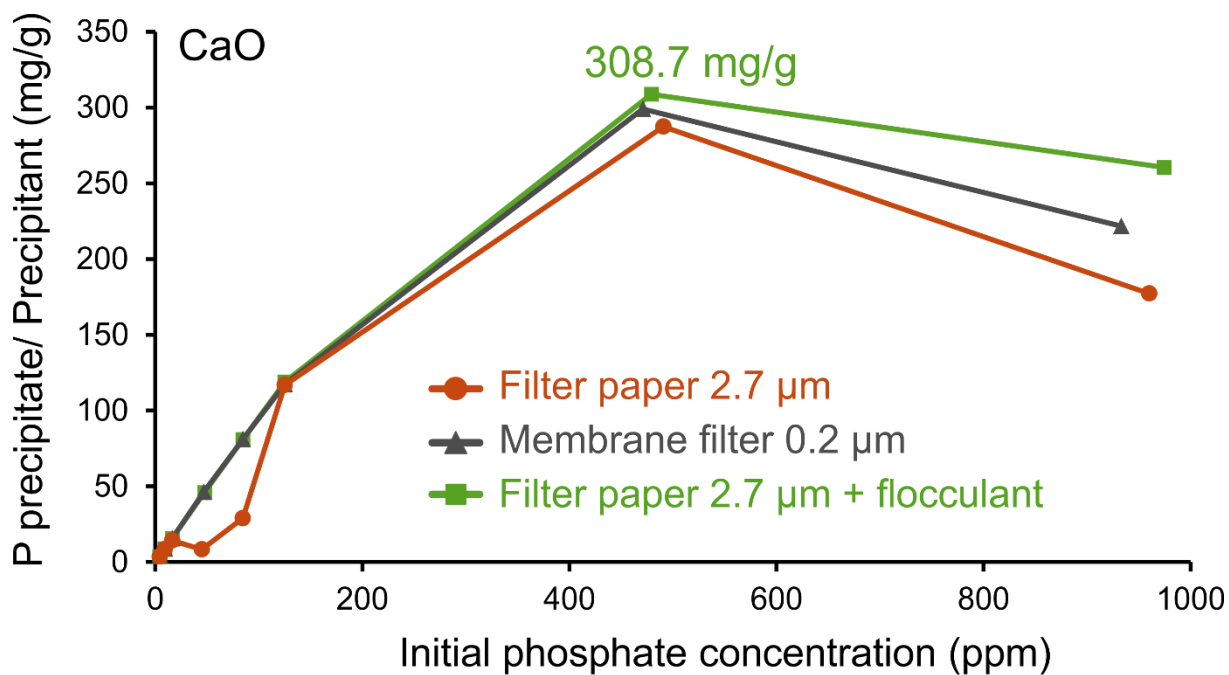
Fig. 2.6. The capacity of phosphate removal of CaO (a) and $Ca(OH)_2$ (b) using different pore size of filter paper with and without flocculants.

The XRD patterns of precipitates formed after the reaction between CaO or Ca(OH)$_2$ and phosphate solution are given in Fig. 2.9. Hydroxylapatite Ca$_{10}$(PO4)$_6$(OH)$_2$, the main crystalline material was generated (Eq. 2.5). It was worth mentioning that hydroxylapatite can be applied as the fertilizer for agricultural activities [71].

$$10Ca^{2+} + 6PO_4^{3-} + 2OH^- \rightarrow Ca_{10}(PO_4)_6(OH)_2 \downarrow \qquad (2.5)$$
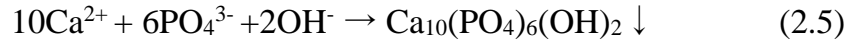
When the mixture of alginic acid, NaHCO$_3$, and CaCl$_2$.2H$_2$O was added to solution, regions of guluronic acid monomers in one molecule of alginate could easily link to others regions of guluronic acid monomers by Ca^{2+} ion [72]. The binding of the alginate chains created the junction zones, leading to the gel formation which was referred to the physical crosslink or connecting bridges [73]. The alginate gels with the high viscosity supported the combination of the suspended precipitates to become coarser; as a result, the phosphate removal rate with the addition of flocculants filtered through 2.7 µm particle retention (3rd type) was similar to membrane filter paper 0.2 µm without flocculants (2nd type).

Crystallite
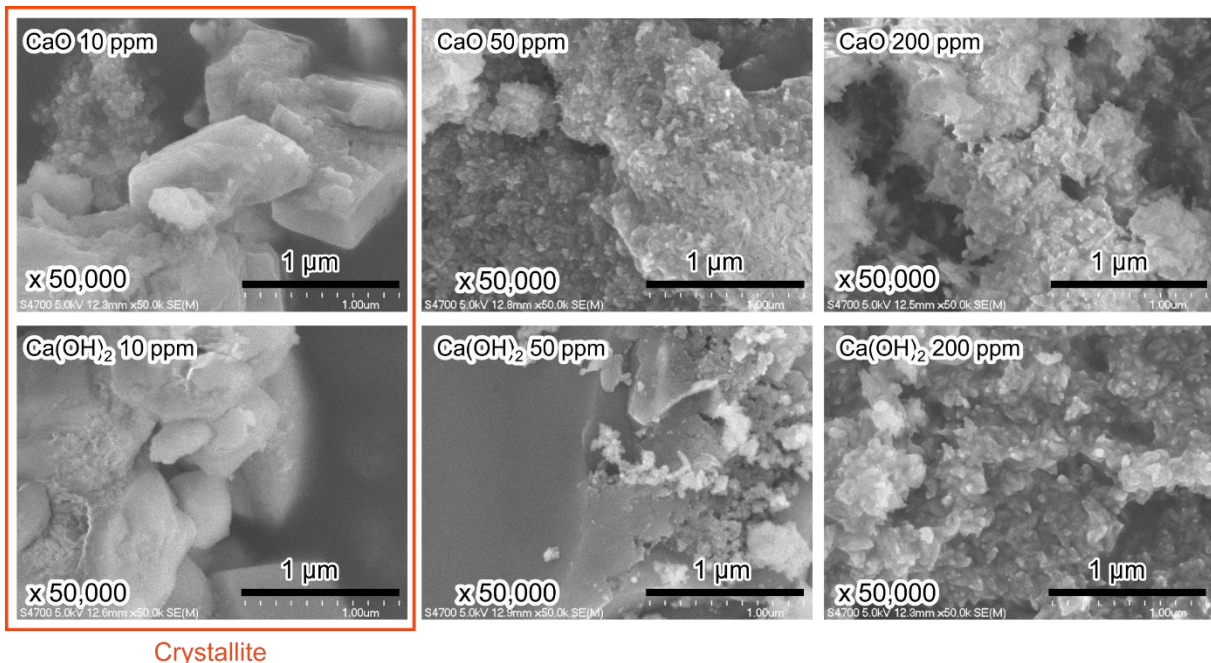
Fig. 2.7. SEM images of precipitate produced after the reaction between CaO or Ca(OH)$_2$ and phosphate concentration at 10, 50 and 200 ppm (x50,000).

Precipitate microsphere (10 ~ 100 μm)
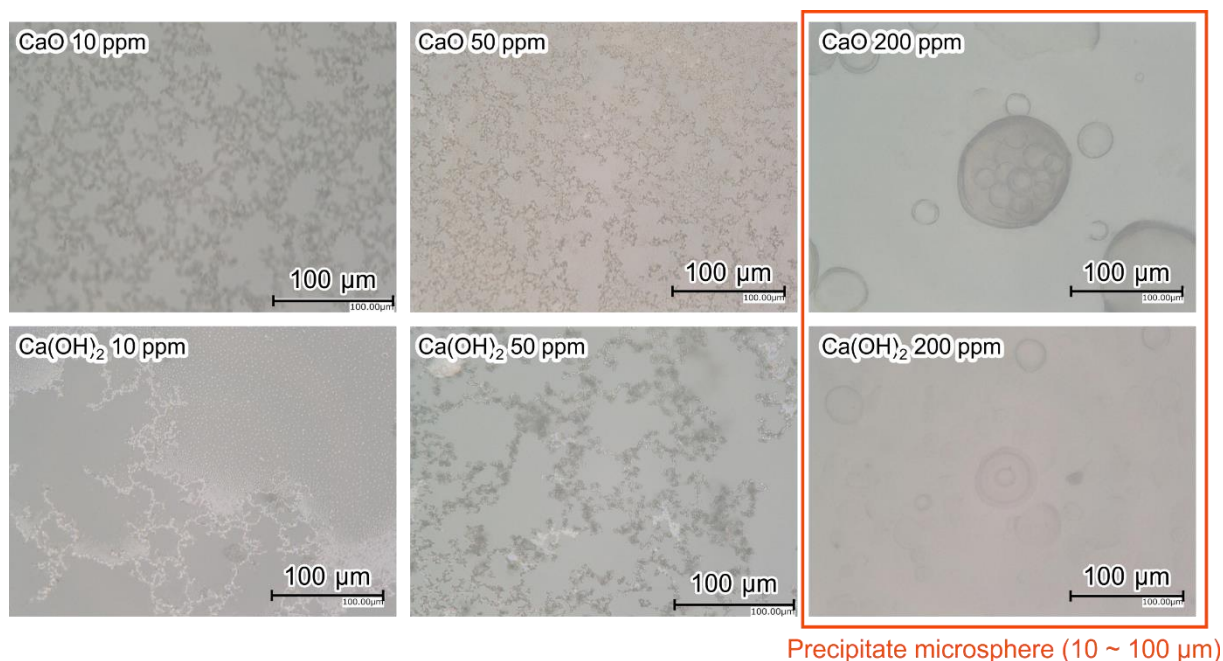
Fig. 2.8. Microscope images of dispersion.
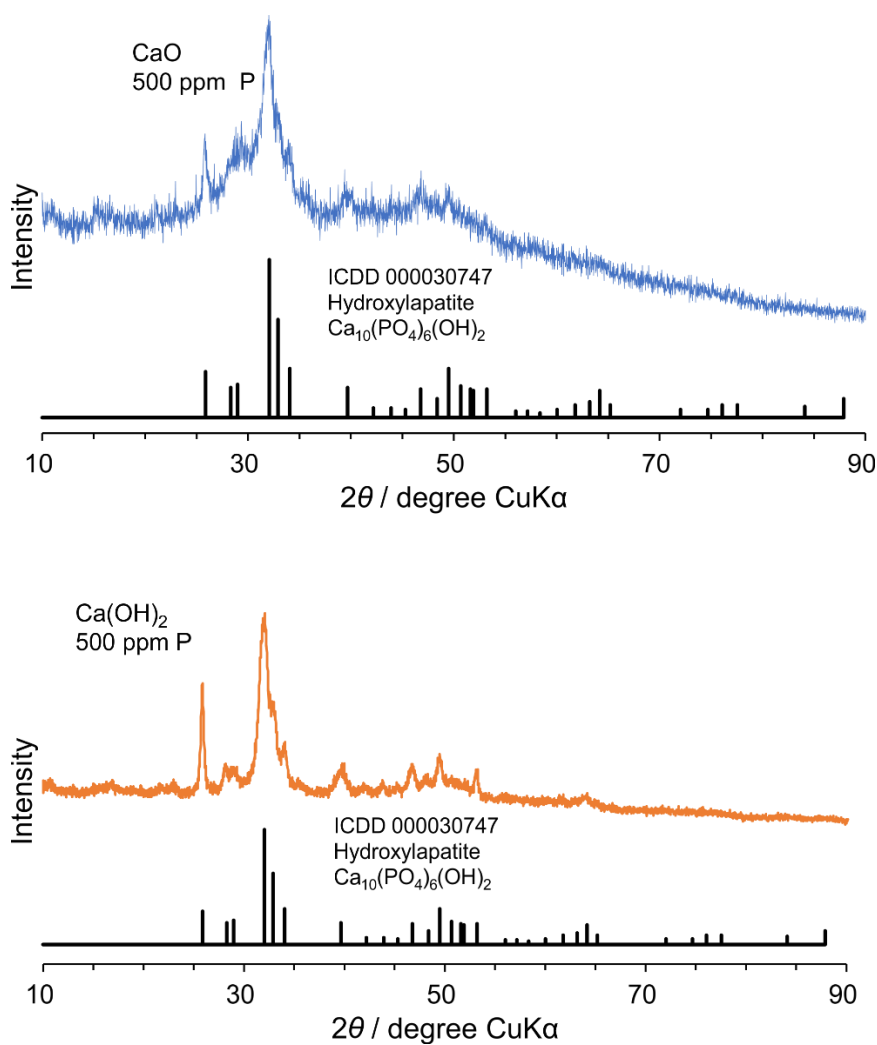
Fig. 2.9. XRD patterns of precipitates produced after CaO (a) and Ca(OH)$_2$ (b) reacted with phosphate solution at 500 ppm.
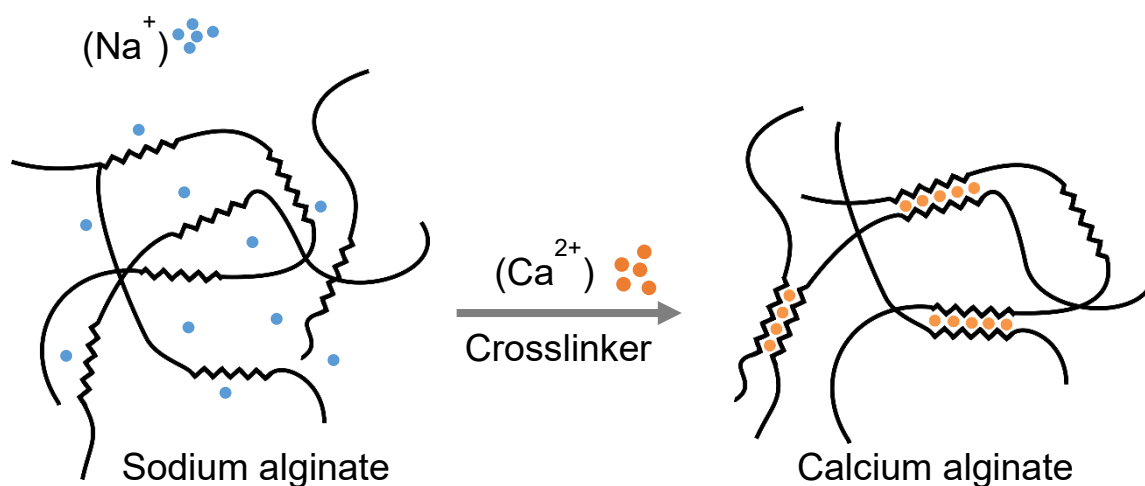
Fig. 2.10. Schematic illustration of alginate gel formation in the presence of calcium cation.

2.4. Conclusion

The formed precipitates between CaO or $Ca(OH)_2$ and phosphate solution at 50 ppm could pass through the 2.7 μm filter paper by filtration. When the flocculants of alginic acid: $NaHCO_3$: $CaCl_2.2H_2O$ with the weight ratio 1: 0.3: 0.02 was added, the phosphate removal rate of samples filtered via 2.7 μm filter paper rose dramatically from 20 to 97%. It is interesting to compare the phosphate removal rate of samples filtered through 0.2 μm membrane filter without flocculants which reached the highest level at 99%. The results suggested that the non-toxic flocculants of alginic, $NaHCO_3$ and $CaCl_2.2H_2O$ are effective for phosphate removal from 20 to 120 ppm. Besides, hydroxylapatite $Ca_{10}(PO_4)_6(OH)_2$ was formed after precipitation could be applied as fertilizer for plants.

Chapter 3

General introduction of boron and its removal processes

3.1. Characteristics of boron and its compounds

3.1.1. Basic chemical properties of boron

Boron is a metalloid in group 13 of the periodic table. The chemical properties of boron are more similar to aluminium, carbon and silicone than elements of its own group [74]. Although the applications of boron compounds were recorded for centuries, it was first isolated as an element by Sir Humphry Davy in England in 1808. After Davy's success, Joseph Louis Gay Lussac and Louis Jaques Thénard found a new method for separating boron from its compound. In 1892, French chemist, Henri Moissan created 98% pure of boron [75]. Boron can be prepared in several allotropic forms including amorphous powder or crystalline forms such as α-rhombohedral, β-rhombohedral, α-tetragonal, and β-tetragonal [76]. It is stressed that boron is hard to prepare in the high purity because of its high melting point.

Boron is comprised of ^{8}B, ^{10}B, ^{11}B, ^{12}B, ^{13}B isotopes. However, the most stable isotopes are the mass of 10 and 11 account for 20:80% ratio, leading to an atomic weight of 10.81g/mol [77]. The electron configuration of this element is $1s^2\,2s^2\,2p^1$, so boron can form three valence bonds. Boron has trivalent oxidation state +3 in its most common compounds such as oxides (e.g. B_2O_3), sulfides (e.g. B_2S_3) and nitrides (e.g. BN). The lower oxidation states +1, 0 or less than 0 exist only in compounds such as higher boranes like B_5H_9, subvalent halides like B_4Cl_4, metal borides like Ti_2B or in some compounds containing multiple B-B bonds [78].

3.1.2. Sources of boron compounds in nature

Boron is never found in nature as an element but always as complex compounds combining with oxygen and other elements as either boric acid (H_3BO_3) or its salts (borates). Economic borate deposits occurring in arid areas are extracted for industrial activities [79]. More than 200 mineral species containing boron are from surface deposits. Approximately 90% of them has commercial significance, and the remaining is considered to the potential minerals. The most extraction activities of borate mineral for commercial applications occur in Turkey, Peru, Chile, Kazakhstan, Argentina, China, Bolivia, The United States and Russia [80]. The list of borate minerals is shown in Table 3.1.

Table 3.1 Borate minerals for industry [79].

Mineral	Formula	B_2O_3 (wt%)
Sassolite	$B(OH)_3$, or $B_2O_3.3H_2O$	56.4
Borax (Tincal)	$Na_2B_4O_7.10H_2O$	36.5
Tincalconite	$Na_2B_4O_7.5H_2O$	48.8
Kernite	$Na_2B_4O_7.4H_2O$	51.0
Ulexite	$NaCaB_5O_9.8H_2O$	43.0
Probertite	$NaCaB_5O_9.5H_2O$	49.6
Priceite (Pandermite)	$Ca_4B_{10}O_{19}.7H_2O$	49.8
Inyoite	$Ca_2B_6O_{11}.13H_2O$	37.6
Meyerhofferite	$Ca_2B_6O_{11}.7H_2O$	46.7
Colemanite	$Ca_2B_6O_{11}.5H_2O$	50.8
Hydroboracite	$CaMgB_6O_{11}.6H_2O$	50.5
lnderborite	$CaMgB_6O_{11}.11H_2O$	41.5
Kurnakovite	$Mg_2B_6O_{11}.15H_2O$	37.3
Inderite	$Mg_2B_6O_{11}.15H_2O$	37.3
Szaibelyite (Ascharite)	$Mg_2B_2O_5.H_2O$	41.4
Suanite	$Mg_2B_2O_5$	46.3
Kotoite	$Mg_3B_2O_6$	36.5
Pinnoite	$MgB_2O_4.3H_2O$	42.5
Boracite (Strassfurite)	$Mg_3B_7O_{13}Cl$	62.2
Datolite	$Ca_2B_2Si_2O_9.H_2O$	21.8
Cahnite	$Ca_2AsBO_6.2H_2O$	11.7
Danburite	$CaB_2Si_2O_8$	28.3
Howlite	$Ca_4Si_2B_{10}O_{23}5H_2O$	44.5
Vonsenite (Paigeite)	$(Fe,Mg)_2FeBO_5$	10.3
Ludwigite	$(Fe,Mg)_4Fe_2B_2O_7$	17.8
Tunellite	$SrB_6O_{10}.4H_2O$	52.9

3.1.3. Distribution of boron in nature

Principal stores and reservoirs of boron in the biosphere were reported as the continental and oceanic crusts, coal deposits, commercial borate deposits, biomass, ice, oceans, groundwater, surface water by Argust [81]. Boron in the environment relates entirely to major and minor environmental transformation. The mobility of boron in the environment is controlled by three chief cycles of atmosphere, terrestrial ecosystems and marine ecosystems. The cycle of boron is given in Fig. 3.1. The diverse inputs of boron to the atmosphere are attributed to the formation of sea salt aerosols, volcanic activities, coal combustion, biomass burning and industrial activities. Total of these sources accounted for 1.796 to 5.3 billion kg B/year [81]. The flow of boron transmitted to the atmosphere from the ocean is identified from 1.3×10^9 to 4.5×10^9 kg B/year by Argust [81], or 1.0×10^9 to 2.3×10^9 kg B/year by Park and Schlesinger [82]. It is noteworthy that boron in the form of gas, minerals and dust returns directly to the ocean or indirectly through passing through soil and drainage systems by wet deposition and dry deposition. Rainwater containing various boron concentrations is recorded in many regions [83, 84].

The average boron content in organic matters such as plants, aquatic life and animals estimates from 30 to 50 ppm [82]. There is a stable equilibrium of boron amount in the organic systems. Boron in the soil and water sources is absorbed by phytoplankton, plants and animals, and it will be returned to the atmosphere by biomass combustion (forest fires, biofuel burning, coal making, coal burning, and the combustion of agricultural residues), or majority is back into the soil and ocean as fossil fuel. The existing of boron in oil is substantially less popular than coal. Indeed, total global boron in oil constitutes 64,000 tonnes, but in coal reaches from 12.7 to 148.1 million tonnes [81].
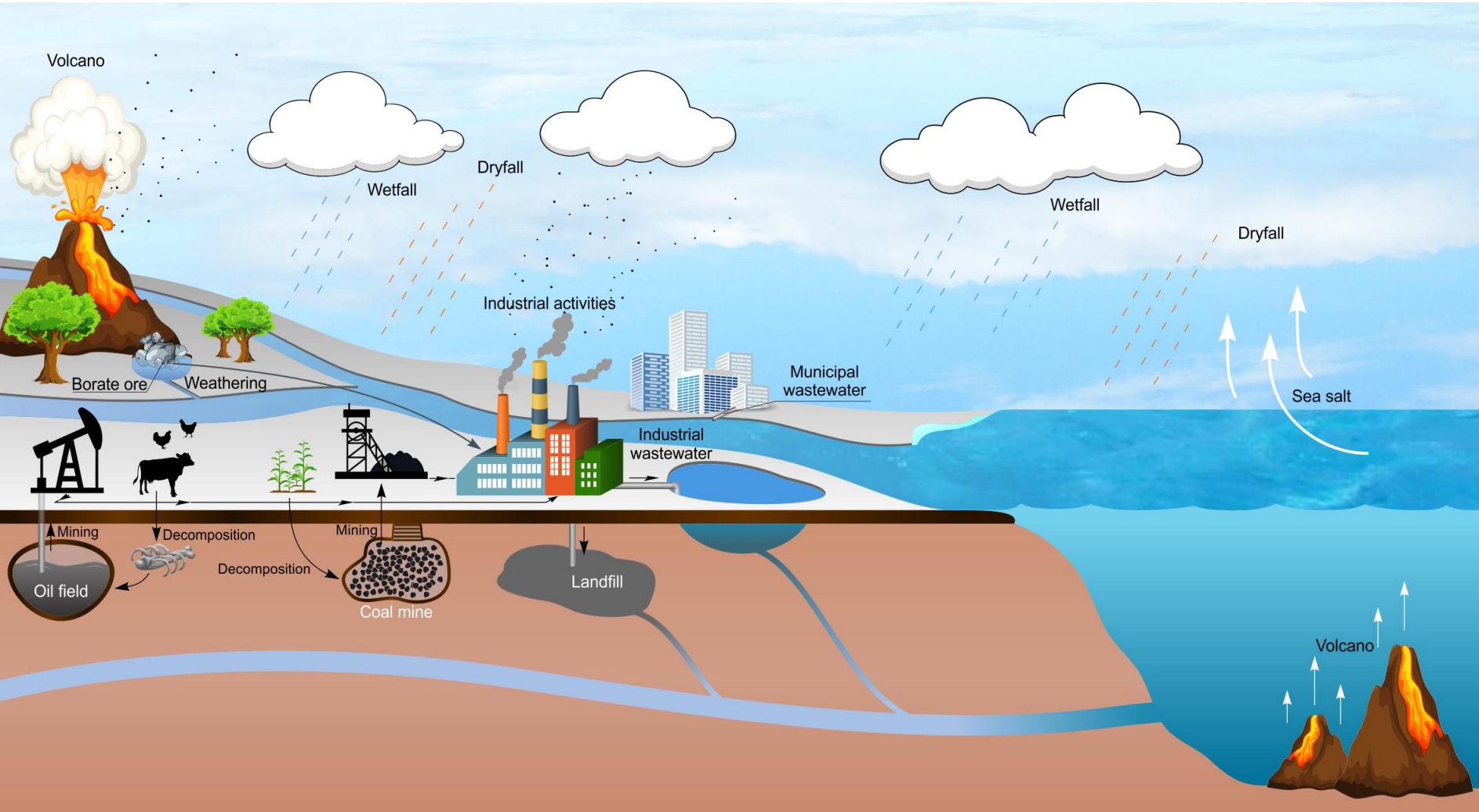
Fig. 3.1. The global boron cycle.

3.1.4. Chemical characteristics of boron in the environment

The dominant form of boron in natural aqueous systems is due to the dissociation of boric acid in water. Boric acid is a kind of solid which can easily dissolve in water with a solubility of 55 g/L at 25 °C, and it is regarded as a weak Lewis acid [85]. Dissociation of boric acid is obtained by accepting hydroxyl ion to generate tetrahydroxyborate ion through the hydrolysis process:

$$\left[\begin{array}{c} HO \\ \quad B-OH \\ HO \end{array}\right]^{0} + H_2O \rightleftharpoons \left[\begin{array}{c} OH \\ HO-B-OH \\ OH \end{array}\right]^{-1} + H^+ \qquad pK_a = 9.23$$
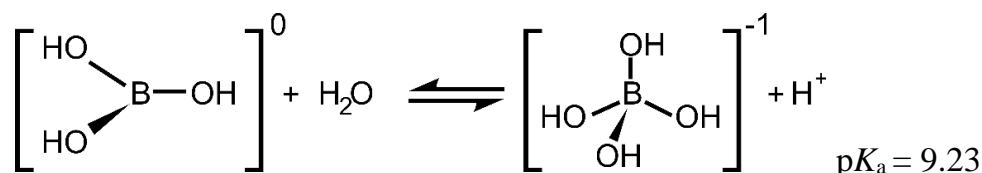
Fig. 3.2. The dissociation of boric acid.

The dissociation constant pK_a ($pK_a = -\log K_a$) of boric acid is found to be 9.23. This value is determined under the standard condition (i.e., at 20 °C, atmospheric pressure, and dilute solution). The actual pK_a depends on certain conditions such as pH, ionic strength, pressure, and temperature. It was found that the actual pK_a increased approximately 2 units when the pressure rose between 0 and 6 kbar (Fig. 3.3a). The relationship of pK_a of boric acid and temperature was reported that there was a drop (roughly 0.3 unit) of pK_a when the temperature increased between 283 and 323 K (Fig.3.3b) [74]. The actual pK_a of boric acid rose from 8.60 to 9.23 when the salinity dropped from 40,000 to 0 ppm (Fig. 3.4) [86].
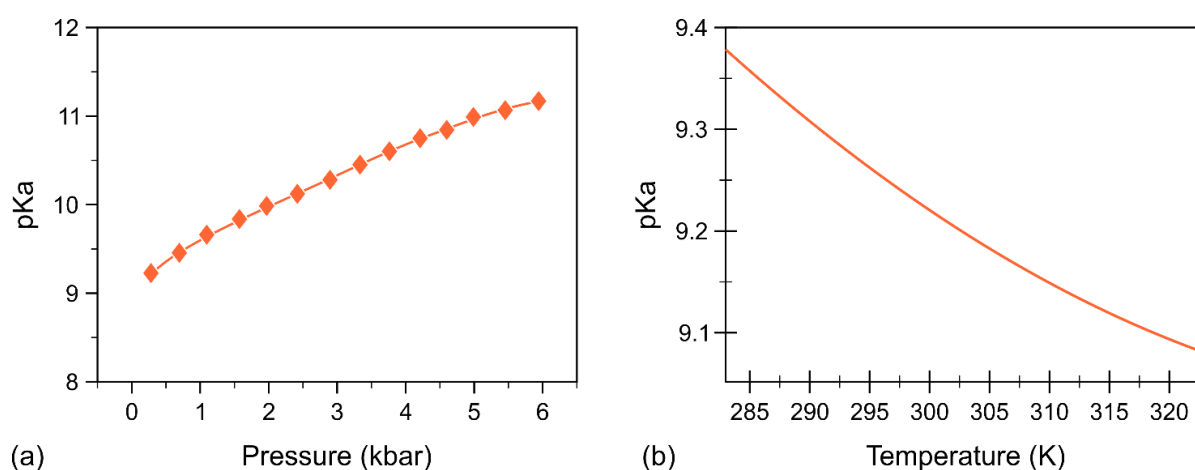
Fig. 3.3. The dissociation of boric acid as a function of temperature and pressure.

(Reproduced from [74])
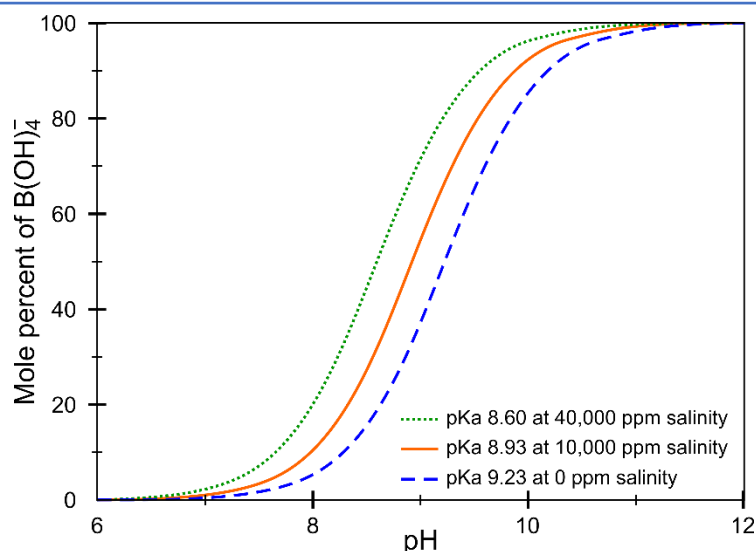
Fig. 3.4. The mole fraction of boric acid as a function of salinity.

(Reproduced from [86])

3.1.5. Distribution of boron species in aqueous solution

Boron is soluble in aqueous solution and variety of boron species are found in the form of boric acid or polyborate which depends on the concentration of boron and pH value. At low boron concentration (< 216 mg/L), soluble mononuclear boron species like $B(OH)_3$ and $[B(OH)_4]^-$ ion are successively formed. At higher concentration (> 290 mg/L) combination of pH between 6 and 11, dissolved polyborate species are chiefly found as polynuclear ions such as $B_3O_3(OH)_4^-$, $B_4O_5(OH)_4^-$ and $B_5O_6(OH)_4^-$ [87]. In aqueous solution, $B(OH)_3$ is capable of reacting with $[B(OH)_4]^-$ ion to form a diversity of polyborate species in accordance with following serial equations [88]:

$$B(OH)_3 + H_2O \rightleftharpoons [B(OH)_4]^- + H^+ \tag{3.1}$$

$$2B(OH)_3 + [B(OH)_4]^- \rightleftharpoons [B_3O_3(OH)_4]^- + 3H_2O \tag{3.2}$$

$$2B(OH)_3 + 2[B(OH)_4]^- \rightleftharpoons [B_4O_5(OH)_4]^{2-} + 5H_2O \tag{3.3}$$

$$4B(OH)_3 + [B(OH)_4]^- \rightleftharpoons [B_5O_6(OH)_4]^- + 6H_2O \tag{3.4}$$
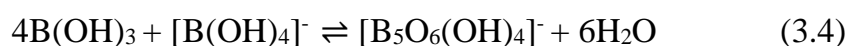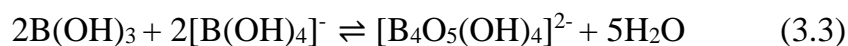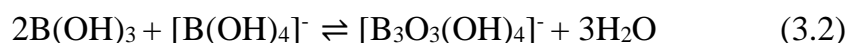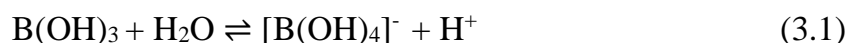
Summary of all the above equations:

$$9B(OH)_3 + 3[B(OH)_4]^- \rightleftharpoons [B_3O_3(OH)_4]^- + [B_4O_5(OH)_4]^{2-} + B_5O_6(OH)_4^- + 13H_2O + H^+ \tag{3.5}$$
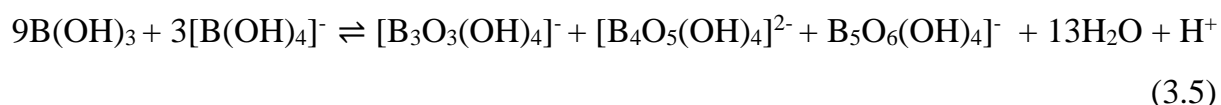
Boric acid + Monoborate (Tetrahydroxodoborate) $\rightleftharpoons$ Triborate + Tetraborate + Pentaborate + Water

The distribution of boron species in various pH and structural formulas of polyborate are illustrated in Fig. 3.5 and Fig. 3.6, respectively. It is obvious that $B(OH)_3$ is dominant at low pH (< 6), whereas various polyborate species preponderate in range of pH from 6 to 10. However, $[B(OH)_4]^-$ ion exists mainly at higher pH (> 10).
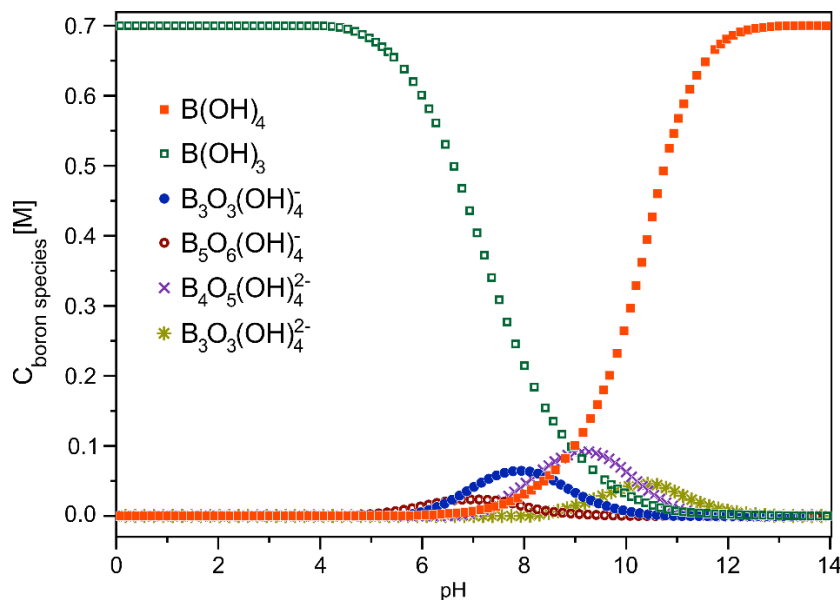
Fig. 3.5. Distribution of boron species in aqueous solution with total boron concentration $C_B = 0.7$ M, ionic strength $I = 0.1$ M in different range of pH. (Reproduced from [89])
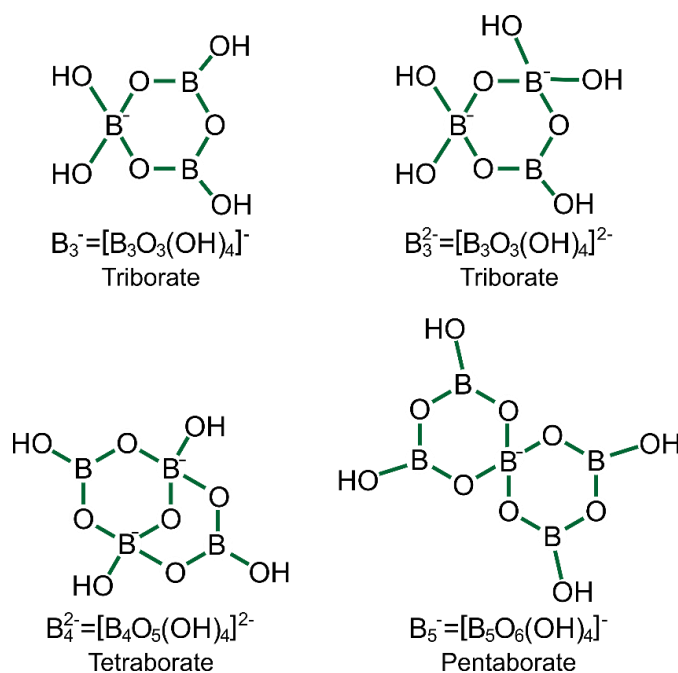
Fig. 3.6. Chemical structure of various polyborate species in aqueous solution [90].

3.1.6. Complexation of boron with compounds containing multiple hydroxyl groups

The formation of various borate complexes is attributed to the interaction of boric acid or borate ions with alcohols, polysaccharide and polyols, which containing multiple hydroxyl functional groups (-OH). Depending on the multiple hydroxyl groups orients suitable to fit structural parameters for tetrahedral boron coordination, strong stable borate complexes will be formed (Fig. 3.7). Thus, the stability of borate complexes significantly relies on the kind of polyols used. The formation of borate complexes relates to the dominant presence of boric acid or borate ion. The complexation process of boric acid or borate ion with polyols is shown in Fig. 3.8. The reaction constants of boric acid with a variety of diols and polyols are reported by previous research in Table 3.2.

After reacting with hydroxyl groups to form borate complexes, boric acid releases protons which raises the acidity of boric acid and borate solution. The derived acids are much stronger than boric acid itself for direct titration with alkali hydroxide solution [91]. It should be noted that it is crucial to neutralize these protons for avoiding ester hydrolysis due to the acidic environment.
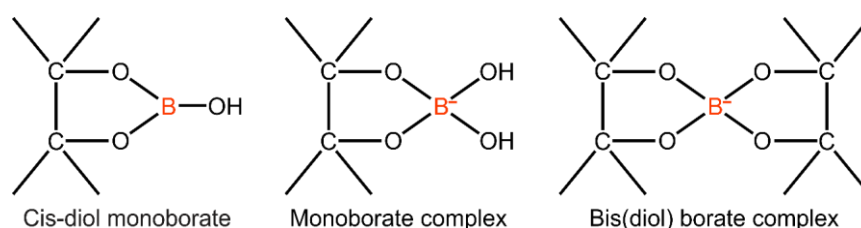
Fig. 3.7 Scheme of borate esters and borate complexes [92].
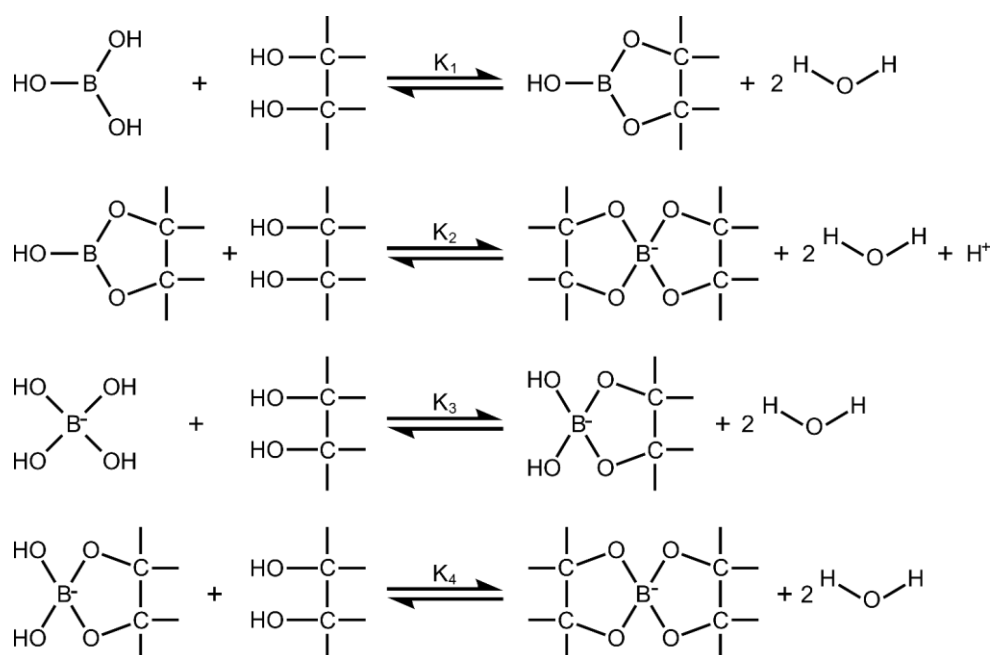
Fig. 3.8. Scheme of borate complexes formation. (Reproduced from [93])

Table 3.2 Equilibrium constants of the reaction of boric acid and different polyols [94].

Polyol	K_1	K_2
1,2-etanediol	2.15	1.15
1,3-propanediol	1.27	0.11
Glycerol	16.0	41.2
Catechol	7.8×10^3	1.42×10^4
D-mannitol	1.10×10^3	1.37×10^5
D-glucose	1.50×10^3	7.60×10^3
D-sorbitol		4.44×10^5
D-ribose		1.57×10^7

3.2. Applications and environmental problems of boron

3.2.1. Applications of boron and its compounds and the sources of boron pollution

Various of boron and its compounds are used in numerous commercial applications of glass, ceramic, abrasives, insulation, semiconductors, cleaning products, agriculture, chemical, cosmetics and pharmaceuticals [95]. Detail applications of boron and its compounds are shown in Table 3.3. Boron is naturally released into the environment by natural factors such as weathering of rocks, leaching of salt and volcanism. However, the most important sources are human activities such as the operation of borate mining, glass and ceramics manufacture, applications of agricultural chemicals and electricity generation using coal or oil, and these activities have caused soil, water and irrigation water contamination [87]. Although glass and ceramic amount to 80% of total borate consumption, these industries are not considered to the main sources of environmental pollution because boron is found immobile form in the manufacture of glass, ceramics and insulation [96]. In contrast, boron has high mobility and solubility in fertilizers, detergents, bleaching agents, antiseptic and wastes of coal combustion.

In the coal-fired power station, coal is the main fuel for electricity generation, and coal combustion residuals (CCRs), also referred to the coal ash including fly ash, bottom ash, boiler slag, flue gas desulfurization material (FGD), and scrubber residues are generated from the combustion of coal, cleaning of gases stack or emission purification

system [97] (Fig. 3.9). CCRs are regarded as one of the largest industrial waste generated in the United States, which made up roughly 130 million tons in 2014 [98]. CCRs are recycled into products like concrete or wallboard; however, they are mainly stored in surface impoundment and landfills. It was reported that approximately 47% of CCR generated was reused, and 53% of the remaining was deposited in the lagoon and landfills in the U.S in 2014 [98]. During the time in the landfills and surface impoundment, many toxic elements are easily leached to the natural water system [99]. Boron has been suggested as a trace element that exceeding the drinking water standard of United States Environmental Protection Agency (USEPA) are the causes related to contaminated groundwater and surface water [100]. Previous studies have found that boron rapidly released from fly ash in aqueous solution because a large fraction of boron in fly ash is in the soluble form [101, 102]. Boron is highly mobile in water and not impacted by redox process even in the conditions with different pH and leaching kinetics [99, 103].
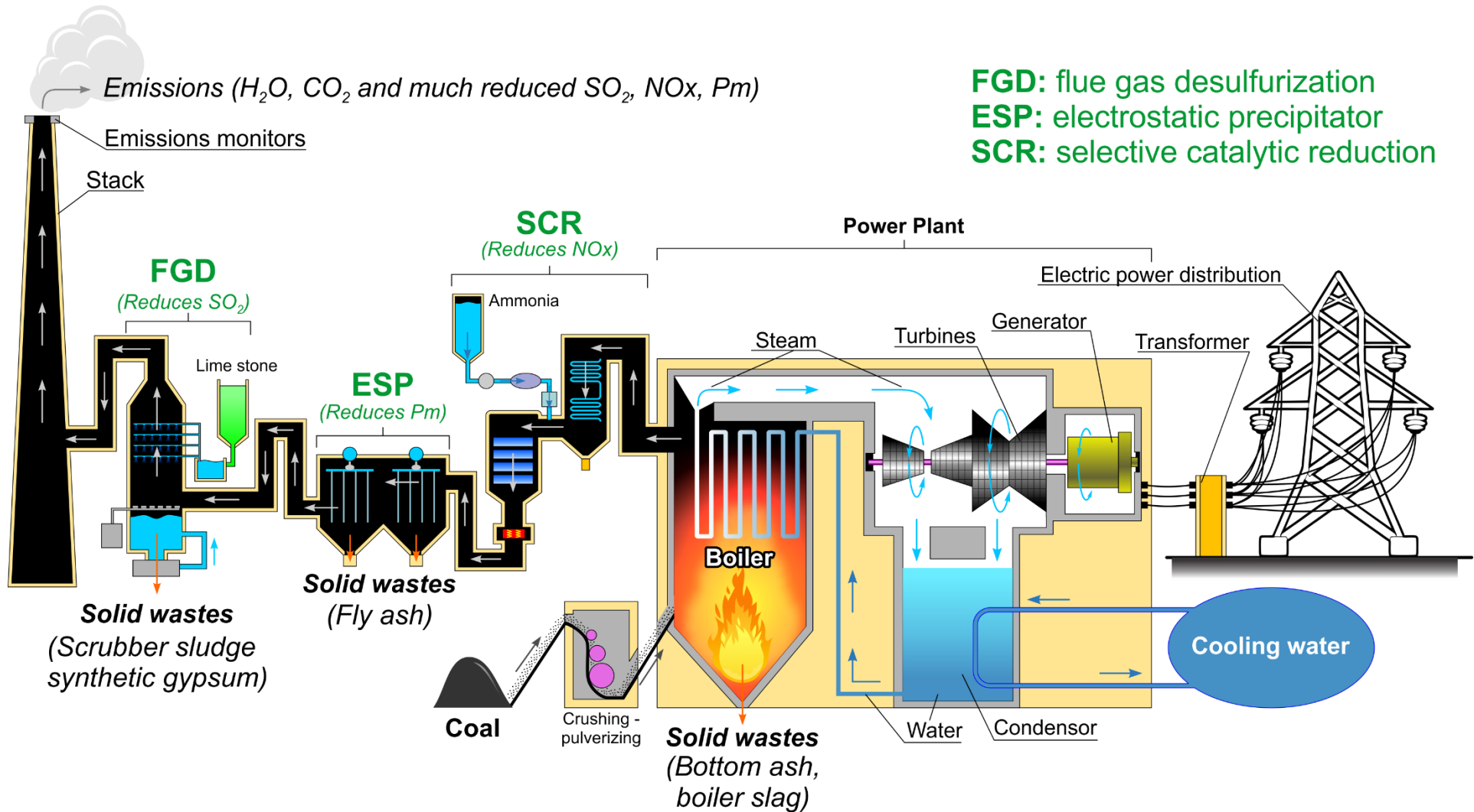
Fig. 3.9. Emission purification system in the coal-fired power station. Different stations use different technologies.

(Reproduced from [104])

Table 3.3 Applications of boron and its compounds [105].

Fields of use	Products
Manufacture of glass	Insulation fiberglass Fiberglass reinforcement Borosilicate glass Textile fiberglass
Agriculture	Fertilizers Insecticides Biocides
Ceramic frits, enamels, glazes	Ceramic glazes – tiles Tableware Sanitaryware Porcelain floor tile Stoneware
Chemical manufacturing	Boron derivatives - Refine boron products (boric acid, boron oxide, borax pentahydrate, borax decahydrate, anhydrous borax, dısodıum octaborate tetrahydrate) - Concentrated boron ores (ulexite, colemanite)
Metallurgy	Steel production Soldering Powder metallurgy Amorphous metals (metallic glasses) and alloys Magnets
Adhesives and coatings	Peptizing agent
	Gelling agent
Oil and gas chemicals	Additives
Detergents	Cleaning agent

Fields of use	Products
	Bleaching agent
Cosmetics	Soap
	Skin lotions
	Hair shampoos
	Cosmetic creams
	Bath salts
Pharmaceuticals	Denture cleaners
	Eye drops
	Cancer-fighting treatments
Flame retardants	Dry powder fire extinguishers
	Fire retardant emulsion paints
	Fire resistance in paper and cellulose insulation
	Wood preservative
	Charcoal briquettes
Abrasives	Saw blades
	Abrasive wheels
	Water jet cutting
	Corrosion inhibitors
Fuel Cells	Hydrogen source
Metal plating	pH adjustment
Nuclear reactions	Neutron screening
	Control nuclear reactions
Photography	Buffering agent to control pH
Construction industry	Gypsum

3.2.2. Effect of boron on plants

Boron is an essential micronutrient for the growth and development of fruits and vegetables. The deficiency of this element involves the decrease in crop productivity and quality of products. It was suggested that boron plays a vital role in cell wall synthesis, maintenance of plasma membrane integrity and its function, metabolism of nucleic acid and protein synthesis, metabolism and transport of carbohydrate, metabolism of nitrogen, synthesis and metabolism of phenolic compounds, the formation of pollen tube, photosynthesis and enzymes interaction [106, 107]. The primary function of boron is to complex with many components of cell wall such as pectin, hemicellulose and lignin. Besides, boron relates to the stability of cell wall matrix by cis-diol groups and cell enlargement exhibited in the growth of leaf, elongation of the root and development of fruit and flower [108].

However, when boron amount is higher than the demand for crops, boron toxicity can decline both crop yields and quality. Numerous data about the adverse effects of boron toxicity on plants have been reported. Biochemical and physiological impacts of boron excess relate to the inhibition of shoot and root system growth, the damage of the photosynthesis process, the promotion of oxidative stress, the reduction of nitrogen metabolism and the carbohydrate metabolism, leading to the limitation of plant growth, decrease in quantity and quality of fruits [109]. The typically visible symptoms of boron toxicity are the leaf diseases (yellow, spot, dryness of leaves), the decay of unripe fruits and even the death of plants in the high level of boron [110, 111]. The boron tolerance level of various agricultural crops was classified in Table 3.4. There is a small range of deficiency and excess of boron which is a beneficial or toxic element for different plants. Excessive presence of boron in soil and irrigation water is more difficult to control than boron deficiency which is solved by providing fertilizer supplements [112].

Flower
· Formation of pollen tube

Damage of shoot development

Leaves
· Photosynthesis

Damage of seed setting

Fruit
· Seed setting
· Fruit quality

Damage of fruit development
· Fruit formation
· Decay of unripe fruits

Stem
· Cell wall synthesis
· Plasma membrane
· Carbohydrate metabolism & transport

Damage of photosynthesis process
· Yellow, spot and dryness

Root
· Formation of root hair
· Nitrogen metabolism

Damage of root development

Fig. 3.10. Functions of boron and its excess in plants.

Table 3.4 Relative boron tolerance of agricultural crops [113].

Boron tolerance (mg/L)	Agricultural crops
Very sensitive (< 0.5 mg/L)	Lemon, blackberry
Sensitive (0.5 – 0.75 mg/L)	Avocado, grapefruit, orange, apricot, peach, cherry, plum, persimmon, fig (kadota), grape, walnut, pecan, cowpea, onion
Sensitive (0.75 – 1.0 mg/L)	Garlic, sweet potato, wheat, barley, sunflower, bean (mung), sesame, lupine, strawberry, artichoke (jerusalem), bean (kidney), bean (lima), groundnut (peanut)
Moderately sensitive (1.0 – 2.0 mg/L)	Pepper (red), pea, carrot, radish, potato, cucumber
Moderately tolerant (2.0 – 4.0 mg/L)	Lettuce, cabbage, celery, turnip, bluegrass (Kentucky), oats, maize, artichoke, tobacco, mustard, clover (sweet), squash, muskmelon
Tolerant (4.0 – 6.0 mg/L)	Sorghum, tomato, alfalfa, vetch (purple), parsley, beet (red), sugarbeet
Very Tolerant (6.0 – 15.0 mg/L)	Cotton, asparagus

3.2.3. Effect of boron on human health

Previous studies in animal and human have reported that boron is a bioactive element in the safe intake that impacts positively on central nervous system functions, growth and maintenance of bone, prevention of arthritis, metabolism of mineral and hormone, cell membrane functions, enzyme reactions and has protective characteristics against some kind of cancers [114, 115]. It was noted that deficiency of boron decreased absorption of calcium, magnesium and phosphorus [114]. Based on the U.S. Institute of Medicine, Food and Nutrition Board, the tolerable upper intake level of boron was established at 20 mg/day for adults [116]. The European Union set an upper intake level for total boron intake based on body weight that equals about 10 mg/day for adults [117]. The World Health Organization (WHO) suggested this value by 0.4 mg/kg body weight per day [118].

Boron can become poisonous with the overdose and long-term consumption of water and food enriching boron amount. While clinical symptoms of acute boron toxicity in human comprise nausea, vomiting, diarrhoea, headache, skin rashes and desquamation, chronic toxicity involves in cardiovascular, nervous and reproductive systems (Fig. 3.11) [119-121].
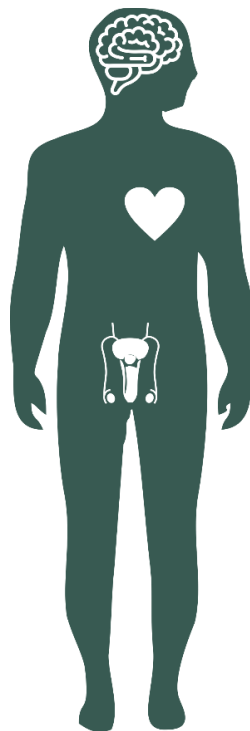
Fig. 3.11. The negative effect of boron on human health.

3.2.4. Standard of boron in drinking water and wastewater

The wide utilization of boron compounds in industrial activities results in an abundance of boron in water sources. Since a series of environmental and health problems have been recorded by boron, the standard of this element was established in drinking water, irrigation water and wastewater. The recommended boron concentration of the World Health Organization (WHO) in drinking water was set at 0.3 ppm in 1993 but there were no technologies could achieve this boron level. Therefore, WHO guideline increased the boron level to 0.5 ppm in 1998, then revised to 2.4 ppm in 2011 [122]. Indeed, the value of 2.4 ppm was set due to the data from the USA and UK on boron dietary intakes, which is acceptable with a required concentration of human body but exceeds the tolerance of crops which are susceptible to boron. For these reasons, many countries still apply for their own standard. There are no federal rules of boron content in the US, where boron regulations depend on the states varying between 0.6 and 1.0 ppm. The maximum boron concentration in the European Union, UK, Singapore, South Korea and Japan is 1.0 ppm. New Zealand and Israel establish boron concentration at 1.4 and 1.5 ppm, respectively. Saudi Arabia is the country obeying the WHO guideline. The recommended boron content in Brazil, Canada and Australia is far higher than WHO guideline, which makes up 5 ppm, 5 ppm, 4 ppm, respectively [123].

In Japan, the tolerable limits of boron and its compounds are limited less than 230 ppm and 10 ppm when the effluent wastewater is discharged by plants, factories or businesses to sea area and other than sea area, respectively [57].

3.3. Removal and regeneration of boron from aqueous solution using various boron-selective adsorbents

3.3.1. Mechanism of boron removal by boron-selective adsorbents

Numerous separation technologies have applied for the removal and recovery of dissolved boron. They can be classified into three main groups i, separation by sorption on solids (adsorption method), ii, separation by membrane filtration (membrane method), iii, separation by a combination of sorption on solids and membrane filtration (hybrid method) [85]. Among these methods, adsorption technique using chelating resins seems to be one of the most effective method for boron removal because of the high efficiency, simple operation, minimal contact time, and capability of water and wastewater treatment with large volume [124]. Chelating resins are the most paramount and effective sorbents for boron removal, and their constituents are made up two chief parts of macroporous polymer support and functional group. The functional group possess at least three functional hydroxyl groups as their ligands. These hydroxyl structure located in cis position of resin, called "*vis*-diols", which can form very stable complexes with boron then immobilized on the resin. This group is not reactive to other elements, leading to the high selectivity of boron [125]. *N*-methyl-D-glucamine (NMDG) is the most popular group among various kinds of functional groups. It is a polyol with five hydroxyl groups and a tertiary amine ends, providing more complexation site boron. Most commercial resins have macroporous polystyrene matrix crosslinked with divinylbenzene and graft to NMDG functional group [126]. The available resins in the market from different manufacturers are shown in Table 3.5.

The mechanism of generation and regeneration of borate complexes is given in Fig. 3.12. In the complexation reaction, tertiary amine plays a crucial role in the neutralization of proton released from the process of borate complex formation. The borate in the complex can be released by hydrolyse process with the addition of an acid. Finally, the resins are regenerated to the original form by the neutralising with a base such as sodium hydroxide (NaOH) [124].
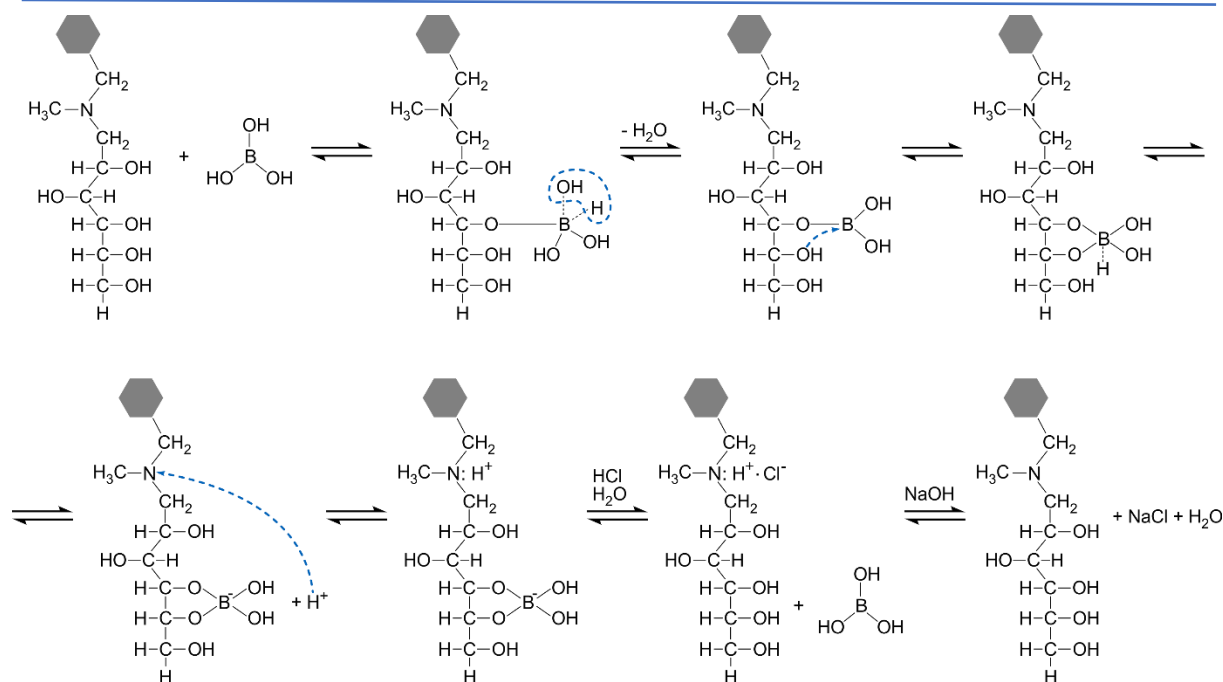
Fig. 3.12. Mechanism of generation and regeneration of borate complexes.

The commercial resins have the challenges of the slow sorption kinetics and the high cost of resins and regeneration, all of which decrease the flexibility and unsatisfactory performance of boron removal [127]. The hydrophobicity of skeleton structure results in the limited surface area which causes the slow kinetics of boron uptake. In fact, the hydrophobic backbone structure declines the process of mass transfer. This is attributed to the decrease in the capacity of boron removal in aqueous media. Moreover, the increase in boron adsorption ability can be conducted by increasing the rate of the functional group [128]. Thus, the characteristics of polymer supports and functional groups have been modified and optimized, and a large number of alternative boron-selective resins have been developed to improve the feasibility of boron removal from aqueous solution for meeting the stringent wastewater discharge standard. The approaches to the development of new boron-selective resins is to focus on the (1) modification of polymer backbone by other synthetic and natural polymers, (2) utilization of alternative multi-vicinal diol ligand, (3) synthesis of hybrid polymers from the integration between organic and inorganic components, and (4) incorporation of above approaches. The abundant alternative boron-selective resins/adsorbents can be classified into four chief groups such as fiber-based adsorbents, synthetic polymer-based adsorbents, natural polymer-based adsorbents, and hybrid organic-inorganic adsorbents. Summary of capacity of boron removal by some new and commercial boron selective resins is shown in Table 3.6.

Table 3.5 List of commonly commercial boron-selective resins.
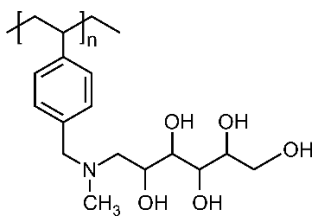
Commercial resins	Type of resin	Matrix structure	Manufacturers	References
Diaion CRB03 & Diaion CRB05	Chelating		Mitsubishi Chemical Co., Ltd, Japan	[129]
Purolite D 4123	Chelating		Purolite International Ltd., UK	[130]
Dowex XUS 43594.00	Weak base anion exchange		Dow Chem., Germany	[131, 132]
Dowex 2x8	Strong base anion exchange		Dow Chem., Germany	[133]
Amberlite IRA 743	Strong base anion exchange		Rohm & Haas Co., Netherlands	[134]

Table 3.6. Boron adsorption capacity of some new and commercial boron-selective resins [124].

Adsorbent	Type	Polymer support	Functional group	Particle/screen size (µm)	Capacity (mg/g)	Experimental condition	Sorption isotherm	Sorption kinetics
Amberlite IRA-743	Commercial	Styrene-Divinylbenzene	*N*-methylglucamine	297-840	7.46	$[B_0]$: 40 mg/L Dosage: 1 g/100 mL pH: 9.5, *T*: 30 ºC	Langmuir	Theoretical model
Dowex XUS 43594.00	Commercial	Styrene-Divinylbenzene	*N*-methylglucamine	250-1000	3.35	pH: 8.4 *T*: 25 ºC	Langmuir	Pseudo second order
Dowex 2x8	Commercial	Styrene-Divinylbenzene	Benzyl-dimethylethanolamine	74-149	36.76	pH: 9 *T*: 25 ºC	Langmuir	Thomas model
Purolite S 108	Commercial	Polystyrence	Complex amino	297-1000	6.27	Dosage: 1 g/500 mL pH: 9.0-9.2 *T*: 30 ºC	Langmuir	Pseudo second order
Diaion CRB 02	Commercial	Polystyrence	*N*-methylglucamine	118-300	7.46	Dosage: 1 g/50 mL pH: 9.0-9.2 *T*: 30 ºC	Langmuir	Pseudo second order
D564	Commercial	Polystyrence	Methylglucamine	250-830	16.43	Dosage: 1 g/50 mL pH: 9 *T*: 25 ºC	-	Pseudo second order
Hybrid Gel	New	Gel precursor ((3-glycidoxypropyl) trimethoxysilane + Tetraethyl orthosilicate)	Methylglucamine	250-830	12.43	Dosage: 1 g/50 mL pH: 9 *T*: 25 ºC	-	Pseudo second order
Glycidyl methacrylate-modified polymer	New	Poly (Glycidyl methacrylate-co-trimethylolpropane trimethacrylate)	*N*-methylglucamine	315-800	12.43	$[B_0]$: 250 mg/L Dosage: 1 g/100 mL pH: 7.5 *T*: 30 ºC	Langmuir	
Glycidyl methacrylate-modified polymer	New	Glycidyl methacrylate-methyl methacrylate-Divinylbenzene	Iminodipropylene glycol	210-420	12.97	$[B_0]$: 40 mg/L pH: 6-6.5	-	Pseudo second order
Glycidyl methacrylate-modified polymer	New	Glycidyl methacrylate-methyl methacrylate-Divinylbenzene	*N*-methylglucamine	110-120	23.24	$[B_0]$: 23 mg/L Dosage: 1 g/30 mL	-	
Chitosan	New	Cross-linked chitosan	*N*-methyl- D-glucamine	100-300	22.70	$[B_0]$: 100 mg/L Dosage: 1 g/100 mL pH: 6.5	Langmuir	Pseudo second order

3.3.2. Classification of boron-selective adsorbents

1. Fiber-based adsorbents

In order to improve characteristics of mass transfer, the chelating resin in the various fiber forms such as fibers and non-woven fabrics have been investigated for more effective boron removal by using radiation-induced graft polymerization technique for modification of polymeric material before chemical treatment with NMDG functional group. Fig. 3.13 shows a schematic representation of boron-selective adsorbent preparation by radiation-induced graft polymerization and immobilization of NMDG functional group.
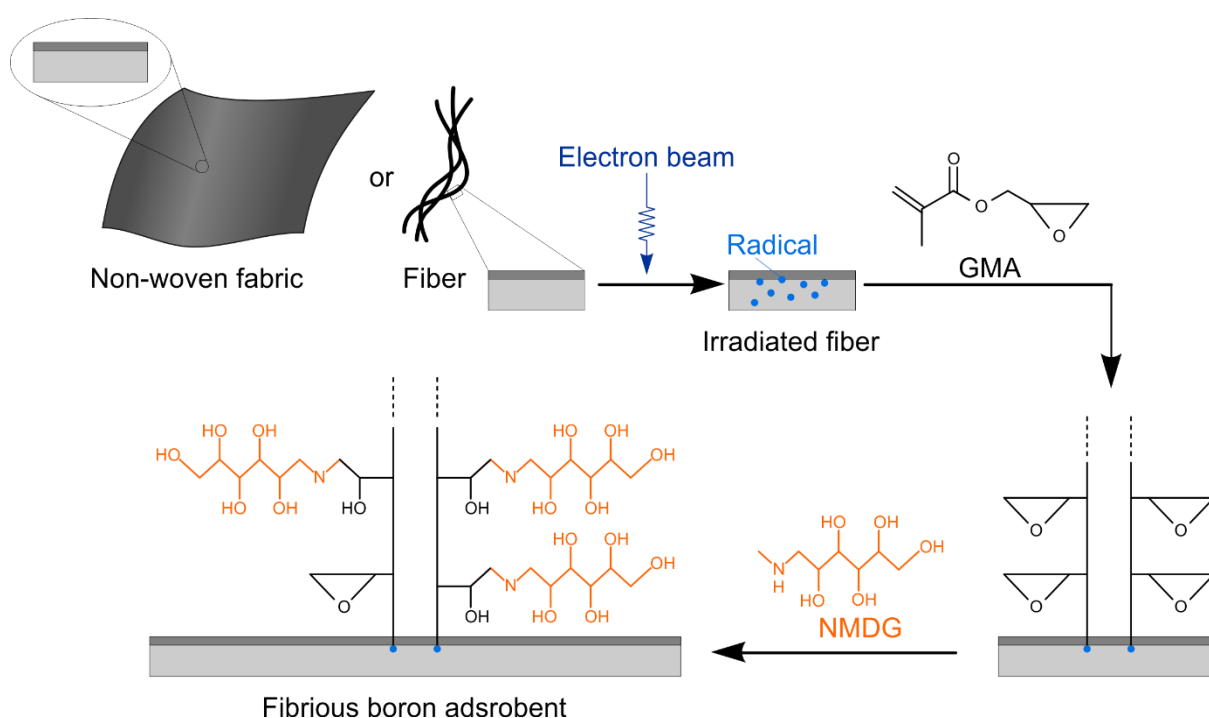
Fig. 3.13. Scheme of boron-selective adsorbent preparation using radiation-induced grafting GMA onto non-woven fabrics or fibres and immobilization of NMDG to the adsorbent. (Reproduced from [135])

Ikeda et al. [135] attached an epoxy-group-containing monomer, glycidyl methacrylate (GMA) to a 6-nylon fiber by using electron-beam-induced graft polymerization. Then NMDG was added to the epoxy group of the grafted polymer chain. As the result, the density of NMDG immobilized in nylon fiber amounted to 2.0 mmol/g, which was 74% of that found in the commercial resin (Diaion CRB05). The maximum boron adsorption capacity of nylon-based chelating fibers was 12 mg/g (fiber diameter of 55 μm, $[B_0] = 150$ ppm, space velocity 20 h^{-1}, 0.38 g adsorbent/mL bed) in

the continuous flow system. The dynamic binding capacity of the chelating fiber-packed bed was 2.5-fold higher than Diaion CRB05 bead-packed bed.

Another kind of boron-selective fibrous adsorbent was studied by grafting GMA onto a non-woven PE fiber using radiation-induced grafting technique. After that, the NMDG functional group was immobilized in the grafted PE fiber. In the range of pH from 3 to 8, more than 90% of boron was adsorbed to obtained adsorbent containing 2.4 mmol/g of NMDG density ($[B_0]$ = 10 ppm, approximately 0.1 g of adsorbent in the square of 1.5 cm x 1.5 cm/50 mL at 25 °C for 1 h). In the test of the comparison conducted in the column mode ($[B_0]$ = 10 ppm, pH 7, space velocity 50 h^{-1}), graft adsorbent had 4 times higher the bed volume at breakthrough point, and 10 times faster boron adsorption capacity than commercial resin (NMDG density 2.2 mmol/g, particle size of 0.8 mm) [136].

A new boron adsorbent was prepared by radiation-induced grafting of GMA onto PE coated PP (PE-PP) non-woven fabric in deoxygenated emulsion solution or solvent of butanol to decrease the cost of radiation grafted adsorbents followed by the functionalization of NMDG. The study found that the emulsion-mediated grafting was effective and economical for the preparation of grafted fibers. In both mediated grafting systems including emulsion and solvent (180% degree of grafting), the density of NMDG introduced in adsorbent made up 2.2 mmol/g adsorbent, the thermal stability remained stable at approximately 260 °C, and the average fiber diameter of 27 μm was smaller than the commercial granular resin (Diaion CRB03) with the diameter of 450 μm. Boron adsorption isotherm and kinetics were carried out in a batch mode ($[B_0]$ = 20 - 200 ppm, pH 6.5, the dosage of 0.5 g adsobent/150 mL solution, stirring speed of 200 rpm at 30 °C). The result showed that the boron adsorption capacity stood at 18.8 mg/L. Besides, the adsorption kinetics was fast, which the adsorption equilibrium of boron onto fibrous adsorbent reached after 30 min compared to 60 min for the commercial resin [137].

2. Synthetic polymer-based adsorbents

Synthetic polymer-based adsorbents are synthesized by using polymerization or copolymerization process to generate precursor, which are subsequently functionalized with the *vis*-diol ligand containing functional hydroxyl group of NMDG or alternative multi-vicinal diol.

A new resin based on the terpolymer of glycidyl methacrylate (GMA), methyl methacrylate (MMA) and divinyl benzene (DVB) in spherical beads were chemically functionalized with NMDG [138]. The resin (105-210 μm) showed the high boron uptake capacity of 23.24 mg/g ($[B_0] = 2660$ ppm, the dosage of 1 g resin/30 mL solution, shaking condition for 6 h), and the exceptional stability without any activity loss. After 20 times of recycling, boron uptake capacity still stayed at the same level of 23.14 mg/g.

Another GMA-MMA-DVB terpolymer as the support functionalized with iminodipropylene glycol functions instead of NMDG was prepared by B. F. Senkal et. al [139]. The resulting beads exhibited the high boron loading capacity of 32.42 mg/g ($[B_0] = 5838$ ppm, pH = 6-6.5, the dosage of 1 g resin/50 mL solution, shaking condition at room temperature for 24 h), fast adsorption kinetics, reasonable regeneration and appreciable selectivity. The synthesis process of GMA-MMA-DVB-NMDG resin and GMA-MMA-DVB- iminodipropylene glycol is given in Fig. 3.14.
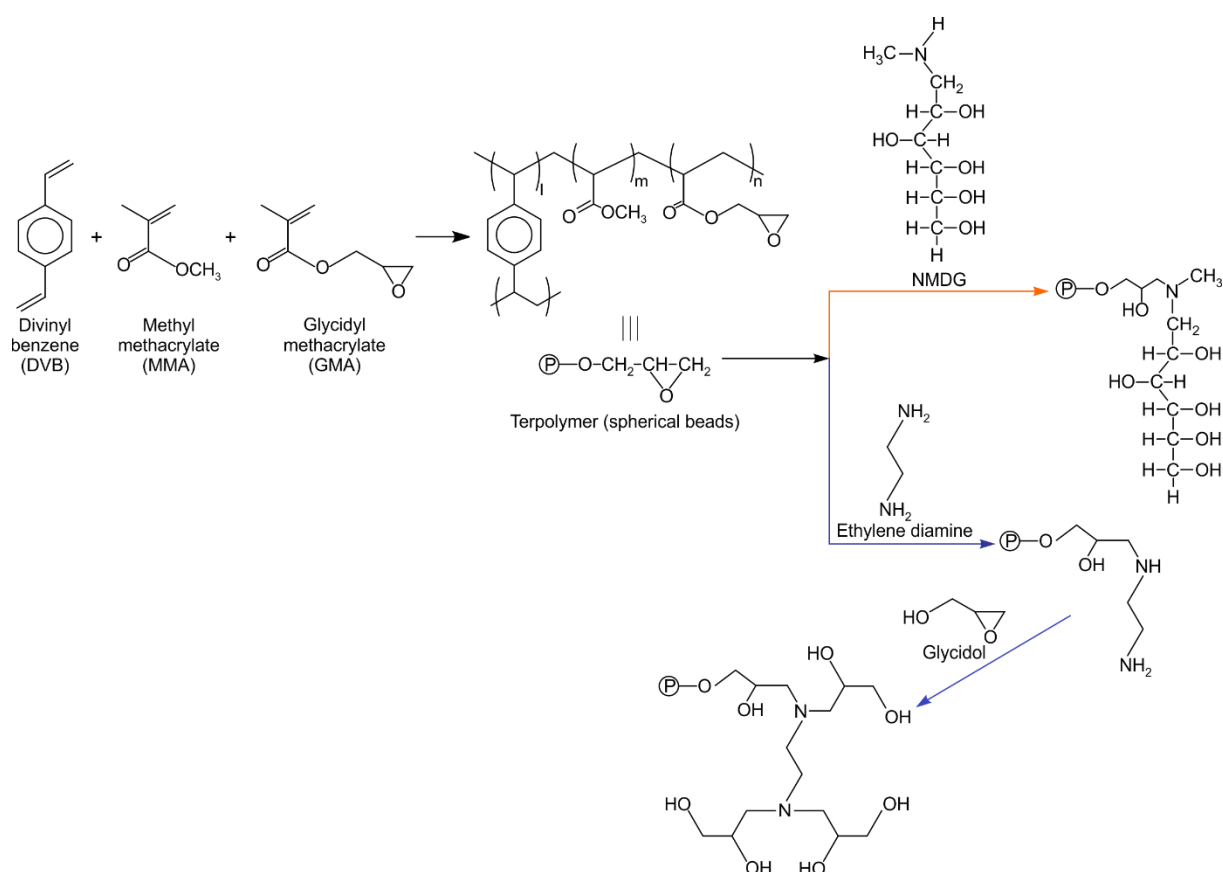
Fig. 3.14. Synthesis of boron-selective resin by polymerization of GMA, MMA, and DVB in spherical beads modified with NMDG and iminodipropylene glycol. (Reproduced from [138, 139])

A novel cross-linked branched polyethylenimine (PEI) beads functionalized with glucono1,5-D-lactone was synthesized with the high density as boron-chelating group (Fig. 3.15) [140]. The spherical resin had boron sorption capacity of 20.87 mg/g and high regeneration efficiency by using 1.0 M HCl solution followed by neutralization with 0.1 M NaOH solution.
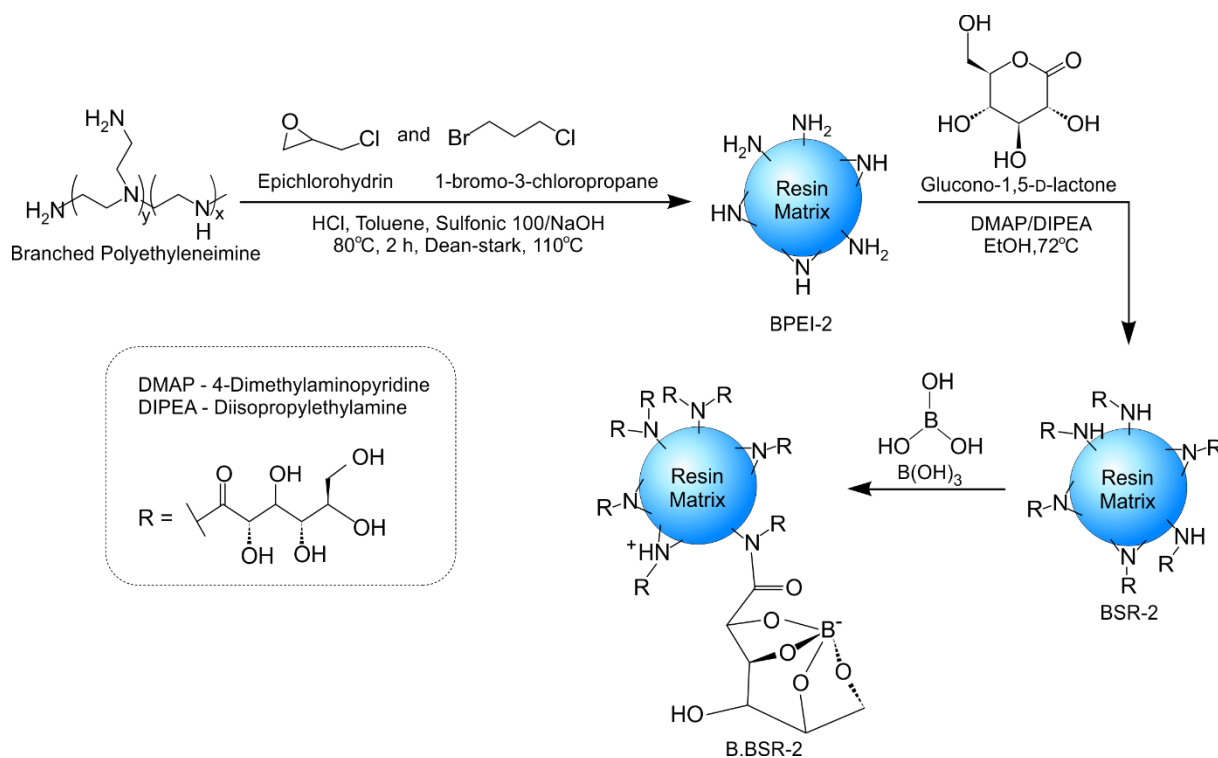
Fig. 3.15. Preparation of PEI resins with boron-chelating groups and mechanism of boron coordination with boron-selective resin. (Reproduced from [140])

A novel Fe_3O_4 nanoparticle core-mesoporous silica shell functionalized with glycidol reagent was synthesized by M. S. Moorthy et al. [141]. Fig. 3.16 shows the synthesis of boron-selective adsorbent. The hybrid nanoparticle showed the high selective-boron adsorption event in the existence of metal ions (Ni^{2+}, Cu^{2+}, Cr^{2+} and Fe^{2+}) and sulphates and chlorides of Na^+, K^+, Ca^{2+} and Mg^{2+}. Boron adsorption equilibrium could be reached within 15-20 min (0.025g/10 mL), and the boron loading capacity was determined at 25.62 mg/g ($[B_0]$ = 100 ppm, pH = 7, 1 g adsorbent/10 mL solution). The magnetic nanoparticles could be easily separated from aqueous solution by an external magnetic field. The adsorbent could be regenerated up to 7 cycles without significant decrease in boron loading capacity and loss of adsorbent.
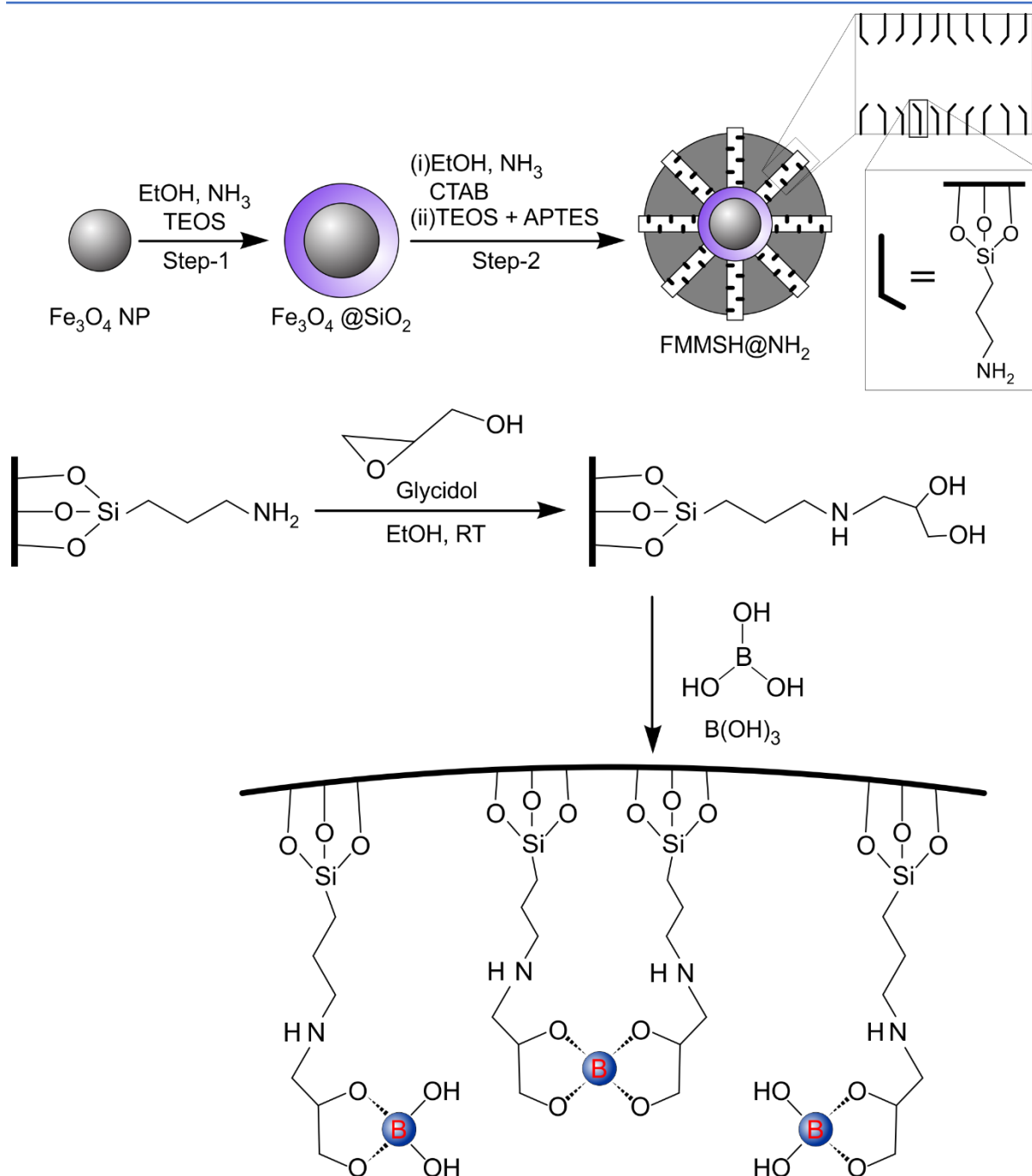
Fig. 3.16. Scheme of hybrid nanoparticle functionalized with glycidol and possible bidentate and/or bis-bidentatate complexation of boron with *cis*-diol group.

(Reproduced from [141])

3. Natural polymer-based adsorbents

Several natural polymers such as chitosan, cellulose and alginates containing abundant amino and hydroxyl groups have been investigated as alternative substrates which are modified and functionalized with boron-chelating groups by NMDG group or hydroxyl group in polysaccharide.

The novel type of crosslinked chitosan resin with NMDG functional group was prepared for boron removal. NMDG was chemically fixed to the base polymer (ethylene glycol diglycidyl ether (EGDE) crosslinked chitosan) through the support of chloromethyl oxirane (Fig. 3.17). The chitosan derivative-NMDG resin exhibited the higher boron sorption capacity and faster sorption kinetics than commercial resins and resins containing synthetic polymer as base material. The boron sorption capacity was 22.7 mg/g, and 100 mg/L of boron passed through column within 10 min ($[B_0] = 100$ ppm, pH 6.5, the dosage of 1 g adsobent/100 mL solution, particle size of 100-300 μm). The resin was also effective for boron removal in water samples (tap water, river, estuarine and groundwater) [127].
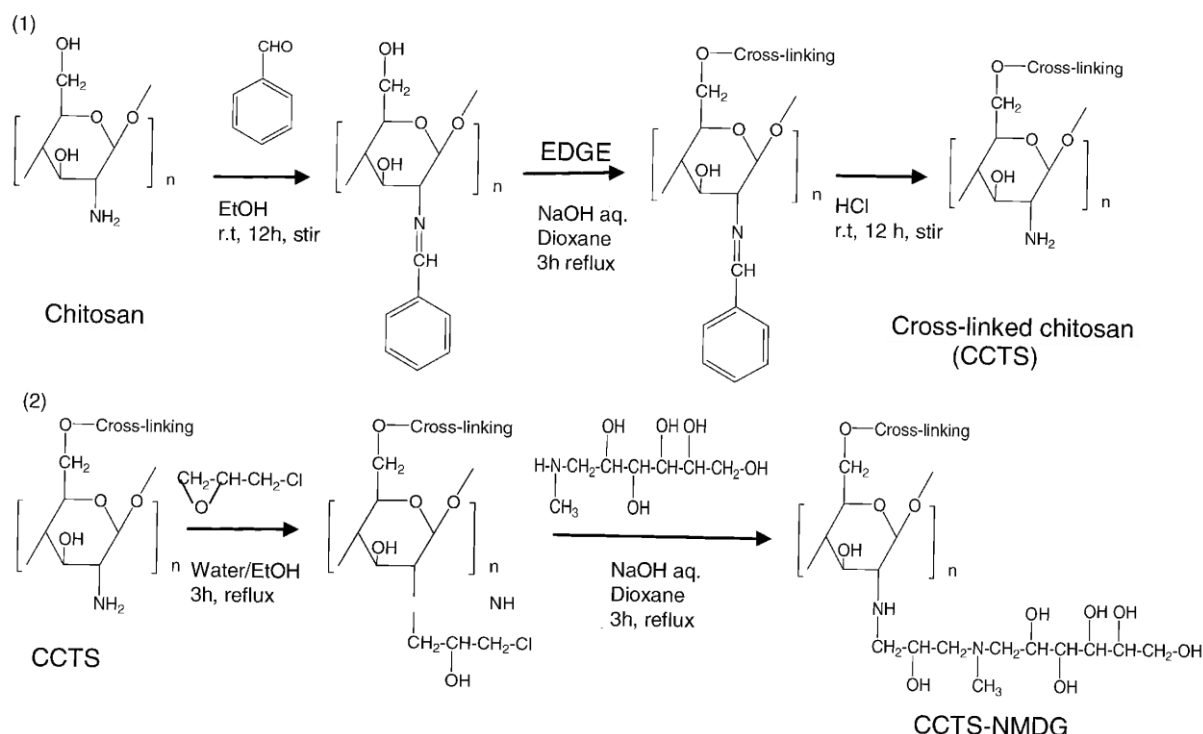
Fig. 3.17. The synthesis scheme of crosslinked chitosan-NMDG [127].

Another new adsorbent based on immobilization of NMDG group to cellulose derivatives was studied by Inukai et al. [142]. In the first step, GMA was introduced to cellulose fiber and cellulose powder by graft polymerization, and cellulose grafted with GMA chains regarded as a polymer support. Subsequently, NMDG functional group was chemically bound in the epoxy group of grafted cellulose products (Fig. 3.18). The maximum value of boron adsorption capacity of powder cellulose reached 11.9 mg/g ($[B_0] = 108$ ppm, the dosage of 0.05 g adsorbent/25 mL solution, shaking condition at 25 ºC for 24 h) which had the similar level in saccharide-chitosan resins and commercial

polystyrene resin. The boron adsorption equilibrium of cellulose derivatives (1 h) was faster than polystyrene resin (5 h) in the range of pH from 8.1 to 8.5.
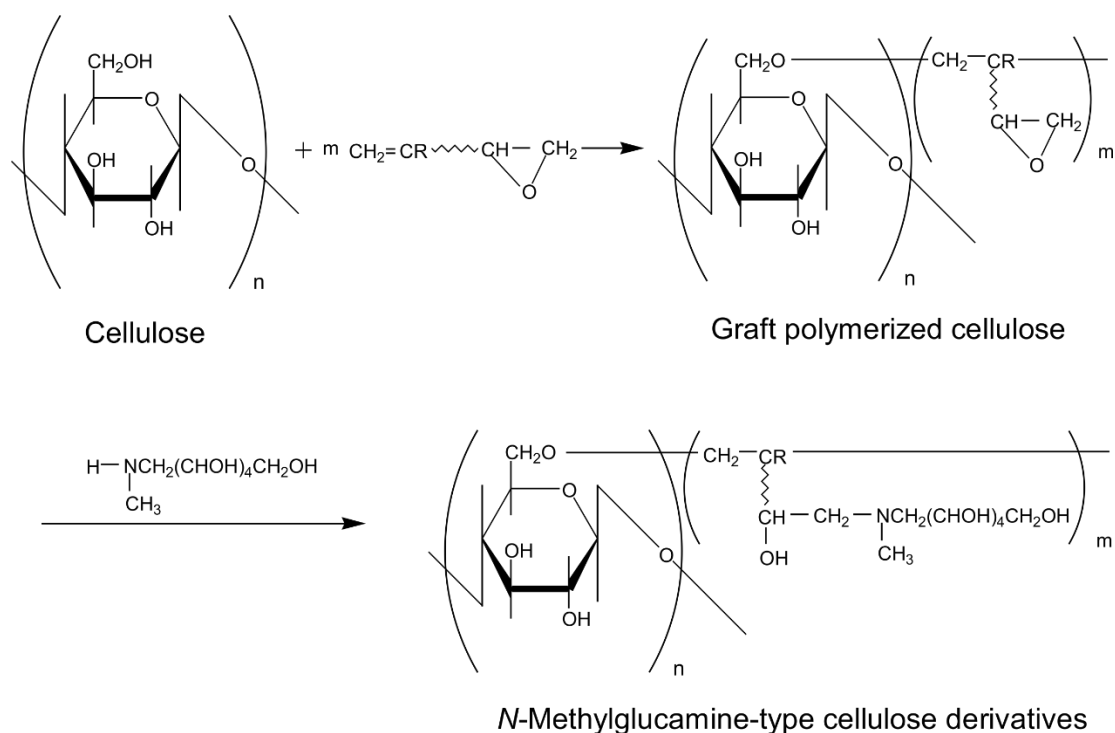
Fig. 3.18. Preparation of *N*-methylglucamine-type cellulose derivatives [142].

A similar adsorbent of microcrystalline cellulose microspheres (MCM) possessing NMDG group was successfully synthesized by S. Liu et al. [143]. In the preparation of adsorbent, 4-vinylbenzyl chloride (VBC) was firstly grafted onto the MCM by simultaneous grafting polymerization, and then VBC grafted cellulose microsphere was functionalized with NMDG (Fig. 3.19). The boron adsorption capacity of resulting adsorbent reached to 12.4 mg/g in the wide range of pH between 5 and 8 ($[B_0] = 30$ ppm, the dosage of 0.02 g adsobent/20 mL solution, average diameters of 390 μm, stirring speed of 230 rpm at 25 °C). While the concentration of NaCl was increased to 40 mmol/L, the boron uptake raised to 14.1 mg/g, and it remained stable with the addition of various chloride salts, which are main salts in seawater with the high concentration. Besides, the thermal stability of adsorbent was about 280 °C. The research indicated that the NMDG-cellulose microsphere was an effective and inexpensive alternative of bio-adsorbent for boron removal from saline water.
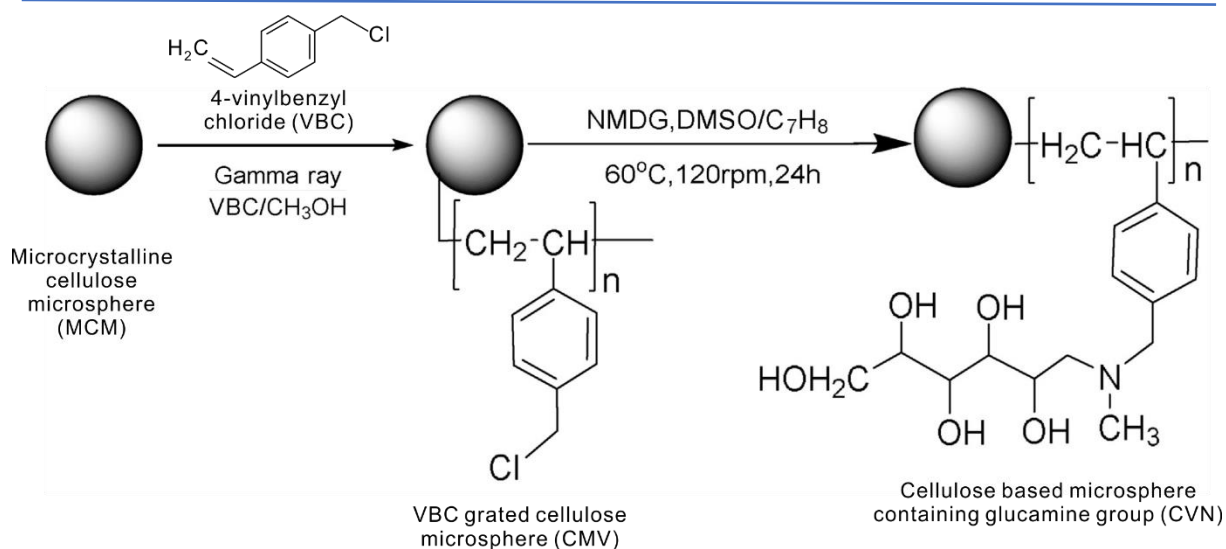
Fig. 3.19. Synthesis of NMDG-cellulose microsphere. (Reproduced from [143])

Saccharides modified chitosan resins (SMC resins) were investigated for boron removal from boron mining and desulfurizing equipment in the coal-fired steam power (Fig. 3.20) [144]. Various saccharides including D-galactose, D-mannose, D-glucose, D-xylose, D-ribose and D-arabinose, which containing hydroxyl group are able to form the stable complexes with boron, were introducing into chitosan by reductive N-alkylation. Then the obtained gel was crosslinked by ethylene glycol diglycidyl ether (EGDE) for the insolubility in acidic and basic solution. The saturated adsorption capacity of boron of SMC resins was from 5.57 to 12.32 mg/g ($[B_0] = 216$ mg/L, 0.05 g adsorbent/ 10 mL solution, shaken condition at 25 $^\circ$C for 48 h).

Gel formation like an egg box occurs when alginate reacts with divalent cations, especially Ca^{2+}. Calcium alginate gel beads having hydroxyl groups can bind boron in the solution (Fig. 3.21). The maximum boron removal efficiency was found at 55.14% ($[B_0] = 50$ ppm using 0.7 g of calcium alginate gel beads/100 mL solution, pH 11, 50 rpm of shaking speed at room temperature) [145].
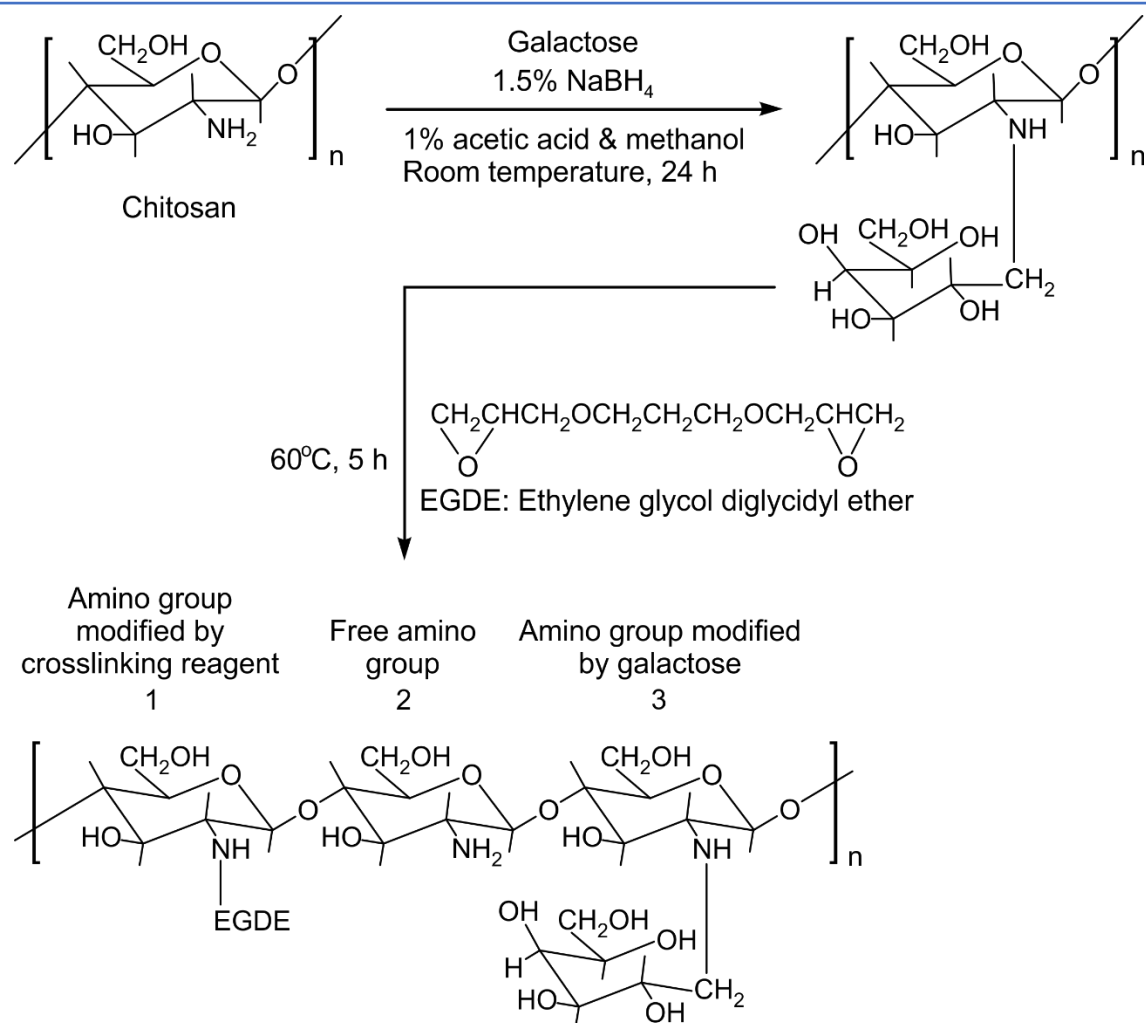
Fig. 3.20. Preparation of saccharides modified chitosan resins. (Reproduced from [144]).
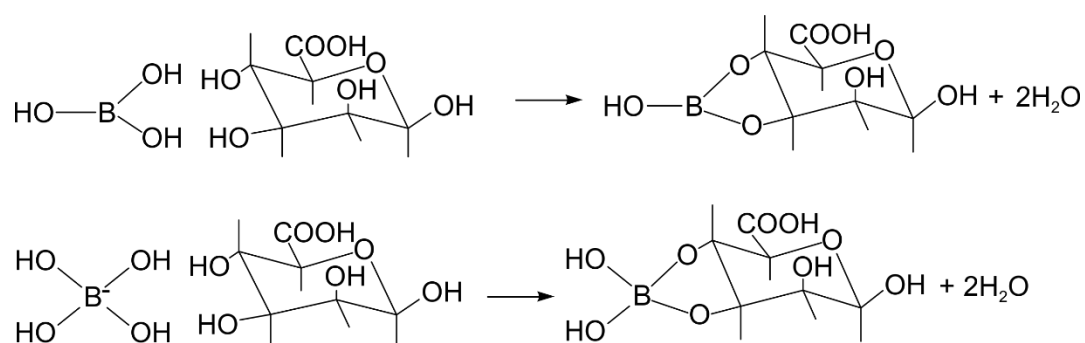
Fig. 3.21. The proposal interaction between boric acid and borate with alginate [145].

A low-cost natural polymer (tannin) extracted from leaves and barks from plants has many hydroxyl groups [146]. The tannin particle was treated by ammonia solution and washed with 1 M HCl solution to obtain the gel (Fig. 3.22). The results displayed the boron uptake capacity of modified tannin gel (3.43 mg/g) was higher than tannin gel (2.48 mg/g) ($[B_0]$ = 10-200 ppm, pH = 8.8, 0.1 g gel/50 mL solution, shaking condition

at 30 °C for 20 h). It was attributed to the stable coordination bond between boron and nitrogen of the amino group in the modified tannin gel (Fig. 3.22).

a

R₁ = OH and R₂ = H, phloroglucinolic;
R₁ = R₂ = H, resorcinolic; R₁ = H and R₂ = OH, pyrogallolic;
R₃ = H, catecholic; R₃ = OH, pyrogallolic
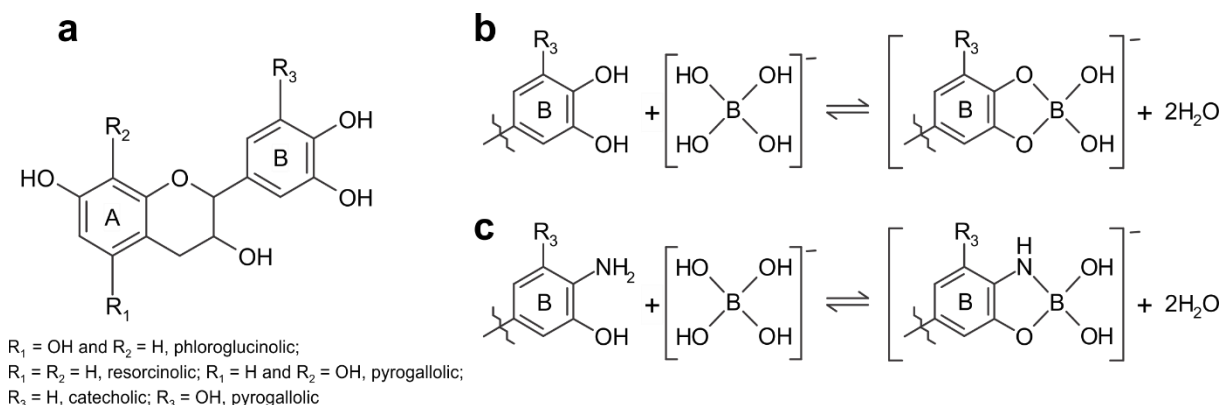
Fig. 3.22. The chemical structure of tannin molecule (a) and boron adsorption mechanisms of tannin gel (b) and modified tannin gel (c) [146].

Although numerous modified biopolymers with boron-chelating groups have been investigated for improving the boron adsorption capacity from the low-cost material, there were little studies investigated the mechanical strength as well as the regeneration feasibility of the adsorbent.

4. Hybrid organic-inorganic adsorbents

H. Demey et al. [147] prepared organic-inorganic composite from chitosan as the encapsulating material and nickel (II) hydroxide named [chiNi(II)]. The composite had a considerable weight loss at roughly 260 °C. The reaction mechanism of composite and boron was shown in Fig. 3.23. The maximum adsorption capacity of [chiNi(II)] was found at 61.4 mg/g (0.04 g adsorbent/100 mL solution for 72 h). Five cycles of boron recovery were conducted using water pH of 12, and the desorption uptake remained higher than 90% in almost of cycles.
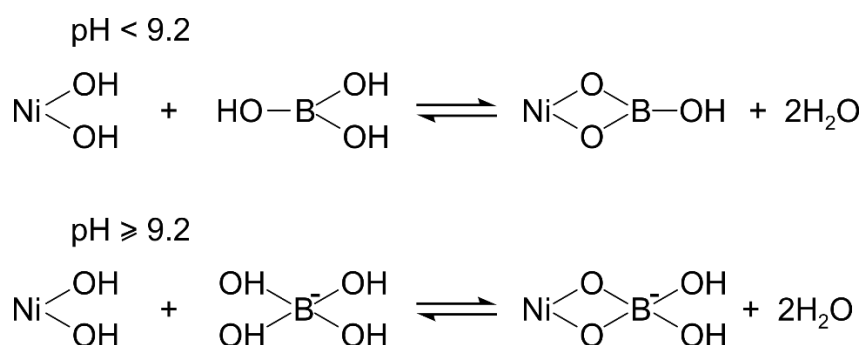
Fig. 3.23. The reaction of boric acid, borate and [chiNi(II)] composite [147].

Magnetic chitosan microbeads (MC) was synthesized and chemically modified with a glycidol to produce magnetic multi-hydroxyl microbeads (MCG) for boron-selective removal [148]. The synthesis procedure of MCG was given in Fig. 3.24. The thermal stability of resulting MCG was significantly high when 37.2% of its residue still remained after heating up 1000 °C. MCG showed the high selective-boron adsorption in the presence of competitive metal ions (Cu^{2+}, Fe^{3+} and Ni^{2+}) and salts of Mg^{2+}, Ca^{2+}, Na^+ and K^+ ions in the optimized condition. MCG exhibited the high boron removal efficiency of 96% as well as boron adsorption capacity of 128. 5 mg/g ($[B_0] = 100$ ppm, pH = 7, 0.1 g adsorben/20 mL solution). The adsorption equilibrium of boron onto adsorbent was reached after 100 min. Due to the magnetic characteristic, MCG could be separated rapidly within 45 s by using an external magnet. The adsorbent could reuse 7 times by 0.1 M HCl solution treatment and reactivate by water at pH 9.
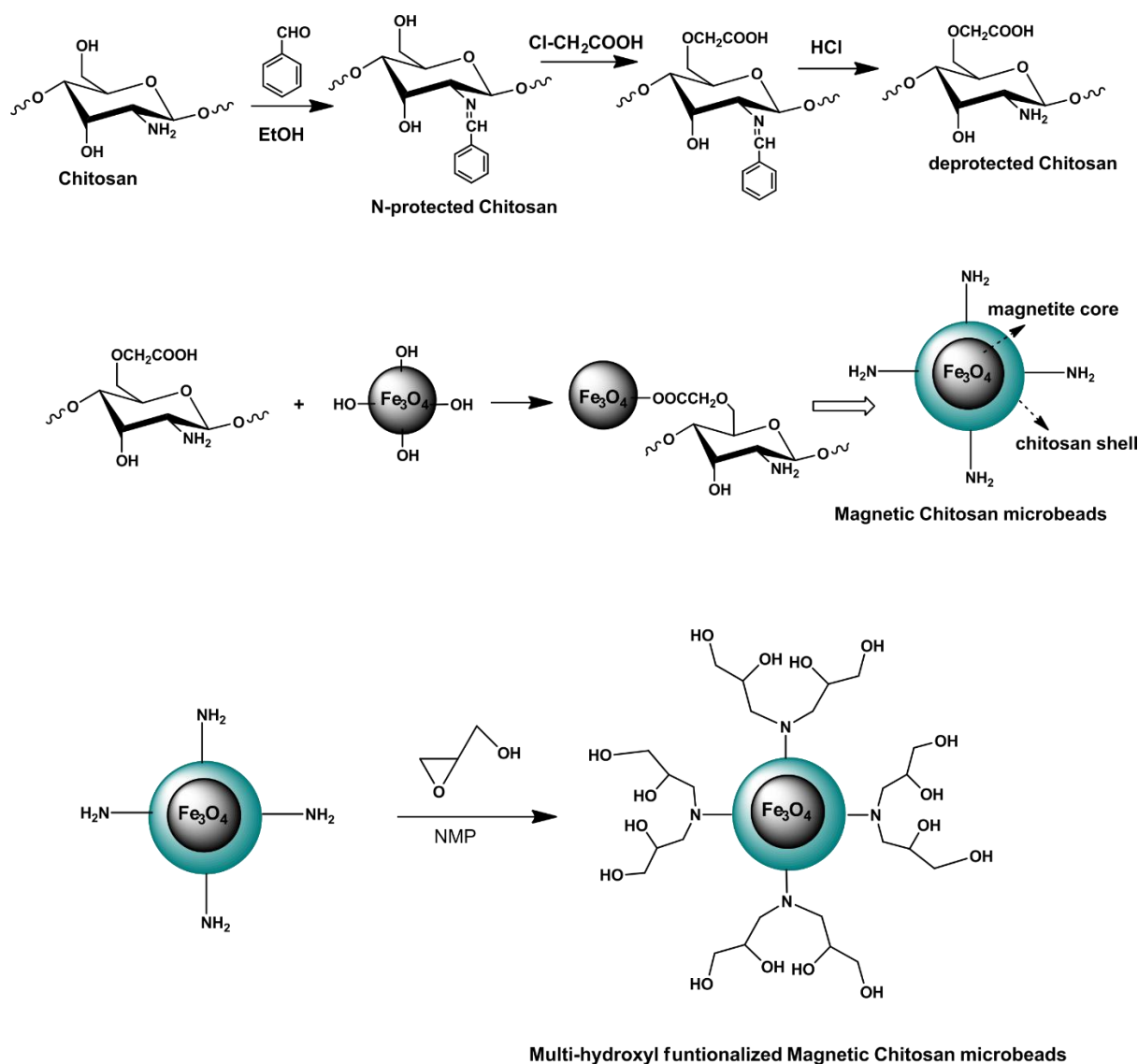
Fig. 3.24. Synthesis of multi-hydroxyl functionalized magnetic chitosan microbeads [148].

3.4. Conclusion

The basic chemical properties of boron were introduced in this chapter. The reaction of boric acid and borate ions with alcohols, polysaccharide and polyols could form various borate complexes due to the multiple hydroxyl functional groups. Owing to the multiple hydroxyl groups orients suitable to fit structural parameters for tetrahedral boron coordination, strong stable borate complexes will be formed. Most commercial resins have macroporous polystyrene matrix crosslinked with divinylbenzene and graft to NMDG functional group as the adsorbents for boron removal. The commercial resins have the weaknesses of the slow sorption kinetics and the high cost. Therefore, alternative boron-selective resins have been developed to improve the characteristics of polymer substrates and functional groups have been modified for boron removal from aqueous solution.

Chapter 4

Simple one-step synthesis of gluconated chitosan for removal of boron

Abstract

The overdose and long-term accumulation of boron can lead to adverse effects on the quality and quantity of crops as well as human health. Boron-selective adsorbents have been developed for boron separation from aqueous solution. Owing to the possession of *vis*-diols, they offer an effective interaction with boron. In this research, gluconated chitosan particles (GChs) were synthesized by the functionalization of chitosan with D-(+)- glucono - 1,5 lactone (GL) in the facile process to provide the adsorbents with boron-selective sections. The adsorption mechanism of GChs was investigated with a batch system. The adsorption equilibrium was reached after 700 min. The maximum boron adsorption capacity of GChs was achieved at 5.8 mg/g. The adsorption isotherm data were well fitted to Langmuir model ($R^2 = 0.9993$). The adsorption kinetics of boron was following the pseudo-second order model. The adsorption process was not considerably affected by pH. Due to the slight increase in boron adsorption after the addition of NaCl, GChs could be applied for boron removal from saline water or sea water. The obtained results apparently indicated that GChs could be the safe and affordable adsorbents for the removal of boron from aqueous solution.

Keywords: boron removal, chitosan, D-(+)- glucono - 1,5 lactone, multi-hydroxyl group, adsorption
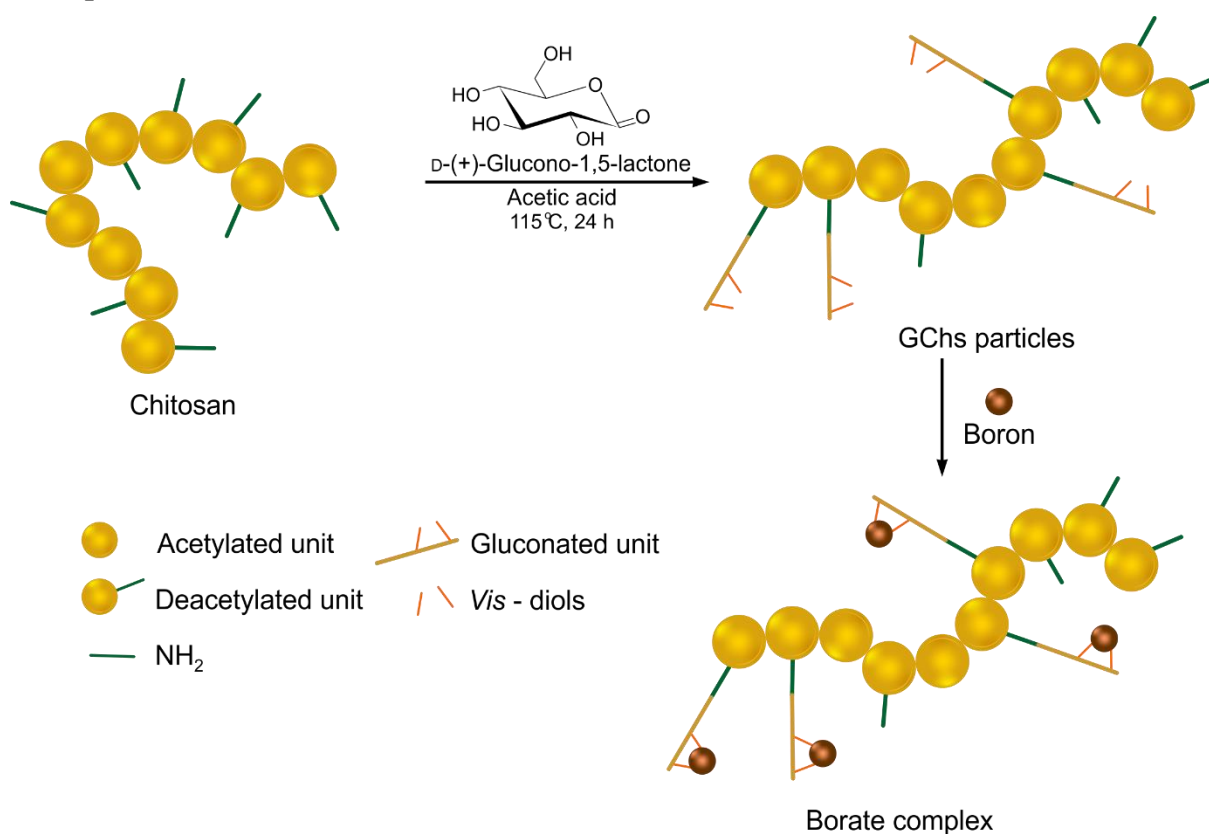
Fig. 4.1. Illustration of synthesis and boron adsorption of GChs.

4.1. Introduction

As an indispensable micronutrient, boron contributes to the synthesis of the cell wall, metabolism and transportation of carbohydrate and the formation of pollen tube [107]. This element plays an important role in the quality and yield crop. Nonetheless, the abundance of boron in irrigation water leads to the leaves diseases and the decay of unripe fruits, especially some plants are sensitive to boron (citrus and blackberry) [113]. In addition, boron damages the cardiovascular, nervous and reproduction system in the long-term uptake [120, 121]. Therefore, the recommended boron concentration of the World Health Organization (WHO) in drinking water was set at 2.4 ppm in 2011 [122]. In Japan, the maximum boron concentration in drinking water was established at 1.0 ppm, and the limitation of boron and its compounds are less than 230 ppm and 10 ppm when the wastewater is discharged by plants, factories or businesses to sea area and other than sea area, respectively. Thus, the level of boron in wastewater need to control in the permissive concentration.

Numerous methods have been applied for boron removal from water and wastewater, such as phytoremediation [149], adsorption [87], reverse osmosis [150], ion exchange [151], precipitation [152], coagulation [153], electrocoagulation (EC) [154], electrodialysis (ED) [155], Donnan dialysis [156] and hybrid process [157, 158]. Among all these methods, adsorption technique using chelating resins has received considerable attention for boron removal due to the high efficiency, easy operation and capability of application in water and wastewater treatment with large scale [124]. Hydroxyl groups located in cis position also called *vis*-diols provide boron-selective sections for the formation of borate complexes. Major commercial resins possess synthetic polymers attached to *N*-methyl- D-glucamine (NMDG) as the functional group, containing *vis*-diols. However, these resins have to face the challenges of high cost which decrease the application of boron removal in large scale and undegradable characteristic of synthetic polymers as the substrate which relates to environmental issues. Thus, the characteristics of polymers and functional groups have been modified and optimized, and a large number of alternative boron-selective resins have been developed to improve the feasibility of boron removal from aqueous solution for meeting the wastewater discharge standard and drop the cost of the materials.

Chitosan is a copolymer composed of a majority of β (1→ 4) linked 2-amino-2-deoxy-β-D-glucopyranose (glucosamine or deacetylated unit) and residues β (1→ 4) linked 2-acetamido-2-deoxy-β-D-glucopyranose *(N*-acetyl- D-glucosamine or acetylated unit) [159]. Due to availability, abundance, biodegradability, non-toxicity and reactivity, chitosan has been extensively applied in agriculture, food industry, pharmaceuticals, cosmetic, and waste and water treatment [160]. Chitosan is produced commercially by deacetylation of acetyl groups from chitin under the alkaline condition at high temperature (above 80 ºC) to convert to free amino groups [161]. In the presence of reactive sites including hydroxyl groups (-OH) and amino groups (-NH$_2$), chitosan can be utilized as an adsorbent for dye and heavy metals removal. After cationization in acidic solution, amino groups give a positive charge which can bind with negatively charged molecules [162]. Furthermore, chitin is the second most ubiquitous natural polymer after cellulose on earth, and it is the principal component in shellfishes such as shrimps, prawns, crabs, lobsters, the exoskeleton of insects, and the cell wall of fungi [163]. Shellfishes are considered to be the major source of pollution in coastal areas [164, 165]. Thus, the large-scale production of chitin and chitosan helps recycle the shell wastes from the food industry.

In this work, gluconated chitosan particles (GChs) were synthesized for boron removal. Chitosan was selected for the substrate and functionalized with D-(+)- glucono - 1,5 lactone (GL) in the facile process to provide the adsorbents with boron-selective sections. Adsorption isotherm and kinetics of boron onto GChs was investigated, and the effects of pH and ionic strength were also studied for the properties of boron adsorption mechanism.

4.2. Experimental

4.2.1. Materials and reagents

Chitosan and D-(+)- glucono - 1,5 lactone (C$_6$H$_{10}$O$_6$) were produced from Tokyo chemical industry Co., Ltd, Japan. Boron standard solution (1000 ppm), boric acid (H$_3$BO$_3$) for preparation of the boron stock solutions containing different boron concentration, hydrochloric acid (HCl) and sodium hydroxide (NaOH) used for pH adjustment were supplied by Kanto, Japan. Dialysis membrane (14,000 MWCO) was purchased from Wako Chemicals USA, Inc. All aqueous solutions were prepared using

Mili-Q water (18.25 MΩ.cm) from Direct-Q UV3, Merck Millipore. All other chemicals used were analytical grade and used as received without further purification.

4.2.2. Synthesis of gluconated chitosan (GChs) particles

GChs were prepared from the chemical modification of chitosan in one step of synthesis, as illustrated in Fig. 4.2. Firstly, 5 g of chitosan flakes were dissolved in 500 mL of acetic acid solution 1% (v,v) at room temperature for 12 h under mechanical stirring. Next, GL was added to the solution following the mole ratio of chitosan : glucono - 1,5 lactone (1 : 5). The reaction mixture was refluxed by heating in an oil bath at 115 °C for 24 h under stirring condition. After the mixture was cool down to room temperature, NaOH 1 M was added dropwise to form the precipitates. Then, the mixture was centrifuged at 4000 rpm, and the precipitates were collected and dipped in acetone. The obtained product was separated by filtration and dried in vacuum overnight. Residuals of free acetic acid and unreacted GL were removed by dialysis against Mili-Q water using dialysis membrane. After the dialysis process was carried out, the precipitates in the membrane were immersed in acetone, sonicated for a few minutes. The product was collected by filtration and dried completely in the vacuum at room temperature. Finally, GChs particles were obtained by crush for homogeneity.
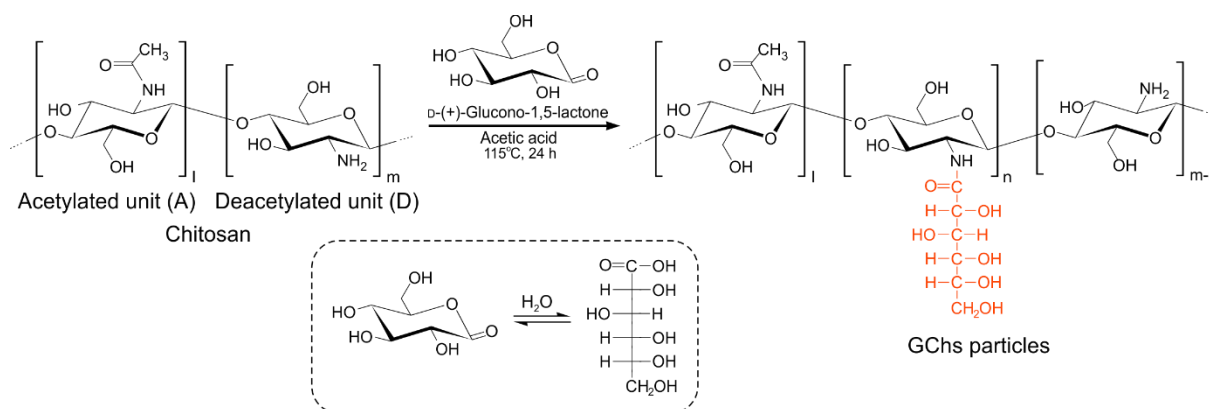
Fig. 4.2. Synthesis of gluconated chitosan derivative.

4.2.3. Boron adsorption

1. Adsorption isotherm

In this experiment, boric acid solution with different boron concentrations varied between 10 and 400 ppm. The adsorbent dosage was 0.2 g/20 mL with 10 and 50 ppm of initial boron concentration while it was 0.8 g/20 mL with samples of 100, 200 and 400 ppm. After shaking at 25 °C for 24 h to reach equilibrium, the mixtures were filtered

through a Whatman 50 filter paper (Whatman International Ltd., England 2.7 μm particle retention) to separate the adsorbent from the aqueous solution.

2. Adsorption kinetics

The adsorption kinetics was conducted by dipping 0.8 g of GChs into 20 mL of boric acid solution as boron 400 ppm. The mixtures were shaken at 25 °C from 0.5 to 24h; afterwards, filtrate samples were collected by filtration.

3. Effect of pH

In order to investigate the effects of initial solution pH on boron adsorption of GChs, 0.8 g of GChs was added to 20 mL of boric acid solution as boron 400 ppm with the initial pH from 5.6 to 9.8. Initial pH solution was adjusted by NaOH 0.1 M using pH meter (F-52, Horiba, Japan). The samples were shaken at 25 °C for 24 h then filtered through filter paper to obtain the filtrate.

4. Effect of ionic strength

0.8 g of GChs was dipped to 20 mL of the boric acid solution as boron 400 ppm containing NaCl from 0 to 1000 mmol/L. The filtrate samples were collected after the mixtures were shaken at 25 °C for 24 h.

The same procedure was also employed with blank samples for each series of the batch experiments. The boron concentration in the filtrate was then analyzed by UV/VIS/NIR Spectrophotometer V-570, Jasco, Japan using azomethine-H method. The boron determination was conducted at 415 nm wavelength which corresponds to the maximum absorbance. The removal efficiency of boron (H) and boron adsorption capacity (q_e) were determined by the equations.

$$H = \frac{C_0 - C_e}{C_0}.100 \quad (\%) \qquad (4.1)$$

$$q_e = \frac{C_0 - C_e}{M}.V \qquad (mg/g) \quad (4.2)$$

Where C_0 and C_e are the initial and equilibrium concentrations of boron (ppm) in the solution, respectively, M is the mass of dry adsorbent (g) and V is the volume of sample (L).

Spectrophotometric methods depend on colourimetric reactions of boron with some specific reagents such as curcumin, carmine, and azomethine-H for colour enhancement [166]. Azomethine-H method is based on the reaction of azomethine-H (8-hydroxy-1-(salicylideneamino)-3,6-naphthalenedisulfonic acid, sodium salt) with boron to form an

orange boron-azomthine-H complex (Fig. 4.3) [167]. EDTA is used in this method to mask copper, iron, and aluminium ions. Azomethine-H is a fast and simple method, and in a comparison of curcumin, and carmine methods, it suffers the least interferences and is the most sensitive, precise and selective [168]. The optical density of the analyzed solution is proportional to the boron concentration in aqueous samples, and the molar absorptivity of the complex detected at 415 nm.

Fig. 4.3. Reaction of boric acid and azomethine-H [167].

Fig. 4.4. Synthesis of GChs particles and boron adsorption experiment.

4.3. Results and discussion

4.3.1. Boron adsorption isotherm

In this study, Langmuir and the Freundlich isotherms models were applied to simulate the experimental data of boron adsorption. The Langmuir isotherm model assumes that maximum coverage can be attained with monolayer adsorption onto the homogeneous

surface of adsorbent that possesses the constant number of the identical energy for all adsorption sites. The non-linear form of Langmuir isotherm can be expressed by Eq. 4.3.

$$q_e = \frac{bq_{max}C_e}{1+bC_e} \qquad (4.3)$$

Where q_e is the amount of adsorbed boron at equilibrium in the solution (mg/g), C_e is the equilibrium boron concentration (ppm), q_{max} is the maximum adsorption capacity (saturation value) (mg/g) and b is the Langmuir constant related to energy of adsorption (L/mg). The linear form of Langmuir equation is given as:

$$\frac{C_e}{q_e} = \frac{1}{bq_{max}} + \frac{1}{q_{max}} C_e \qquad (4.4)$$

The Freundlich isotherm model was used to describe the assumption of multilayer adsorption on heterogeneous surfaces having unequal available sites with different energies of adsorption [169]. The non-linear form of Freundlich isotherm is represented by Eq. 4.5.

$$q_e = K_F C_e^{1/n} \qquad (4.5)$$

Where K_F and n are the Freundlich constants related to the adsorption capacity and the adsorption intensity, respectively.

The linear form of Freundlich equation is calculated according to Eq. 4.6.

$$\log q_e = \log K_F + \frac{1}{n} \log C_e \qquad (4.6)$$

The estimation of the non-linear isotherm parameters was carried out by minimizing the error values of experimental data and isotherm models by using Solver Add-in of Microsoft Excel. The adsorption parameters of Langmuir and Freundlich models and correlation coefficient (R^2) are listed in Table 4.1. From this table, the maximum boron adsorption capacity of GChs was determined at 5.80 mg/g by Langmuir model. The correlation coefficient obtained from Langmuir model ($R^2 = 0.9993$) was higher than Freundlich model ($R^2 = 0.8506$), implying that the fitting of experimental data and Langmuir isotherm model was better than Freundlich isotherm model (Fig. 4.5 and Fig. 4.6). This finding indicated that the monolayer coverage on the surface of GChs was the principal adsorption mechanism.

Furthermore, the Langmuir isotherm can be used to predict that if the adsorption of boron by GChs is favorable or not, and the dimensionless separation factor of the equilibrium parameter, R_L is shown by Eq. 4.7.

$$R_L = \frac{1}{1 + bC_0} \qquad (4.7)$$

Where C_0 is the initial concentration of boron in the solution (ppm). R_L indicates the type of the process of boron adsorption to be unfavorable ($R_L > 1$), linear ($R_L = 1$), favorable ($0 < R_L < 1$), or irreversible ($R_L = 0$). In this work, the R_L values shown in Table 4.1 are calculated in the range of 0.071 - 0.7480, which indicated that process of boron adsorption on GChs was favorable in the range of boron concentration used in this investigation.
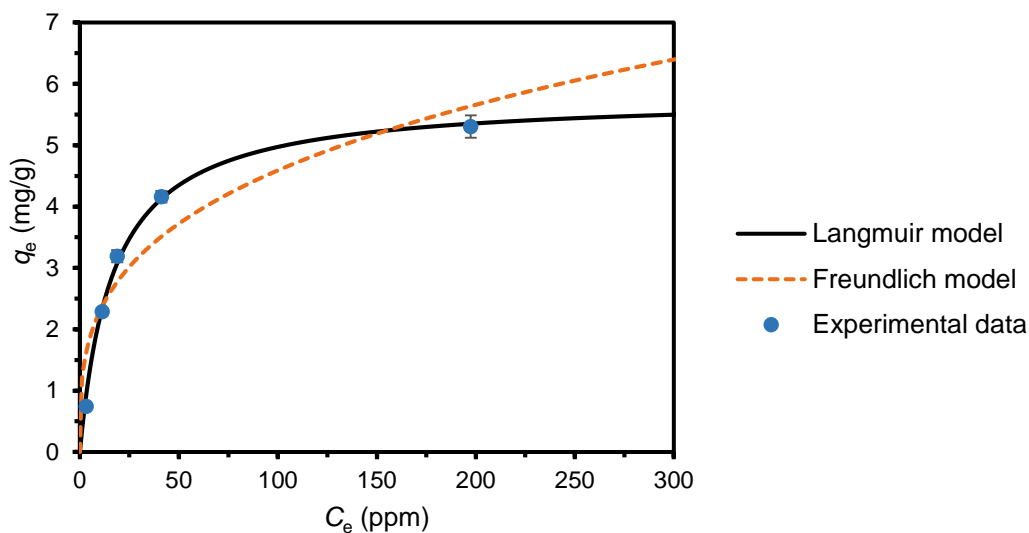
Fig. 4.5. Adsorption isotherm of boron on GChs particles by fitting Langmuir and Freundlich models (Initial boron concentration 10 - 400 ppm, mass of adsorbent 0.2 g in the samples of 10 and 50 and 0.8 g in the samples of 100 to 400 ppm, pH 5.4, V 20 mL and contact time 24 h).

Table 4.1. Langmuir and Freundlich isotherm parameters and correlation coefficient at 25 °C for adsorption of boron by GChs particles.

q_{exp} (mg/g)	Langmuir model					Freundlich model		
	q_{max} (mg/g)	b (L/mg)	R^2	R_L range		K_F	n	R^2
5.31	5.80	0.060	0.9993	0.071 - 0.7480		1.141	3.309	0.8506
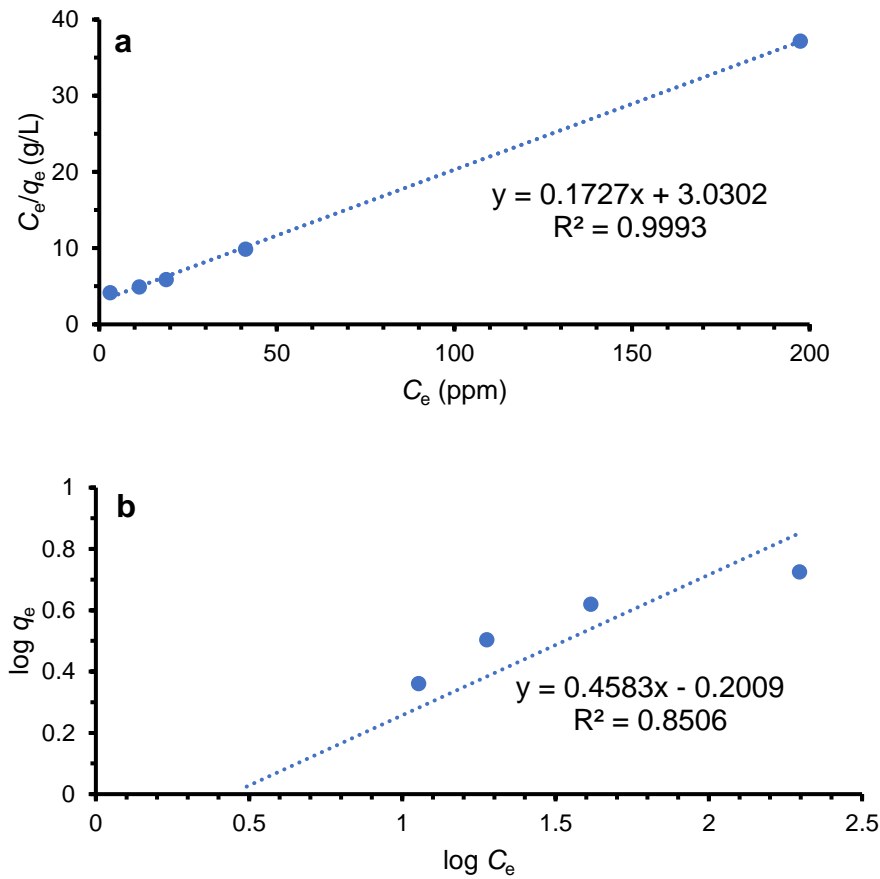
Fig. 4.6. Langmuir (a) and Freundlich (b) plots for boron adsorption by GChs particles.

4.3.2. Boron adsorption kinetics

The adsorption kinetic of boron on the GChs was investigated by employing the pseudo-first order and pseudo-second order model. The kinetic equation for the pseudo-first order model was firstly proposed by Lagregan [170]. This model is described as:

$$\frac{dq_t}{d_t} = k_1(q_e - q_t) \qquad (4.8)$$

Where q_e and q_t (mg/g) are the boron uptake at equilibrium and at time t (min), respectively, and k_1 (g mg^{-1} min^{-1}) is the rate constant of the pseudo-first order adsorption model. Integrating Eq. 4.8 for the boundary conditions $t = 0$ to $t = t$ and $q_t = 0$ to $q_t = q_t$:

$$\ln(q_e - q_t) = \ln q_e - k_1 t \qquad (4.9)$$

The linear form of Eq. (4.9) is given as:

$$\log(q_e - q_t) = \log q_e - \frac{k_1 t}{2.303} \tag{4.10}$$

The non-linear form of Eq. 4.9 can be written as:

$$q_t = q_e \, (1 - \exp(-k_1 t)) \tag{4.11}$$

The pseudo-second order kinetic model was proposed by Blanchard [171], may be expressed as:

$$\frac{dq_t}{(q_e - q_t)^2} = k_2 d_t \tag{4.12}$$

Where k_2 (g mg^{-1} min^{-1}) is the rate constant of the pseudo-second order model. Integrating Eq. 4.12 for the boundary conditions $t = 0$ to $t = t$ and $q_t = 0$ to $q_t = q_t$:

$$\frac{1}{q_e - q_t} - \frac{1}{q_e} = k_2 t \tag{4.13}$$

The linear form of Eq. 4.13 introduced by Ho is given as:

$$\frac{t}{q_t} = \frac{1}{k_2 q_e^2} + \frac{t}{q_e} \tag{4.14}$$

The initial adsorption rate, h (g mg^{-1} min^{-1}) at t = 0 is expressed as:

$$h = k_2 q_e^2 \tag{4.15}$$

The non-linear form of (17) can be written as:

$$q_t = \frac{k_2 q_e^2 t}{1 + k_2 q_e t} \tag{4.16}$$

Similar to the calculation of non-linear isotherm parameters, kinetic parameters of both models were determined by using Solver Add-in of Microsoft Excel, as summarized in Table 4.2. It can be found that the time of boron adsorption to equilibrium was 700 min, and the q_t values of the experimental data were close to both kinetic models (Fig. 4.7). However, the pseudo-second order kinetic model produced a better correlation coefficiency ($R^2 = 0.9933$) than the pseudo-first order kinetic model ($R^2 = 0.9884$) for the adsorption of boron (Fig. 4.8). This result suggested that the kinetics of boron adsorption can be represented by pseudo-second order model. Thus, the

mechanism of boron adsorption onto the surface of GChs was probably controlled by chemisorption process via ion exchange between boron ions and functional groups of the adsorbent.

Table 4.2. Kinetics parameters at 25 °C for adsorption of boron by GChs.

q_{exp}	Pseudo-first order model			Pseudo-second order model		
(mg/g)	$q_{e,1}$	k_1	R^2	$q_{e,2}$	k_2	R^2
	(mg/g)			(mg/g)		
5.31	5.31	0.0054	0.9884	6.15	0.0011	0.9933
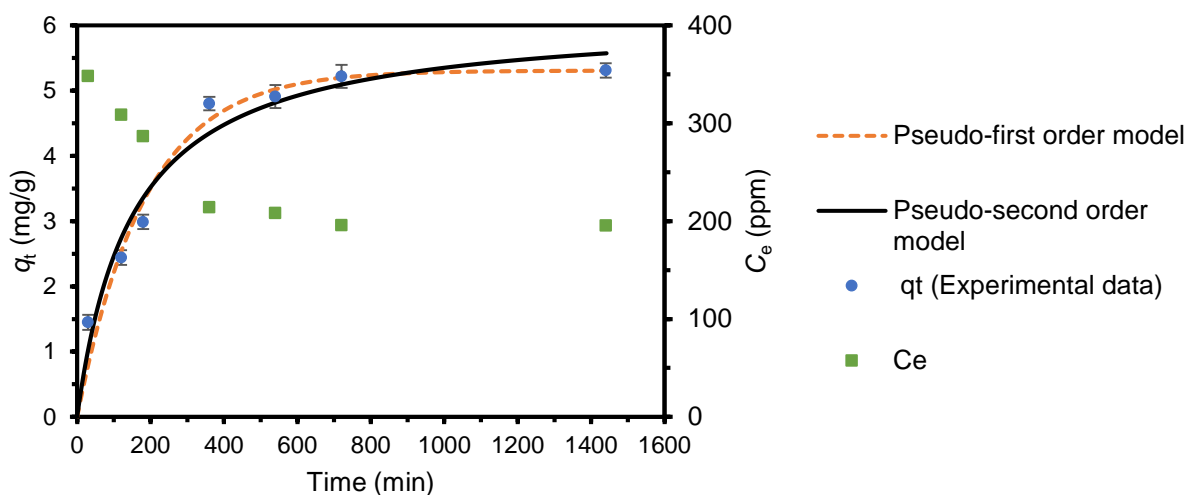
Fig. 4.7. Adsorption kinetics of boron on GChs (Initial boron concentration 400 ppm, mass of adsorbent 0.8 g, pH 5.6 , V 20 mL and contact time 24 h).
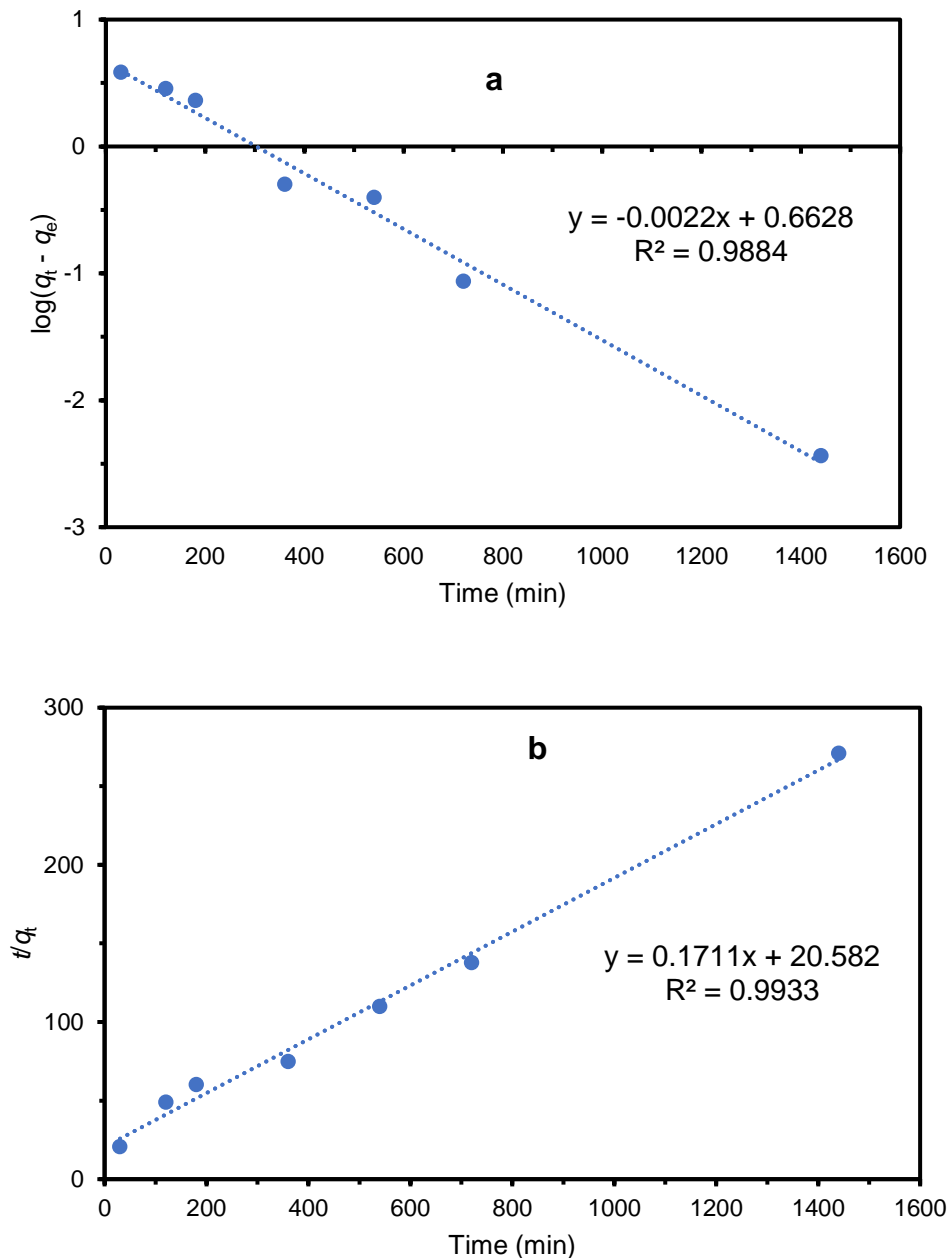
Fig. 4.8. Pseudo-first order model (a) and Pseudo-second order model (b) plots for boron adsorption by GChs particles.

4.3.3. Effect of pH

The influence of pH on the behavior of boron uptake was investigated in the range of pH between 5.6 and 8.9. As can be seen from Fig. 4.9, there was no considerable change in the boron adsorption in the wide range of pH, and pH values before and after adsorption were not substantially different. This finding revealed that the process of boron uptake was not dependent on pH solution. Our findings are consistent with those of Ö. Kaftan et al. and S. Liu et al. [143, 172].
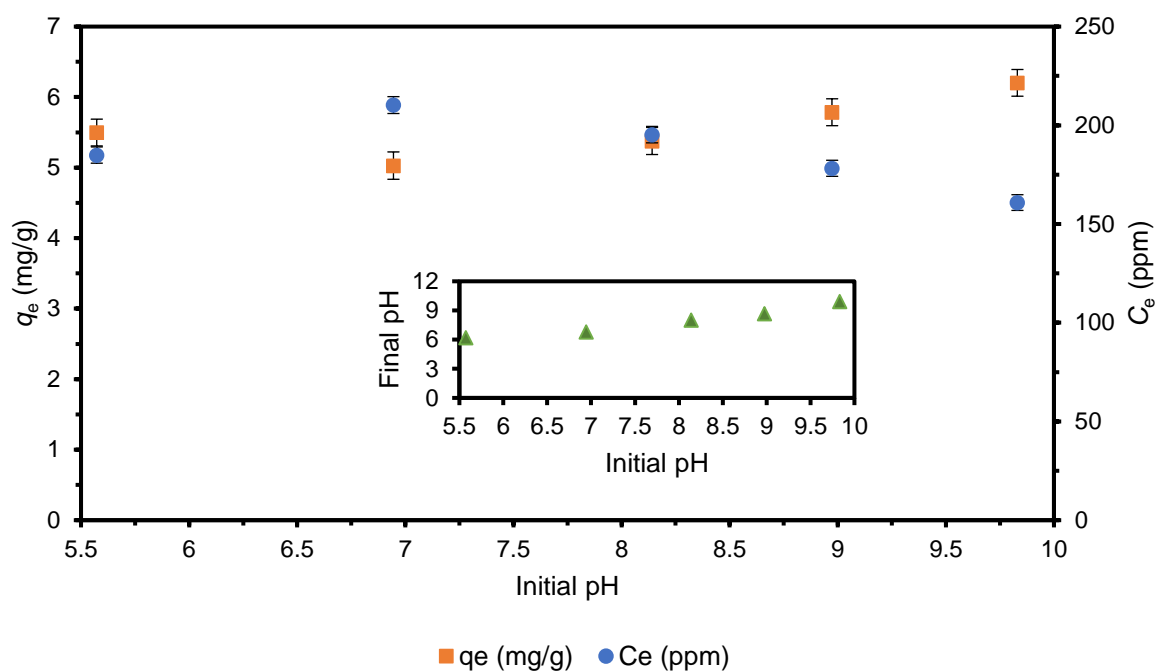
Fig. 4.9. Effect of pH on boron adsorption by GChs and final pH (inset) (Initial boron concentration 400 ppm, mass of adsorbent 0.8 g, V 20 mL, contact time 24 h).

4.3.4. Effect of ionic strength
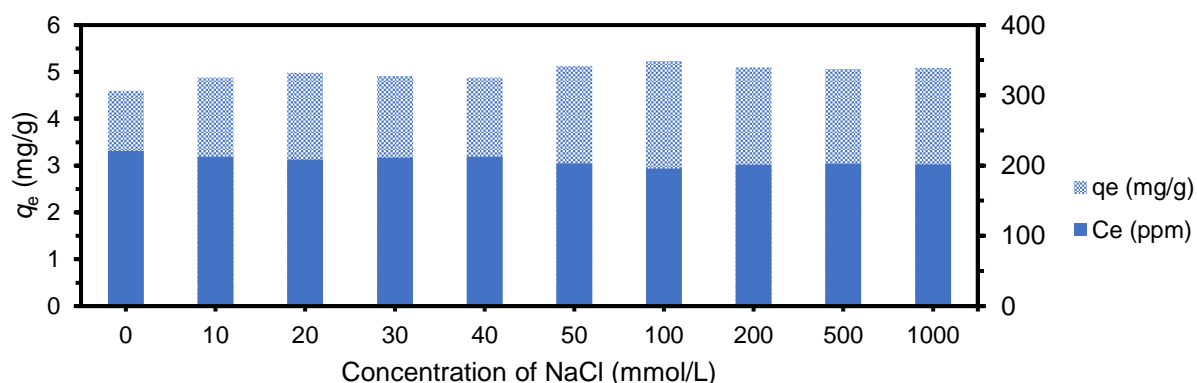
Fig. 4.20. Effect of NaCl concentration on boron adsorption by GChs (Initial boron concentration 400 ppm, mass of adsorbent 0.8 g, pH 5.6, V 20 mL, contact time 24 h).

Fig. 4.20 displays the impact of ionic strength on the adsorption of boron into GChs particles. It can be observed that there was a slight increase in boron uptake in the presence of NaCl salt (10-1000 mmol/L). Boron adsorption capacity rose gradually from 4.6 to 4.9 mg/g when the concentration of NaCl increased from 0 to 10 mmol/L, and the value of boron adsorption stayed stable in the range of NaCl concentration between 10 and 40 mmol/L. After this stage, boron uptake grew minimally to 5.1 mg/g and remained

steady with the concentration of NaCl from 50 to 1000 mmol/L. In addition, equilibrium boron concentration decreased from 220.98 to 201.76 ppm as NaCl concentration raise between 0 and 1000 mmol/L. These results indicated that higher boron adsorption was attained in the presence of NaCl; nevertheless, there was no impact on boron uptake at high NaCl concentration.

The possible mechanism of boron adsorption on GChs and the reaction between borate complex and NaCl are illustrated in Fig. 21. In aqueous solution, boric acid can be easily dissolved in water as a weak Lewis acid to generate tetrahydroxyborate ion through the hydrolysis process. The formation of the boron complex between boron ions and *vis*-diol groups relates to the growth of negative charge on the surface of the adsorbent. The high concentration of NaCl raising the capacity of boron adsorption is possible due to the reduction of the negative charge of the surface areas in the aqueous system. However, following this growth, boron adsorption stays at the same level even larger amount of NaCl concentration. It is attributed to the balance of electric charges on the surface of GChs. The similar reports have been reported for the effect of ionic strength in previous studies. Owing to not decreasing the capacity of boron adsorption in the appearance of NaCl salt, GChs can be used in the application for boron removal from saline water or seawater.
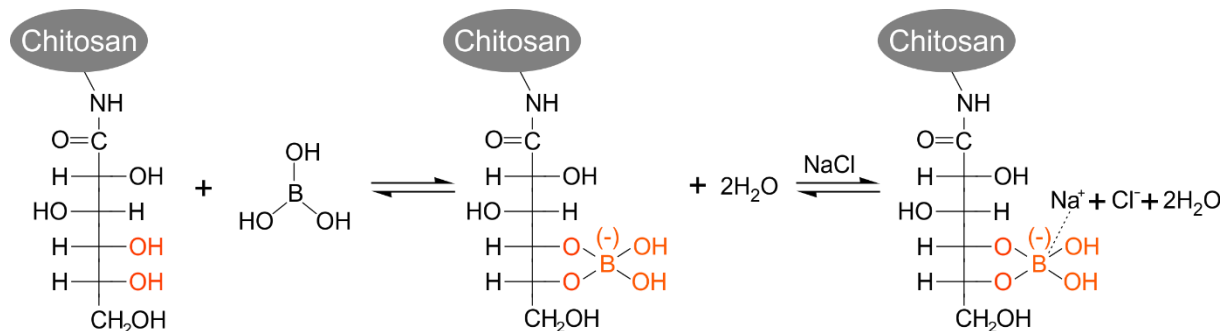
Fig. 4.21. Proposal of borate complex formation and the effect of NaCl on capacity of boron adsorption.

4.4. Conclusion

In this study, chitosan-based adsorbent (GChs) containing gluconated groups was successfully synthesized in a simple process and applied for boron removal. GChs exhibited the maximum adsorption capacity at 5.8 mg/g after 700 min. Moreover, the change of pH has not impacted on the capacity of boron adsorption in the wide range of pH from 5.6 to 8.9, indicating the pH adjustment is not required for the treatment of wastewater contaminated by boron. This finding results in the less use of reagent in the boron removal using GChs. There was a slight increase in boron adsorption in the presence of NaCl salt; therefore, GChs may be applied for boron removal from saline water or seawater.

Chapter 5

Green synthesis and characterization of the novel multi-hydroxyl
functionalized with chitosan nanofibers
to approach the removal of boron

Abstract

Although chitosan exhibited remarkable properties of biodegradability, non-toxicity, macromolecular structure and reactivity, its low porosity limited the capacity of adsorption process. In this work, chitosan nanofibers (ChNFs) containing amino groups was grafted with D-(+)- glucono - 1,5 lactone (GL) to form gluconated chitosan nano fibers (GChNFs) sponge as the novel material for boron removal. The optimal conditions for introducing GL into ChNFs were carried out by the batch investigation of parameters (the kinds of reactor, reaction time, reaction temperature, the use of acid for dissolution of ChNFs and the neutralization by sodium hydroxide). The degree of gluconated units (DG%) of GChNFs sponge synthesized in pressure condition at 115 $^{\circ}$C for 12 h amounted to 48.82%, whereas this value of gluconated chitosan (GChs) particles prepared from chitosan flake in reflux condition at 115 $^{\circ}$C for 24 h was 13.90%, which determined by colloidal titration. In the synthesis process of GChNFs sponge, the disappearance of acid for protonating amino groups and sodium hydroxide for the formation of particles led to the less use of reagents. The SEM images presented the fiber structure in GChNFs sponge which provided the large surface for enhancing the mass transfer in boron adsorption. The results of this study showed that ChNFs are the promising nanomaterial for green synthesis in the field of boron removal.

Keywords: chitosan nanofibers, degree of deacetylated units, degree of gluconated units, colloidal titration, NMR spectroscopy, green synthesis
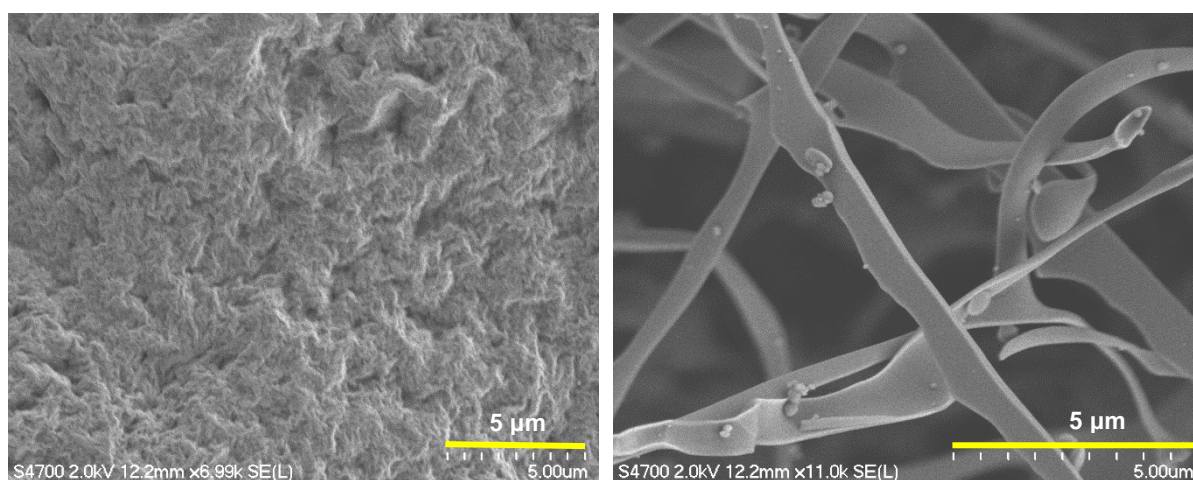
Fig. 5.1. SEM images of GChs particles prepared from chitosan flake in reflux at 115 $^{\circ}$C for 24 h and GChNFs sponge synthesized from ChNFs in pressure at 115 $^{\circ}$C for 12 h.

5.1. Introduction

Chitosan, a natural polymer, is made from the dominant deacetylated units and residue acetylated units. Chitosan is prepared from chitin by deacetylation. In this process, acetylated groups of chitin are hydrolyzed and transform to free amino groups in the alkaline environment. The degree of deacetylated units (*DD%*) is affected by the concentration of sodium hydroxide, time and temperature [161]. Chitosan has attracted tremendous interest due to its outstanding properties such as high adsorption capacity for dyes and toxic heavy metals, macromolecular structure, abundance and low cost [173]. Containing ample amino and hydroxyl groups, chitosan has been investigated as alternative substrate which is modified and functionalized by NMDG group or hydroxyl groups. Crosslinked chitosan resin with NMDG functional group was prepared for boron removal by Sabarudin et al. [127]. In this research, NMDG group was chemically fixed to the base polymer (ethylene glycol diglycidyl ether (EGDE) crosslinked with chitosan) through the support of chloromethyl oxirane. In another study, D-galactose, D-mannose, D-glucose, D-xylose, D-ribose and D-arabinose, which containing hydroxyl groups were introduced into chitosan by reductive N-alkylation. Then the obtained gel was crosslinked by EGDE for the insolubility in acidic solution [144].

Nevertheless, pH susceptibility has a significant effect on the solubility of chitosan. Depending on the pH values, chitosan can dissolve or generate gel. This polymer is not soluble in water, alkaline environment and organic solvents due to the hydrogen bonds in the repeat units [174]. In contrast, chitosan dissolves in the acidic solutions that indicate the use of acids. When chitosan is dissolved in acidic solution, free amino groups are protonated and the cationicity of this material is increased. The protonation of amino groups resulting in the formation of $(NH_3)^+$ enhances the electrostatic interaction between chitosan and negatively charged molecules [175]. Chitosan flakes and powder exhibit their limitations such as crystalline structure, low porosity, low surface area and high hydrophobicity that restricts the mass transfer and the performance of the adsorption process. The transformation of chitosan structure from flakes or powder to gel such as beads, film or membrane improve the characteristics of the raw chitosan [176-178]. These physical modification declines the crystallinity and increases the surface area and porosity of chitosan. Besides, the expansion of polymer chains contributes to the rises of the activity of functional groups like hydroxyl, free amino

groups as well as diffusion mechanism. Firstly, chitosan flakes or powder are dissolved in acidic media to generate a chitosan solution. The chitosan beads can be formed by dropping the chitosan solution into an alkaline media, and the product is obtained by drying. The formation of chitosan membranes and films are carried out by the solution casting method. Chitosan solution is poured in flat disk then dried completely. The film and membrane are removed from the mould and available to use for further experiment or immersed in the alkaline solution to increase the porosity. Since the conservation of involved chains and intermolecular interaction, the chitosan films are formed. It is attributed to the rise in chitosan concentration leads to the generation of hydrogen bonds in the drying activity which plays a vital role in polysaccharide structure [179]. In order to solve the brittle character of films or membranes, the introduction of plasticizers is essential to enhance their mechanical properties [180].

Although chitosan displays excellent properties, the low surface area and low porosity in the form of flakes, powder, films and membranes can limit their potential. For this reason, chitosan nanofibers (ChNFs) considering to be the promising nano biomaterial offers advantages that overcome the drawbacks of the conventional rigid porous structure of chitosan. ChNFs provides the larger surface area to volume ratio than the material in the nanoparticles. A flexible porous texture in ChNFs is an energetic system where the shape and pore size can adjust [181]. Furthermore, characteristics such as high porosity, interconnection, small pores size and higher mechanical strength have allowed ChNFs to be widely used in food technology (active food packaging, nanofood carrier and enzyme immobilization), biomedical application (wound dressings, drug delivery, artificial organs, tissue engineering scaffolds) [182-184].

In this work, gluconated chitosan nanofibers (GChNFs) in the form of sponge were synthesized by grafting D-(+)- glucono - 1,5 lactone (GL) into ChNFs. Various parameters of reaction time, reaction temperature, pressure, the necessity of the use of acid to dissolve ChNFs and reaction solution neutralized or not neutralized by NaOH were investigated in order to find the highest degree of gluconated units (*DG%*). The degree of deacetylated units (*DD%*) and degree of gluconated units (*DG%*) of samples were determined by ^{1}H NMR and colloidal titration. Other characterizations of samples

were conducted by Cosy NMR and SEM. Finally, The potential of chitosan nano fibers-based adsorbent applied for the removal of boron was also discussed.

5.2. Experimental

5.2.1. Materials and reagents

Chitosan flake and D-(+)- glucono - 1,5 lactone (GL) were produced from Tokyo chemical industry Co., Ltd, Japan. ChNFs were purchased from Sugino, Japan. N/400 potassium polyvinyl sulfate solution (N/400 PVSK) was produced from Fujifilm Wako, Japan. Dialysis membrane (14,000 MWCO) was purchased from Wako Chemicals USA, Inc. All aqueous solutions were prepared using Mili-Q water (18.25 MΩ.cm) from Direct-Q UV3, Merck Millipore. All other chemicals used were analytical grade and used as received without further purification.

5.2.2. Synthesis

1. Synthesis of GChs and GChNFs particles with the addition of acid

Firstly, 5 g of chitosan flakes were dissolved in 500 mL of acetic acid solution 1% (v,v) at room temperature for 12 h under mechanically stirring. Next, GL was added to the solution following the mole ratio of chitosan : GL (1 : 5). The reaction mixture was refluxed by heating in an oil bath at 115 °C for 24 h with stirring. After the mixture was cool down to room temperature, NaOH 1 M solution was added dropwise to form precipitates. Then, the mixture was centrifuged at 4000 rpm, and the precipitates were collected and dipped in acetone. The obtained product was separated by filtration and dried in vacuum overnight. Residuals of free acetic acid and unreacted GL were removed by dialysis against Mili-Q water using dialysis membrane. After the dialysis process, the precipitates in the membrane were immersed in acetone and sonicated for a few minutes. Next, the product was collected by filtration and dried completely in the vacuum at room temperature. Finally, GChs particles were obtained by crush for homogeneity. The synthesis of GChNFs particles is similar to the above process using ChNFs solution 2% (v,v).

2. Synthesis of GChNFs particles without acid

The mixture of ChNFs solution 2% (v,v) and GL with the molar ratio (1 : 5) was refluxed at 115 ºC for 24 h in mechanical stirring. The next steps were carried out the same as the synthesis of GChNFs particles with the addition of acid.

3. Synthesis of GChNFs sponge without acid

a. Synthesis of GChNFs sponge without acid in reflux condition

ChNFs solution 2% (v,v) and GL with the molar ratio (1 : 5) was refluxed at 115 ºC for 12 h in the condition of mechanical stirring. The reaction solution was kept cool down to the room temperature, and the dialysis against Mili-Q water was carried out to remove the residuals of unreacted GL. The dialysed solution was concentrated by evaporation, freeze-drying and vacuum-drying to form the sponge.

b. Synthesis of GChNFs sponge without acid in pressure condition

The mixture of ChNFs solution 2% (v,v) and GL with the molar ratio (1 : 5) was heated in the pressure vessel. Next, the oven was turned off, and the solution was kept cool down to the room temperature. Subsequently, unreacted GL was removed by dialysis. The product in the form of sponge was obtained after evaporation, freeze-drying and vacuum-drying.

In order to find the optimal condition for introducing the gluconated units to ChNFs, several parameters were investigated. The reaction time was tested at 4, 8, 12, 24 h at 115 ºC. Afterward, the temperature was examined at 70, 100 and 115 ºC for 12 h. The synthesis process of GChs and GChNFs is illustrated in Fig. 5.2.
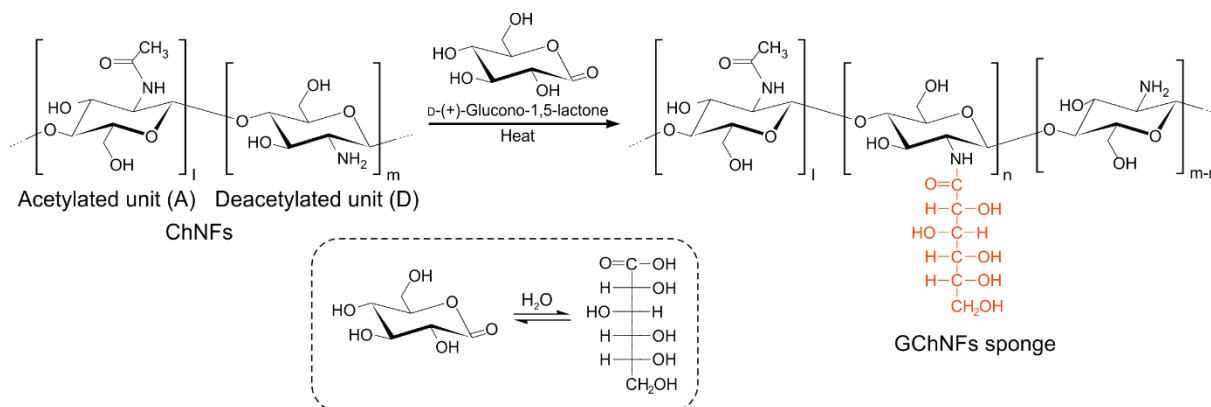

Fig. 5.2. Synthesis of GChs and GChNFs.

5.2.3. Characterization of chitosan flake, ChNFs, GChs and GChNFs

1. Proton nuclear magnetic resonance (^{1}H NMR)

^{1}H NMR data of samples dissolved in trifluoroacetic acid (CF$_3$COOH) 2% (v,v) with the solvent of deuterium oxide (D$_2$O) or only D$_2$O were recorded by JNM-ECZ400S, Jeol, Japan. The equipment was operated at 400 MHz with a pulse accumulation of 128 scans.

2. Cosy NMR

Cosy NMR spectra were collected by JNM-ECZ400S, Jeol, Japan, using a pulse accumulation of 32 scans. The samples were dissolved in CF$_3$COOH 2% (v,v) solution or only D$_2$O solvent.

3. Determination of the degree of deacetylated units (DD%) of different chitosans and degree of gluconated units (DG%) on GChs and GChNFs by colloidal titration and ^{1}H NMR methods

DD%, the mole fraction of deacetylated units in the chain and *DG%*, the mole fraction of gluconated units in the polymer are the most significant characteristics of chitosan and chitosan derivatives, which were examined by using colloidal titration and ^{1}H NMR methods. In the colloidal titration experiment, 0.1 g of sample and 8.6 mL of acetic acid solution 3 M were added to 200 mL volumetric flask, then MiliQ water was filled to reach the etched line. The completed dissolved solution was titrated by N/400 PVSK solution using toluidine blue as the indicator [185]. The endpoint was obtained when the solution changed from blue to purple pink. The titration experiment was performed in quintuplicate. *DD%* was calculated as follows:

$$DD(\%) = \frac{d}{\dfrac{W - 161d}{204} + d} \, 100 \qquad (5.1)$$

Where d is the mole of deacetylated unit (mol) and W is the dry weight of sample (g).

4. SEM analysis

Sample morphology was examined by field emission scanning electron microscope (Hitachi S-4700 FE-SEM, Japan).
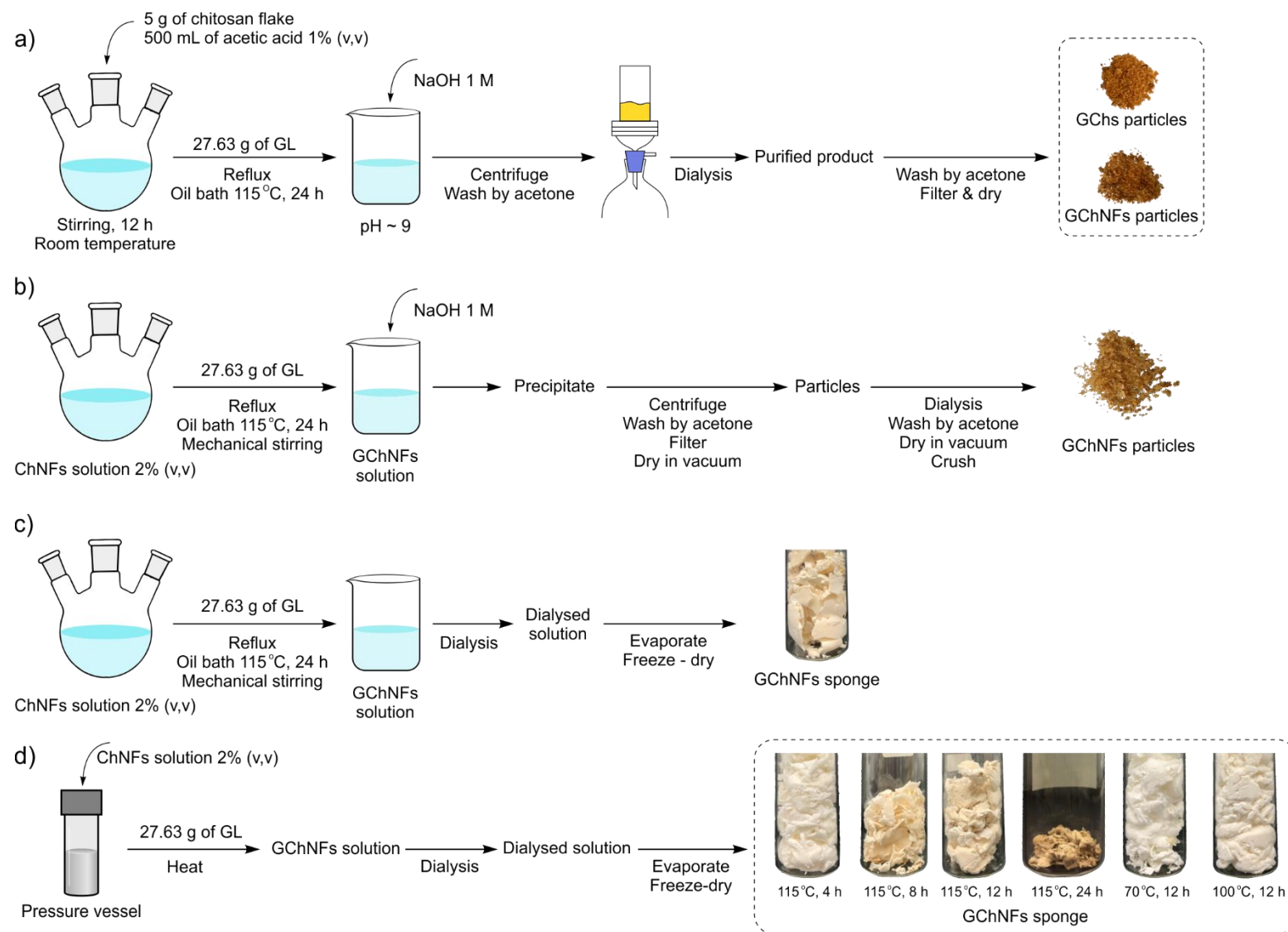
Fig. 5.3. The batch experiments of chitosan derivative and ChNFs derivatives synthesis.

5.3. Results and discussion

5.3.1. *^{1}H NMR and Cosy NMR spectra of samples*

1D NMR and 2D NMR analysis were performed to find out the structure of samples. 1D NMR offers the information about different kinds of protons but the results are sometimes limited because of the overlapping signals. This drawback can deal with 2D NMR through the correlation between protons and protons. The ^{1}H NMR spectra of chitosan flake, ChNFs, GL, chitosan derivative and ChNFs derivatives are given in Fig. 5.4 and Fig. 5.5. The highest peak at 4.79 ppm was represented to the solvent (CF$_3$COOH in D$_2$O). ^{1}H NMR spectrum of ChNFs in Fig. 5.5b exhibited the overlapping signals from 3.68 ppm to 3.84 ppm were corresponded to the protons H3 to H6 of the deacetylated units and H2 to H6 of the acetylated units in chitosan backbone glucopyranose ring [186, 187]. The proton observed independently at 3.10 ppm and 2.01 were assigned to the H2 of the deacetylated units and three methyl protons of the acetylated units, respectively. Besides, a coupling interaction shown in Fig. 5.7 was attributed to the correlation between H2 (D) and H3. The disappearance of H1 (A) and H1 (D) spots in diagonal peaks confirmed the overlap of these protons to the solvent [188]. The similar results were found for the sample of chitosan flake (Fig. 5.4b and Fig. 5.6).

As shown in Fig. 5.5a, the signal at 4.41 ppm was assigned to H7, whereas the signal developed at 4.10 ppm was related to H8 of GL. The broad signal from 3.93 to 3.61 ppm corresponded to H9 to H11. In the Cosy spectrum of GL, there was a correlation between H7 and H8. In addition, H8 was supposed to couple to H9 (Fig. 5.8).

After functionalizing by GL, the presence of a new signal at 3.93 was attributed to H8 in the sample of GChs particles_acetic acid_reflux_NaOH_115 ºC_24 h (Fig. 5.4c) [189, 190]. The remaining signals of protons H9 - H11 were overlapped with chitosan skeleton [191]. From Cosy spectrum in Fig. 5.9, it was assumed that H2 was coupled to H3, and H8 was coupled to H9. It was found that the signal at 4.16 ppm and the small signal at 4.24 ppm were both coupled to H8, indicating the splitting of H7 by H8. These results matched two samples of ChNFs derivatives in the form of particles. However, Cosy spectra of GChNFs derivatives in the form of sponge from Fig. 5.5c to Fig. 5.5i demonstrated the splitting of H8 proton which was coupled to H9. Furthermore, there

was a coupling interaction between H7 and H8, as given in Fig. 5.10 to Fig. 5.12. All above results proved that the ring of GL was opened and successfully grafted onto the chitosan and ChNFs.

5.3.2. DD% and DG% of samples

DD% of samples calculated by using the data provided from ^{1}H NMR spectra was presented by Eq. 5.2. The calculation of *DG*% values was based on (i) the integrals corresponding to H2 proton of deacetylated units compared to the integrals corresponding to methyl protons of acetylated units for all samples (Eq. 5.3) and (ii) the integrals of new peaks compared to the integrals of methyl protons of acetylated units (Eq. 5.4). According to the intact peaks, *DG*% was determined by the integrals corresponding to H7 proton of gluconated units compared to the integrals corresponding to methyl protons for GChNFs derivatives in the form of sponge or calculated by the integrals corresponding to H8 proton of gluconated units compared to the integrals corresponding to methyl protons for GChs and GChNFs in form of particles.

$$DD(\%)=\left\{1-\left[\frac{\frac{1}{3}I_{CH_3}}{\frac{1}{6}\left(I_{\substack{H2\text{-}H6(A)\\H3\text{-}H6(D)}}+I_{H2(D)}\right)}\right]\right\}100 \quad (5.2)$$

$$DG(\%)=DD(\%)-DA(\%)\,\frac{I_{H2}}{\frac{I_{CH_3}}{3}} \quad (5.3)$$

$$DG(\%)=DA(\%)\,\frac{I_{H7}\text{ or }I_{H8}}{\frac{I_{CH_3}}{3}} \quad (5.4)$$

Where I_{CH_3}, $I_{H2(D)}$, I_{H7} and I_{H8} and $I_{\substack{H2-H6(A)\\H3-H6(D)}}$ are the integral intensities of methyl protons (acetylated untits), protons connected to C2 (deacetylated units), C7, C8, C2-6 (acetylated units) and C3-6 (deacetylated units), respectively.

The results of *DD*% and *DG*% determined by ^{1}H NMR and colloidal titration are shown in Table 5.1. The *DD*% of both two kinds of chitosan amounted to approximately 86.00% by the calculation of ^{1}H NMR, and this value of chitosan flake (84.65%) was smaller than ChNFs sample (88.11%) as follow the colloidal titration. It was obvious

that the *DG*% of GChs particles had the lowest level, which made up from 11.74 to 13.90%. While the *DG*% of GChNFs particles with the use of acid solution constituted between 13.02 and 29.67%, the value of GChNFs particles without using acid increased slowly (13.88 to 35.49%) in the same conditions of reflux, reaction temperature and reaction time; in contrast, there was a marked rise in the *DG*% of GChNFs sponge, which was between 17.83 and 50.35% although the reaction time reduced a half. These results indicated that GL was able to introduce directly into ChNFs solution without acid, whereas the form of chitosan solution required the use of acid. Secondly, the *DG*% of GChNFs sponge higher than GChNFs particles was attributed to the surface area of GChNFs sponge larger than GChNFs particles, indicating the unnecessary of NaOH presence.

In order to find out the optimal conditions for grafting GL, the reaction was investigated in the same pressure at 115 °C with the variety of reaction time from 4 to 24 h. It was clear that the more reaction time was carried out, the more *DG*% level was obtained, and this value reached the highest level from 27.81 to 52.42% in the sample of 24 h. Moreover, the colour changed from yellow (4 h) to brown (12 h) and turned out black (24 h) was explained by the chemical reaction between amino groups in chitosan and GL at the high temperature which was referred to Maillard reaction [192]. It is worth mentioning that the production of antioxidants and antibiotic compounds were found after browning reaction [193]. The decomposed compounds were regarded as the cause of black solution at 115 °C for 24 h. This confirmed that the new peaks of this sample were observed in ^{1}H NMR spectrum (Fig. 5.5f). Therefore, GChNFs sponge synthesized in pressure for 12 h was chosen for the further investigation with the different temperature at 70, 100 and 115 °C, and the sample tested at 115 °C had the highest level (23.47 - 48.22%). Comparing to GChNFs sponge was refluxed at 115 °C for 12 h, this sample had the similar *DG*% following the colloidal titration but its *DG*% was much higher based on ^{1}H NMR. For these reasons, GChNFs sponge prepared by the reaction between ChNFs and GL in pressure at 115 °C for 12 h was chosen for the further experiment.

5.3.3. SEM analysis

The morphology of the obtained samples was observed by FE-SEM. The images of chitosan flakes in Fig. 5.13 displayed the various pieces with a smooth and tight surface, whereas ChNFs showed a homogeneous system of fibrous layers (Fig. 5.14). After grafting GL into chitosan and ChNFs, GChs and GChNFs particles possessed a much porous and rough surface (Fig. 5.15 and Fig. 5.16); however, the fiber structure was disappeared and replaced by the porous structure in GChNFs particles with and without acid (Fig. 5.16 and Fig. 5.17). In contrast, Fig. 5.18 to Fig. 5.24 showed both GChNFs sponge synthesized in the condition of reflux or pressure with freeze-drying still sustained the fiber structure. It was suggested that the conversion of chitosan in the acid solution to the particles in the presence of sodium hydroxide could enhance the porosity of chitosan derivatives. Nevertheless, NaOH solution was able to compress the fiber, leading the transformation from fiber to porous structure in the process of precipitate formation. All these results were supposed the decrease of $DG\%$ in GChNFs particles that given in ^{1}H NMR calculation. As shown in Fig. 5.21, the SEM images of GChNFs sponge prepared in pressure at 115 ºC for 24 h provided several microspheres, indicating the decomposed compounds in the synthesis process at high temperature for long reaction time. This result was consistent with ^{1}H NMR analysis.

Chitosan undergoes the drawbacks of low porosity and surface area, resulting in the limitation of mass transfer and a decrease in the capacity of adsorption. In order to overcome these disadvantages, chitosan has been modified by physical methods in the previous researches. Firstly, chitosan flake or powder was dissolved in an acidic solution to expand the polymer chain, leading to the activation of functional groups. Next, chitosan solution turned to beads, membrane or film with the support of sodium hydroxide solution. This physical modification enhanced the porosity, surface area and activity of functional groups in chitosan and improved its swelling and diffusion characteristics. In our work, ChNFs demonstrates the excellent material owning the large surface area with the fiber structure. In particular, acid solution is not required in the process of extending the chain in the polymer, and the addition of sodium hydroxide in unnecessary to improve the porosity of ChNFs. Physical modification of chitosan from the form of flake or powder to nanofibers provide the new method for enhancing the properties of chitosan. Furthermore, the synthesis process of GChNFs sponge from ChNFs is considered to the green synthesis due to the decrease in the use of reagents.

Table 1 Characteristics of chitosan, ChNFs, chitosan derivative and ChNFs derivatives.

Sample	^{1}H NMR			Colloidal titration		Solubility [3]			
	DD (%)	DG (%) (H2:CH$_3$)	DG (%) (H7:CH$_3$) or (H8:CH$_3$)	DD (%)	DG (%)	HCl 0.1 M	Boric solution [4]	Water	Borax solution [5]
Chitosan flake	86.02			84.65 ± 0.63					
ChNFs	85.98			88.11 ± 0.45					
GChs particles_acetic acid_reflux_NaOH_115 ºC_24 h		11.74	13.46 [1]		13.90 ± 0.29	+	-	-	- o
GChNFs particles_acetic acid_reflux_NaOH_115 ºC_24 h		14.05	13.02 [1]		29.67 ± 0.33	+	-	-	- o
GChNFs particles_no acid_reflux_NaOH_115 ºC_24 h		13.88	17.51 [1]		35.49 ± 0.41	+	-	-	- o
GChNFs sponge_no acid_pressure_freeze drying_115 ºC_4 h		13.00	10.88 [2]		40.91 ± 0.29	+	+	+	+
GChNFs sponge_no acid_pressure_freeze drying_115 ºC_8 h		14.81	20.82 [2]		44.37 ± 0.26	+	+	+	+
GChNFs sponge_no acid_pressure_freeze drying_115 ºC_12 h		27.40	23.47 [2]		48.82 ± 0.26	+	+	+	+
GChNFs sponge_no acid_pressure_freeze drying_115 ºC_24 h		35.55	27.81 [2]		52.42 ± 0.29	+	+	+	+
GChNFs sponge_no acid_pressure_freeze drying_70 ºC_12 h		15.37	1.72 [2]		36.63 ± 0.33	+	+	+	+
GChNFs sponge_no acid_pressure_freeze drying_100 ºC_12 h		18.69	16.56 [2]		49.98 ± 0.25	+	+	+	+
GChNFs sponge_no acid_reflux_freeze drying_115 ºC_12 h		18.02	17.83 [2]		50.35 ± 0.25	+	+	+	+

[1] *DG*% values were calculated from the integrals corresponding to H8 proton of gluconated units compared to the integrals corresponding to methyl protons of acetylated units.

[2] *DG*% values were calculated from the integrals corresponding to H7 proton of gluconated units compared to the integrals corresponding to methyl protons of acetylated units.

[3] "-": represents soluble, "+": represents insoluble and "o": represents swelling.

[4] Boric acid solution as B 400 ppm (pH 5.57)

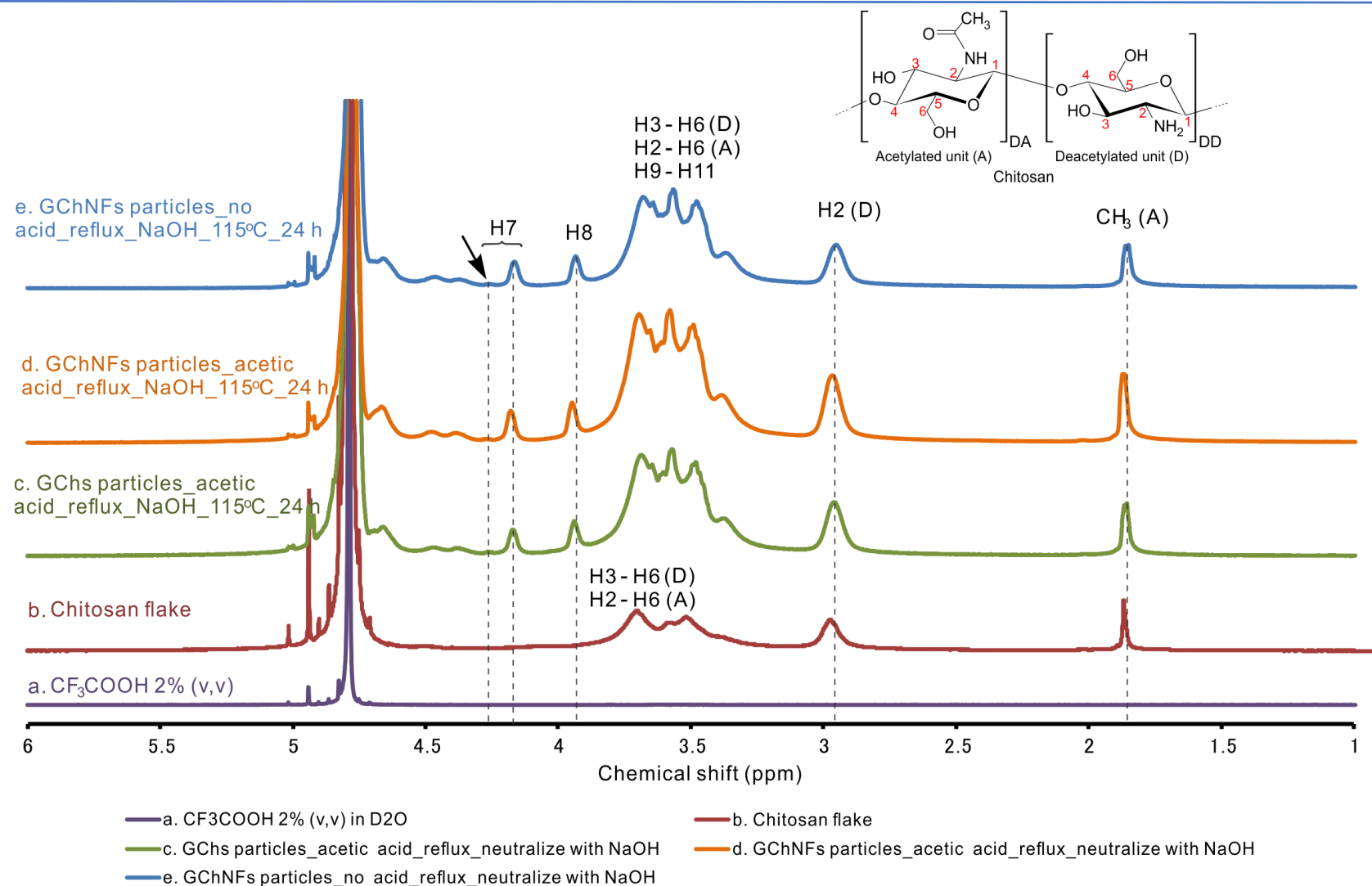[5] Borate solution as B 400 ppm (pH 9.27)

Fig. 5.4 ^{1}H NMR spectra of CF$_3$COOH 2% (v,v) (a), chitosan flake (b), chitosan derivative (c) and ChNFs derivatives (d) - (e) with the neutralization of NaOH 1M. Sample (b) to sample (e) were dissolved in CF$_3$COOH 2% (v,v) solution.

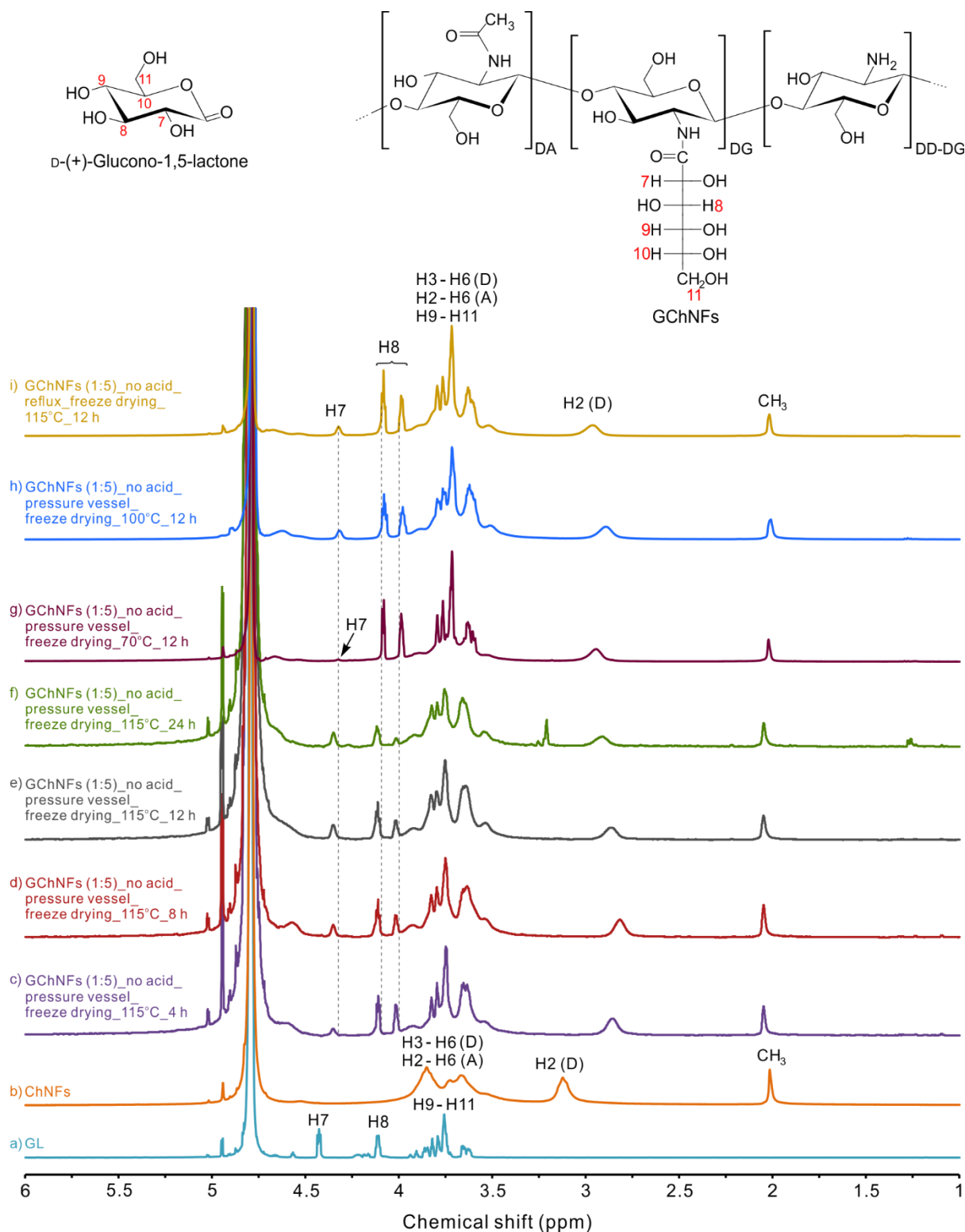Fig. 5.5. ^{1}H NMR spectra of GL (a), ChNFs (b) and GChNFs derivatives (c) - (i). Sample (a) and sample (c) to sample (i) were dissolved in D$_2$O. Sample (b) was dissolved in CF$_3$COOH 2% (v,v) solution.
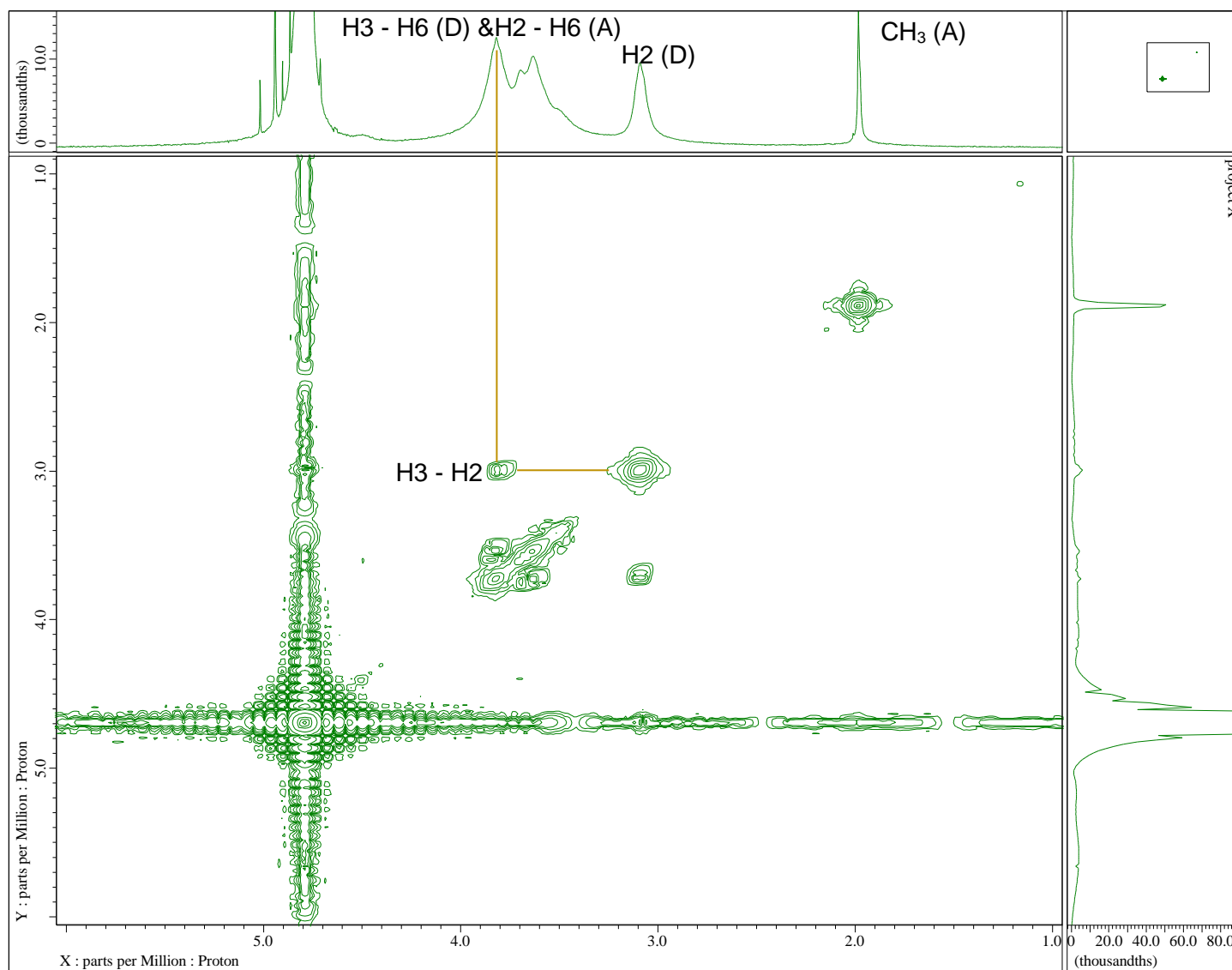
Fig. 5.6. Cosy NMR spectrum of chitosan flake.
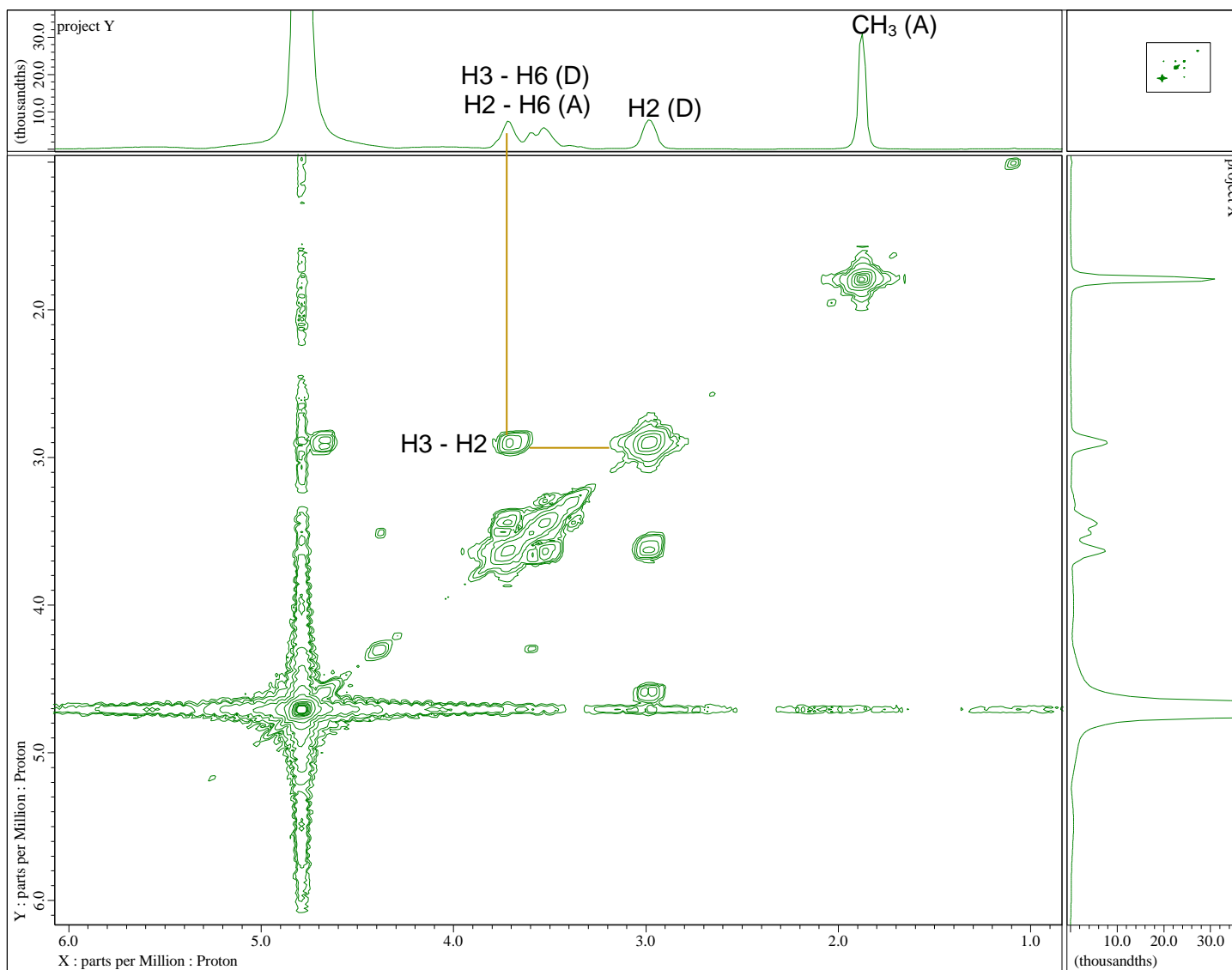
Fig. 5.7. Cosy NMR spectrum of ChNFs.
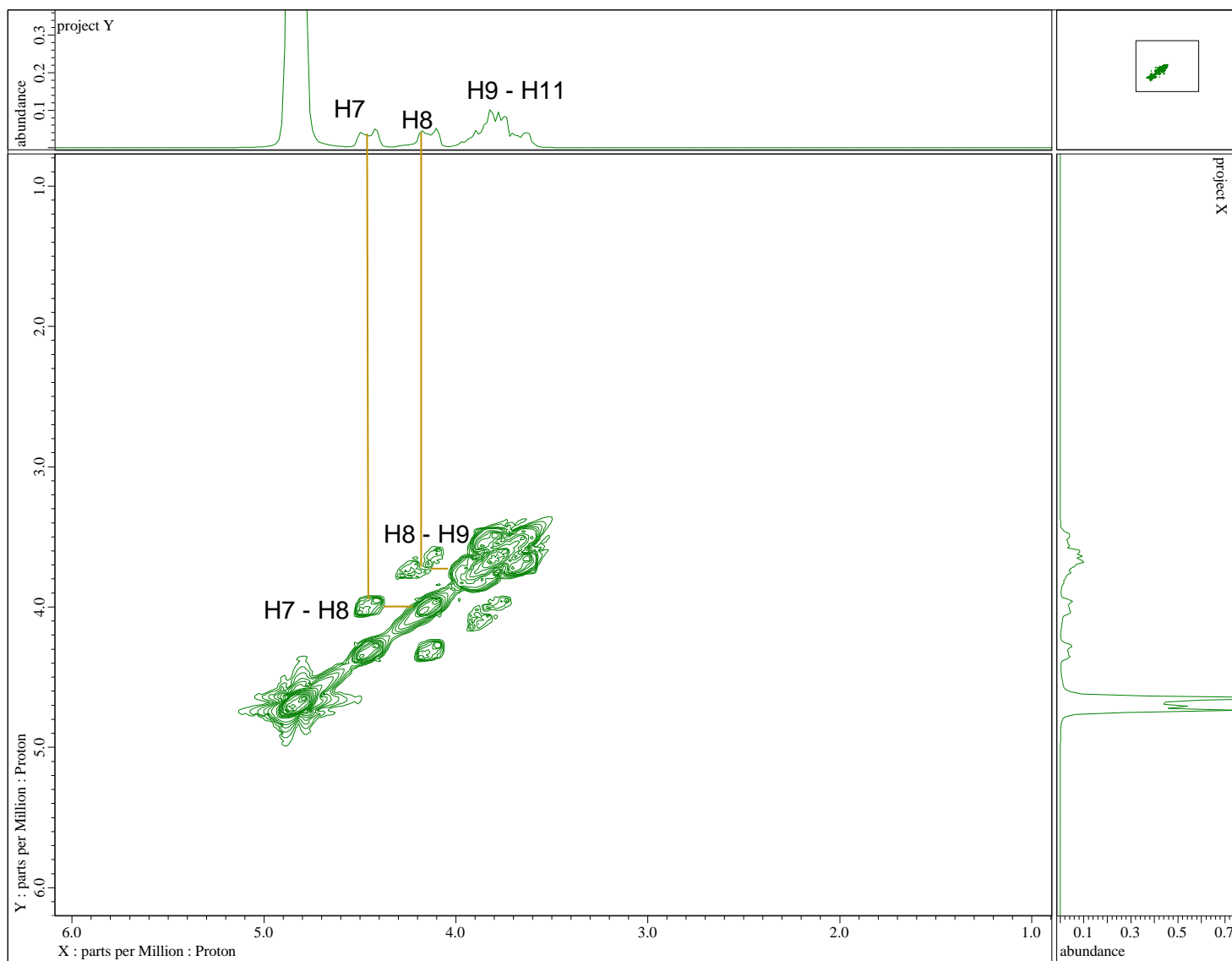
Fig. 5.8. Cosy NMR spectrum of GL.
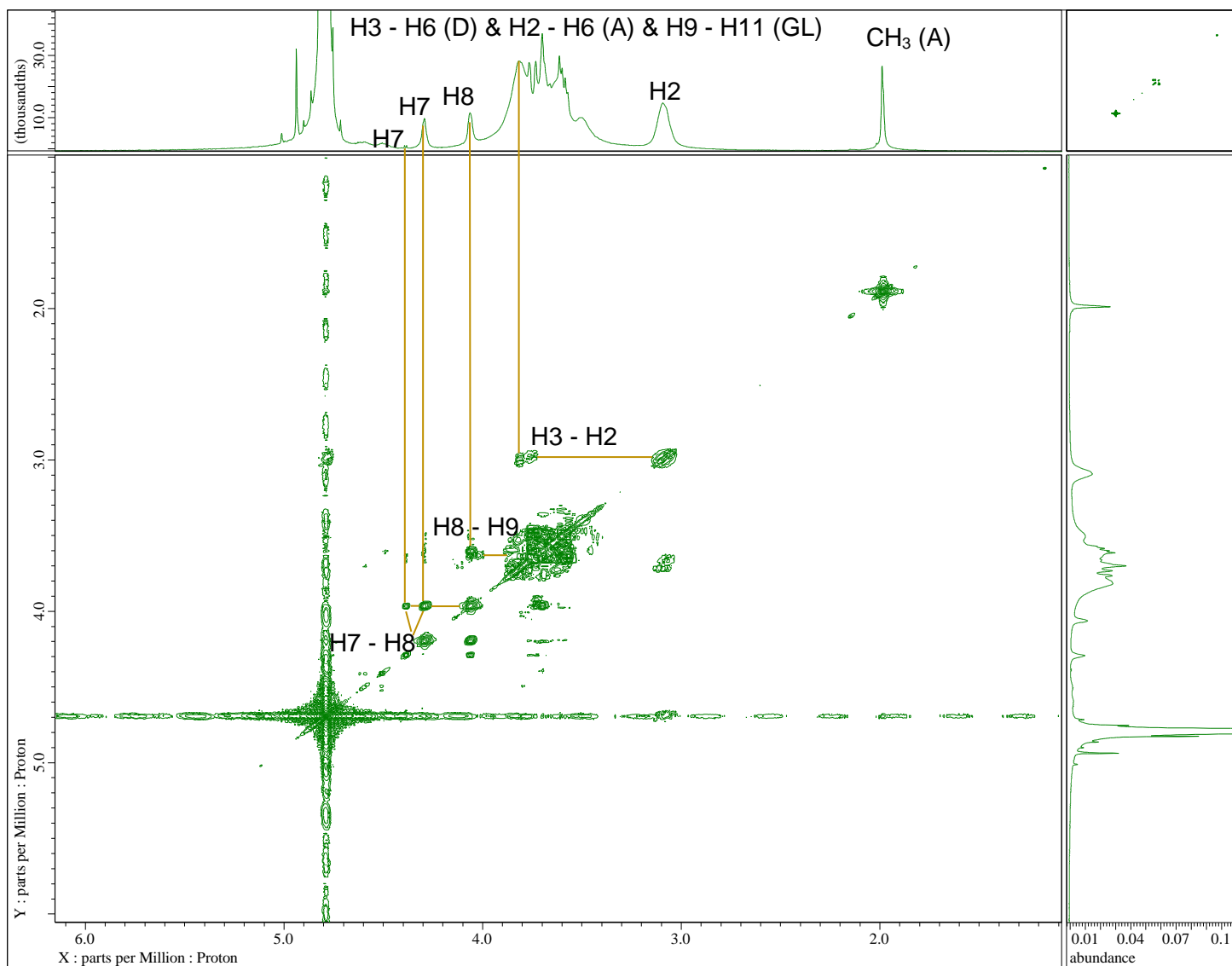
Fig. 5.9. Cosy NMR spectrum of GChs particles_acetic acid_reflux_NaOH_115 ºC_24 h.
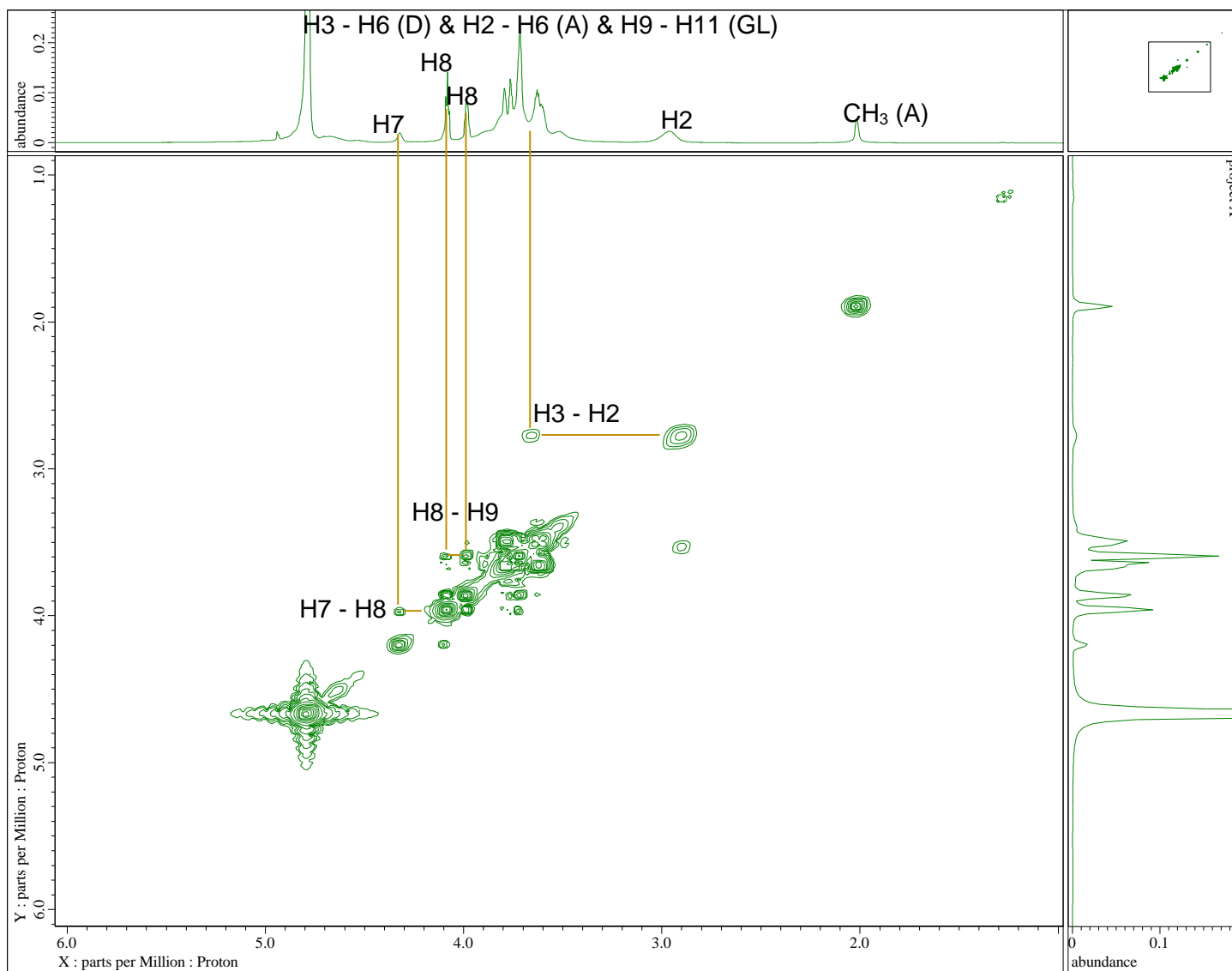
Fig. 5.10. Cosy NMR spectrum of GChNFs sponge_no acid_pressure_freeze drying_100 ºC_12 h.
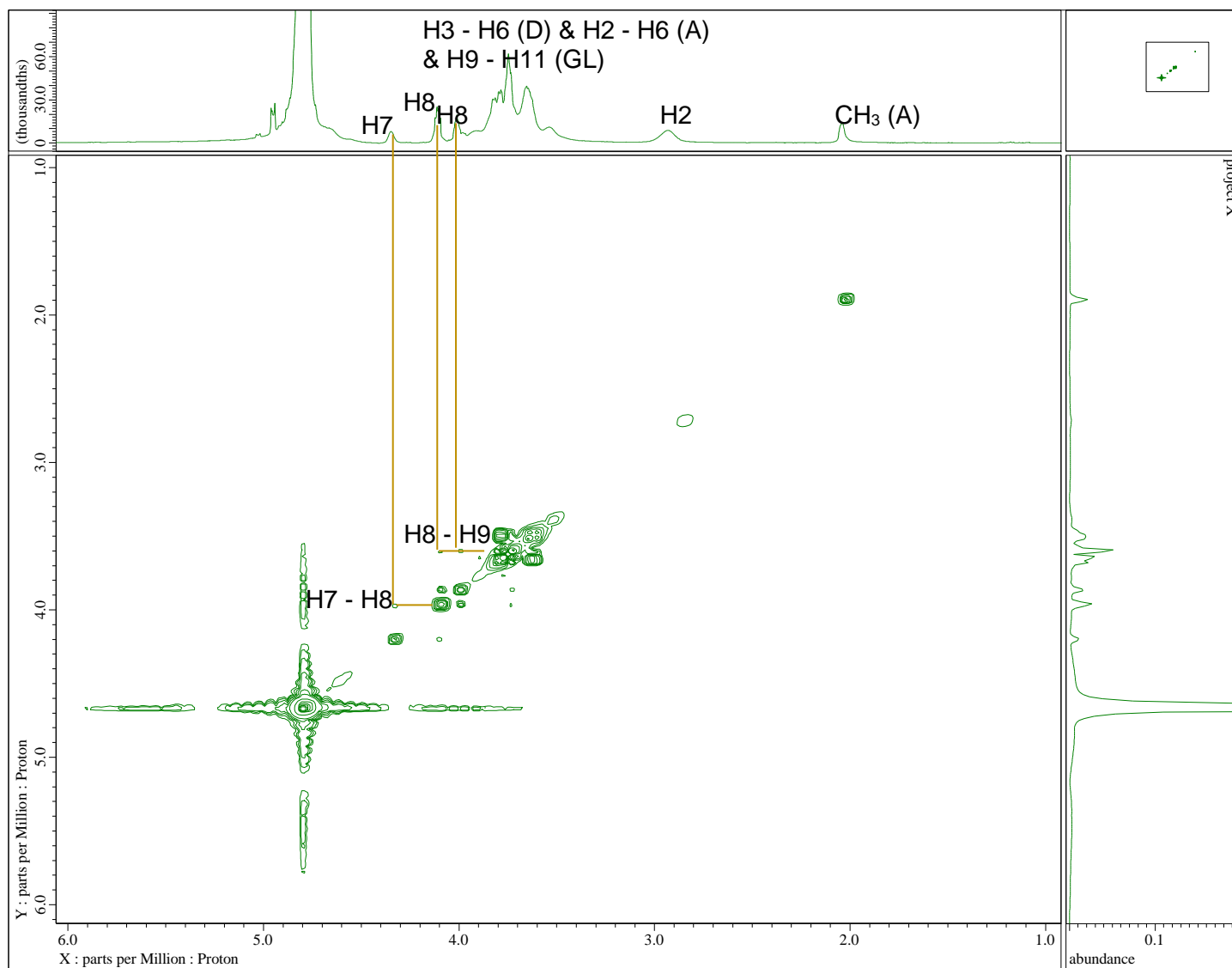
Fig. 5.11. Cosy NMR spectrum of GChNFs sponge_no acid_pressure_freeze drying_115 ºC_12 h.

Fig. 5.12. Cosy NMR spectrum of GChNFs sponge_no acid_reflux_freeze drying_115 ºC_12 h.

Fig. 5.13. SEM images of chitosan flake.
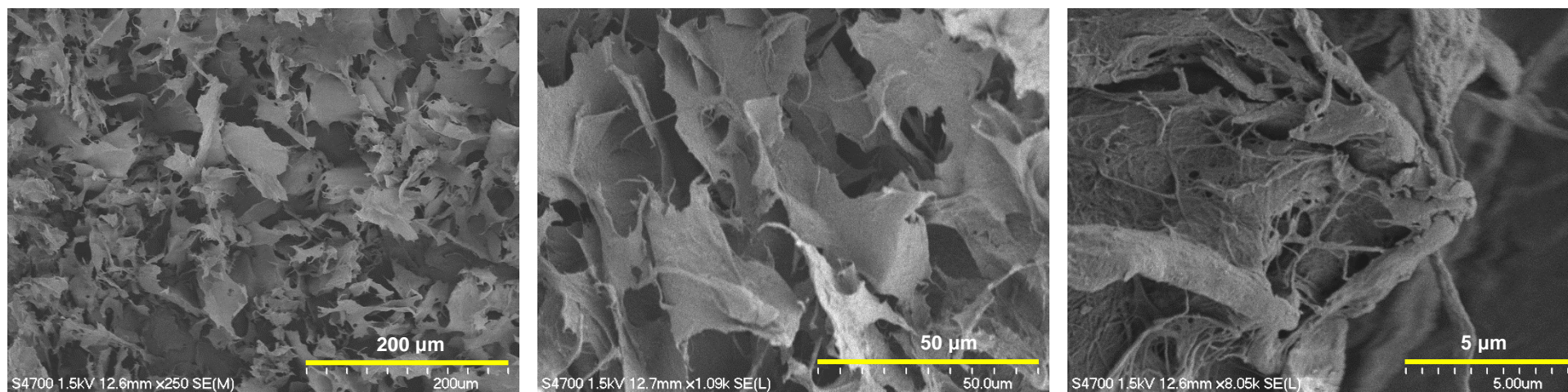
Fig. 5.14. SEM images of ChNFs sponge after freeze drying.
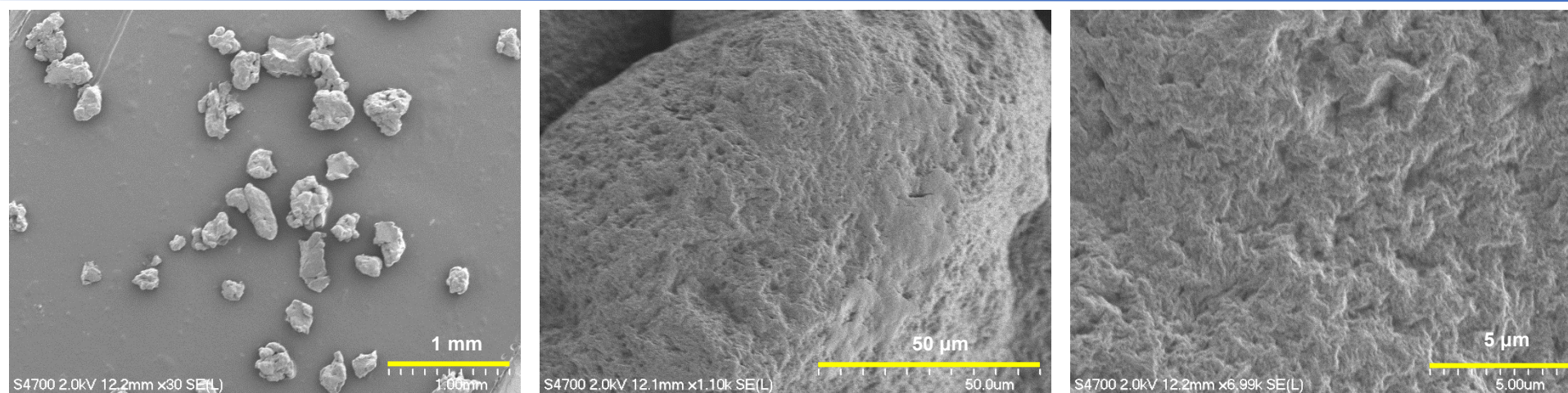
Fig. 5.15. SEM images of GChs particles_acetic acid_reflux_NaOH_115 ºC_24 h.
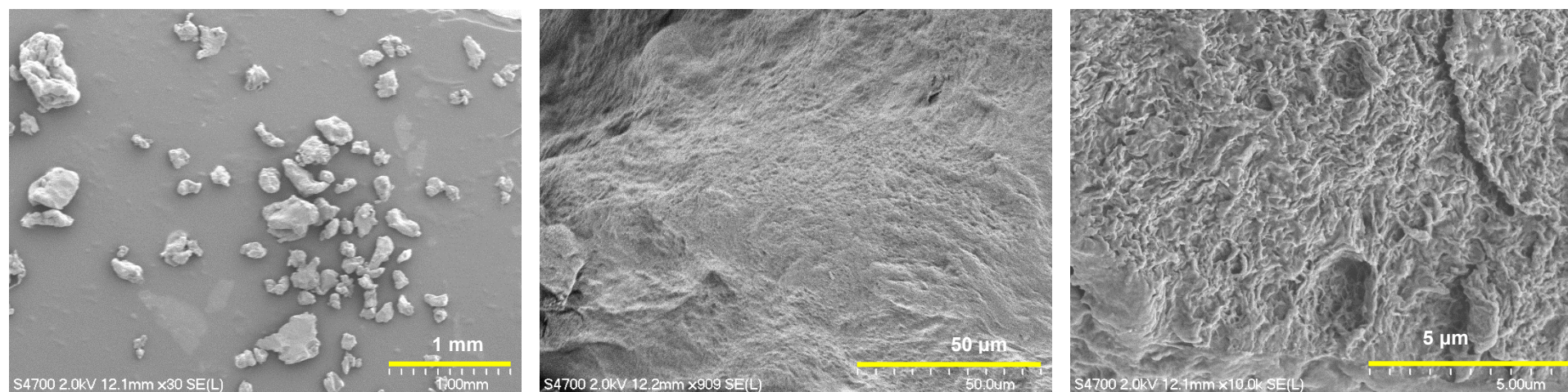
Fig. 5.16. SEM images of GChNFs particles_acetic acid_reflux_NaOH_115 ºC_24 h.
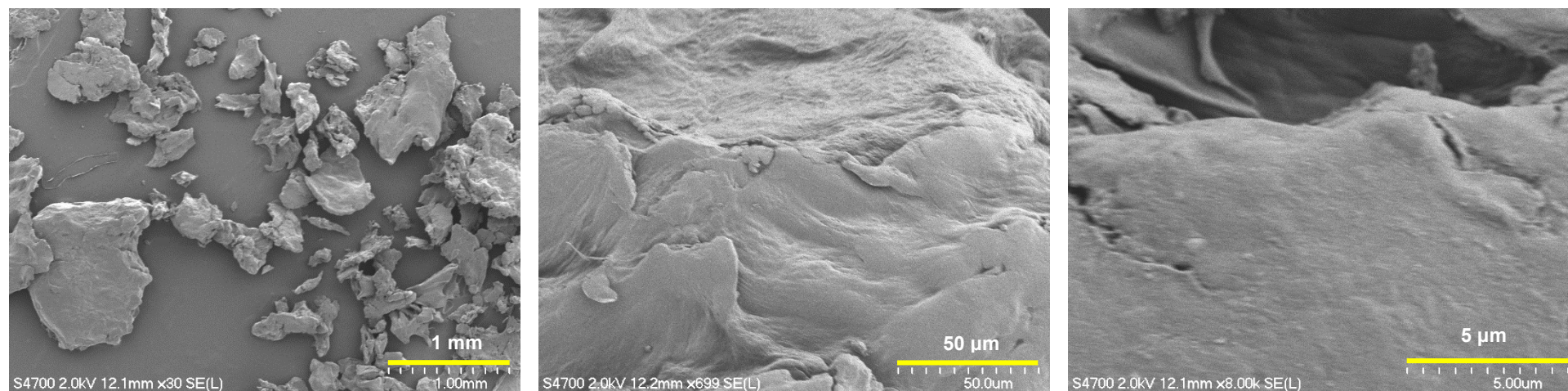
Fig. 5.17. SEM images of GChNFs particles_no acid_reflux_NaOH_115 ºC_24 h
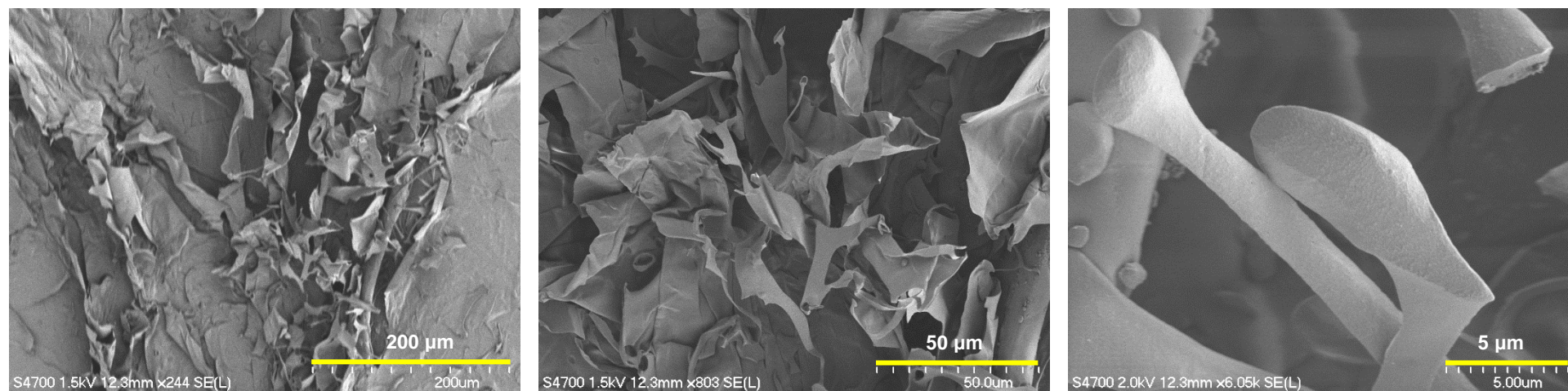
Fig. 5.18. SEM images of GChNFs sponge_no acid_pressure_freeze drying_115 ºC_4 h.
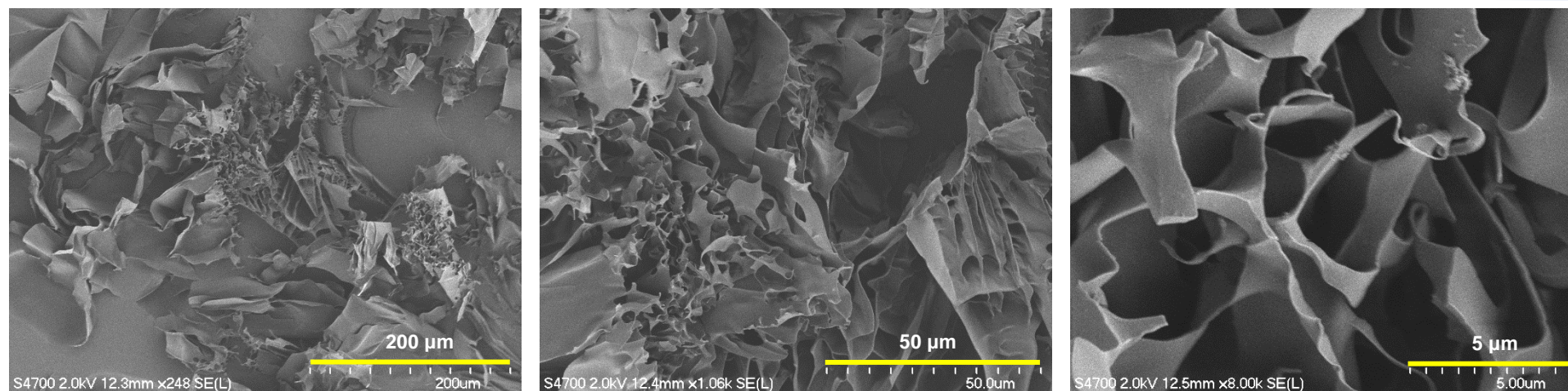
Fig. 5.19. SEM images of GChNFs sponge_no acid_pressure_freeze drying_115 ℃_8 h
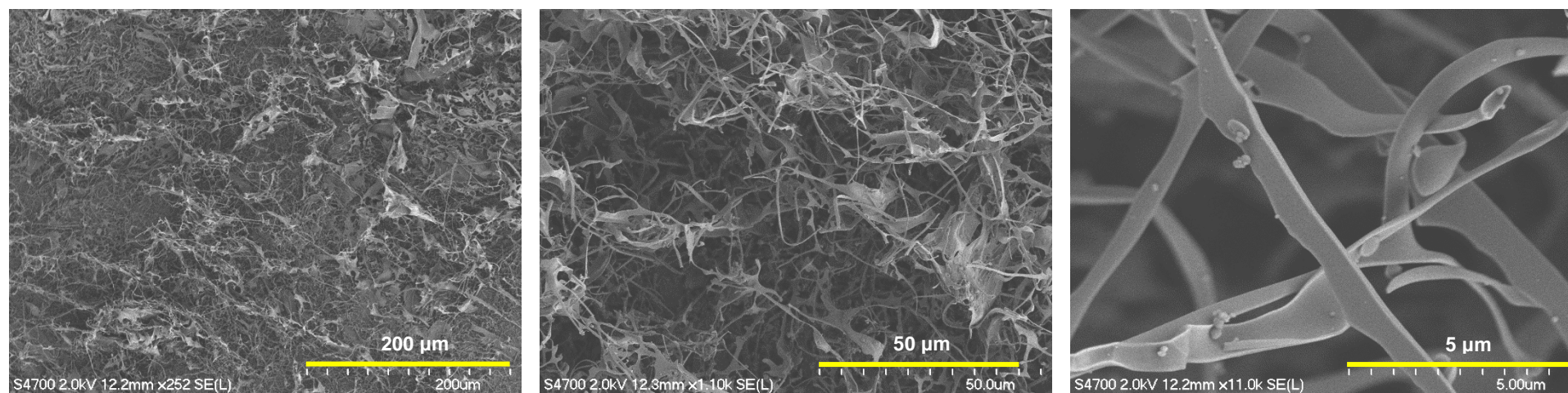
Fig. 5.20. SEM images of GChNFs sponge_no acid_pressure_freeze drying_115 ℃_12 h
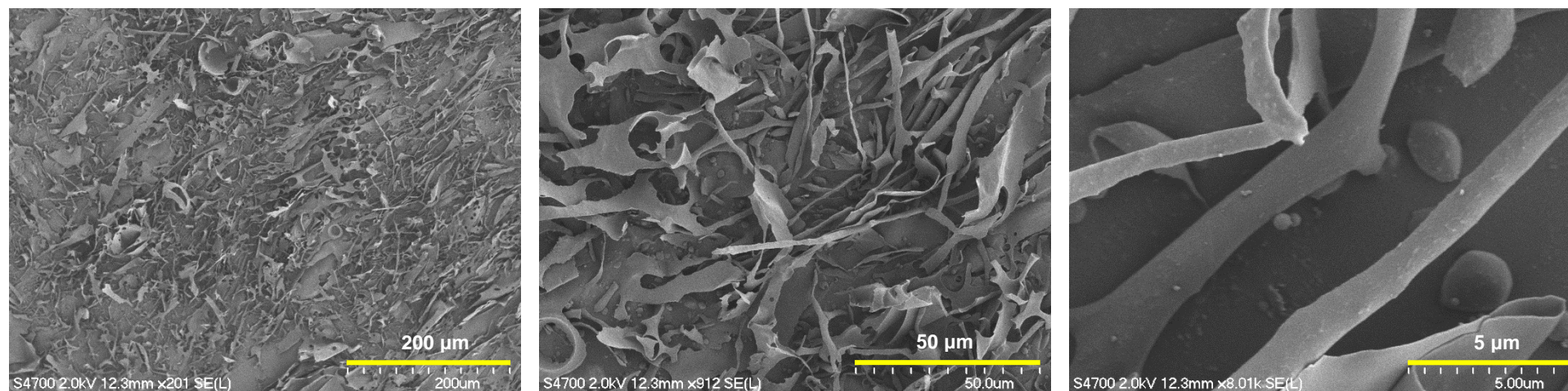
Fig. 5.21. SEM images of GChNFs sponge_no acid_pressure_freeze drying_115 ºC_24 h.
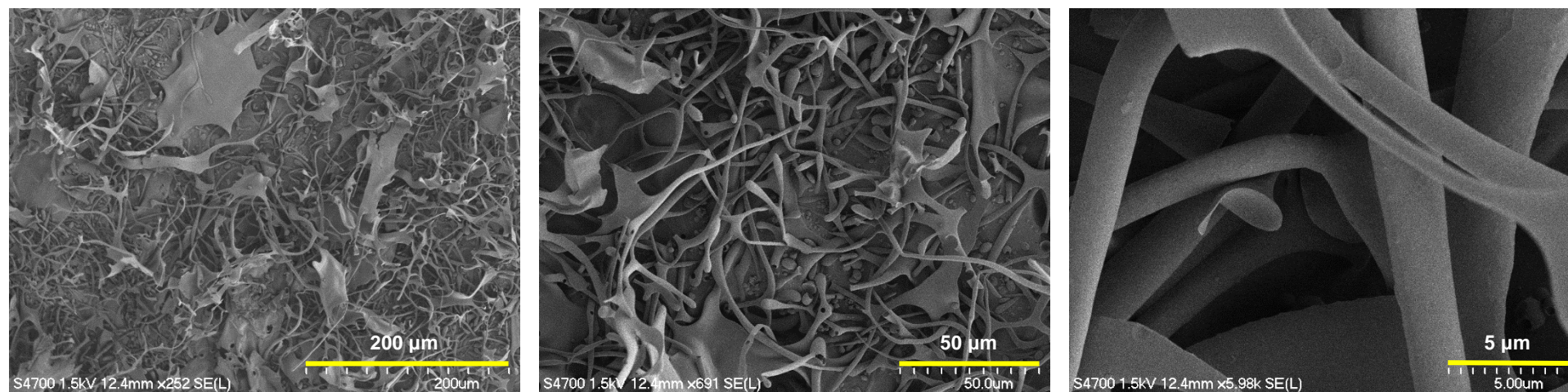
Fig. 5.22. SEM images of GChNFs sponge_no acid_pressure_freeze drying_70 ºC_12 h
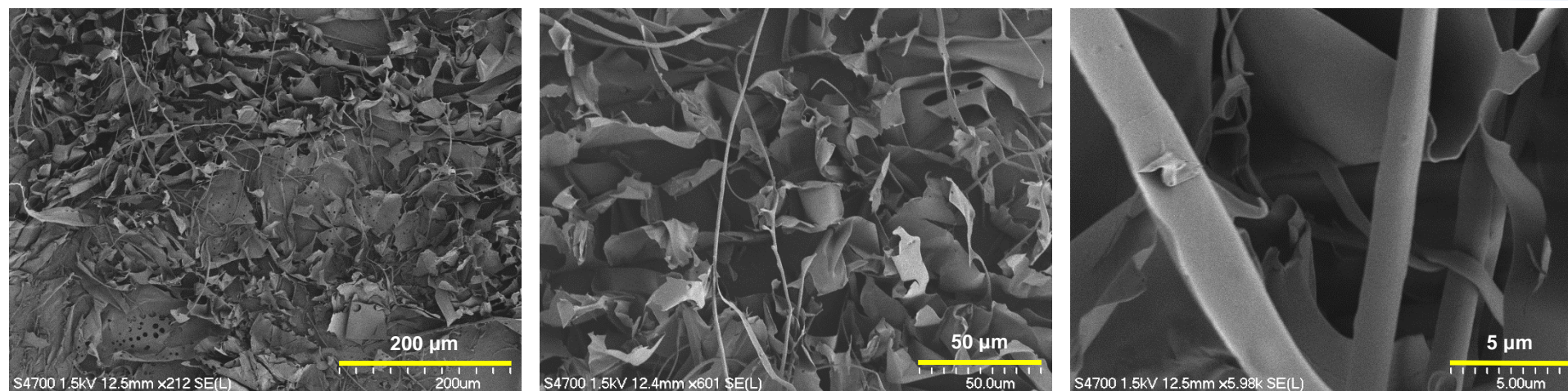
Fig. 5.23. SEM images of GChNFs sponge_no acid_pressure_freeze drying_100 ºC_12 h

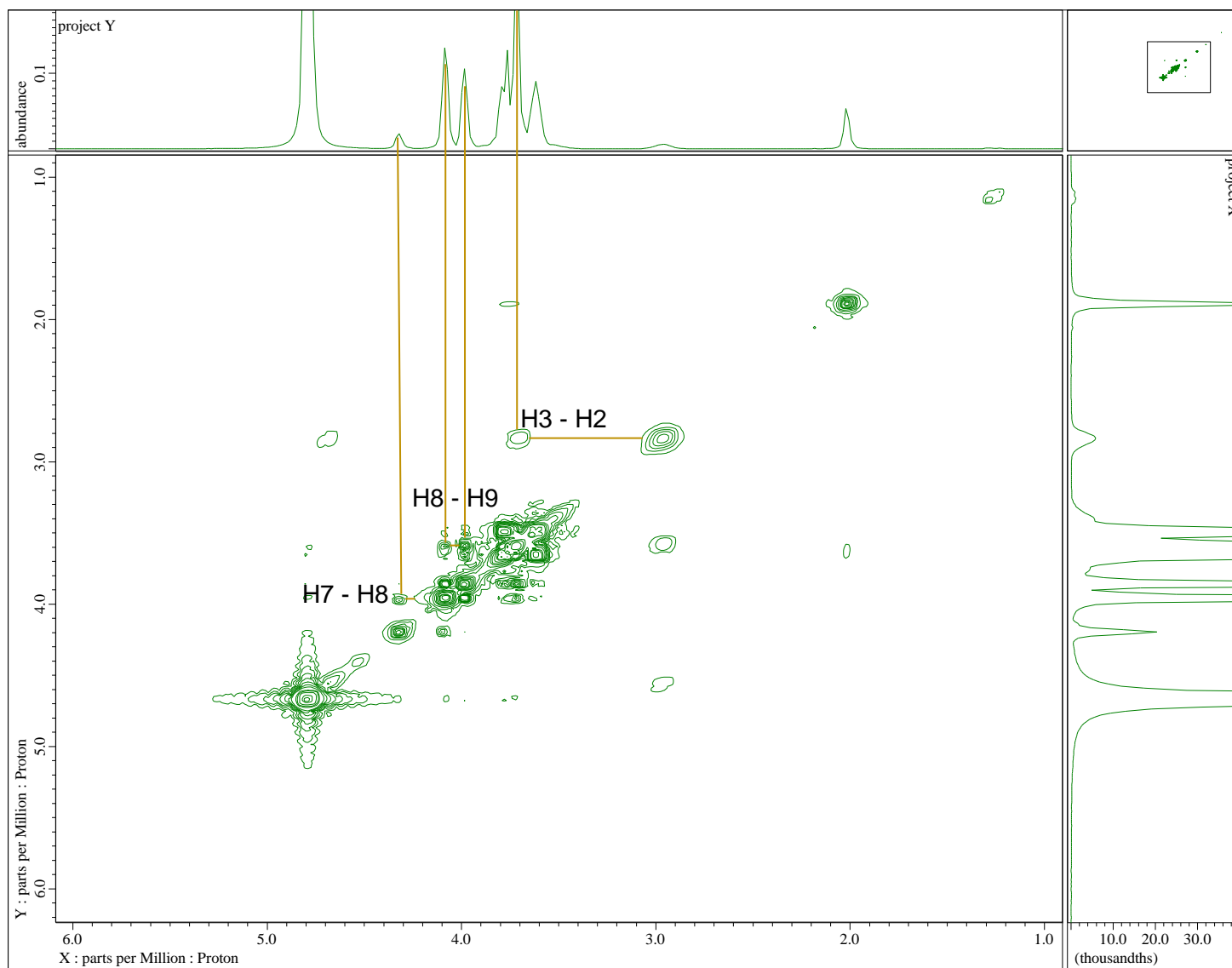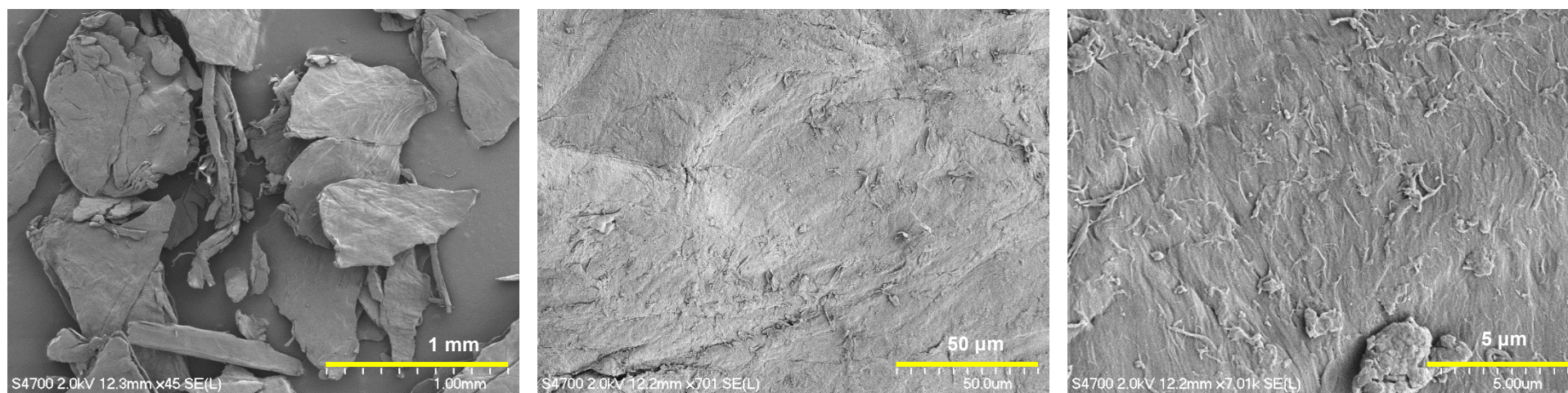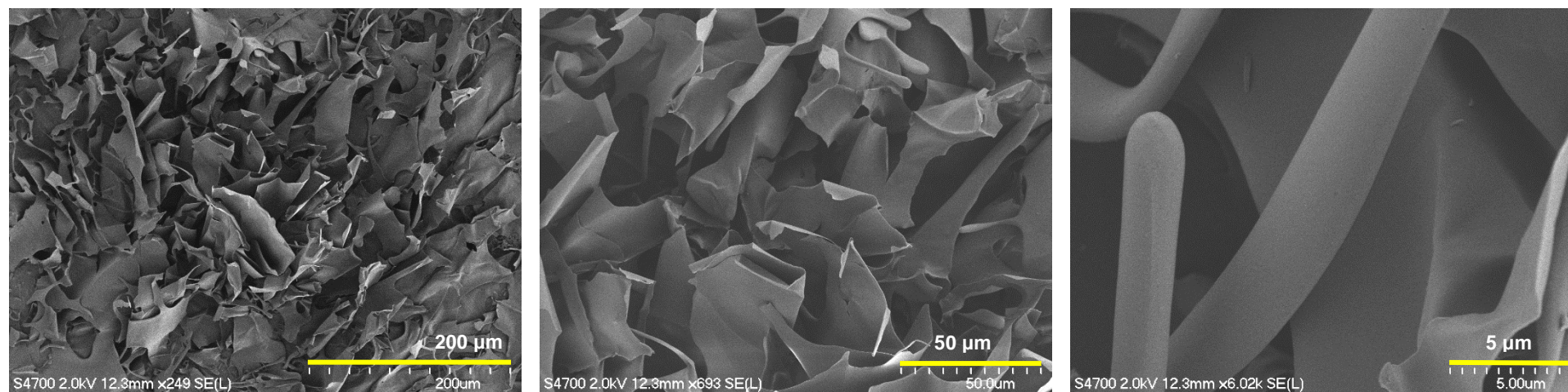Fig. 5.24. SEM images of GChNFs GChNFs sponge_no acid_reflux_freeze drying_115 ºC_12 h.

5.4. Conclusion

ChNFs were successfully functionalized with GL to develop the novel material with the high content of *vis*-diols for enhanced boron removal. GChNFs sponge prepared in pressure condition at 115 ℃ for 12 h had the *DG*% determined by colloidal titration 3.5 times higher than GChs particles prepared from chitosan flake in reflux condition at 115 ℃ for 24 h. ChNFs was able to react directly with GL without using acid, and the products were obtained with the absence of sodium hydroxide. SEM images showed the fiber structure in GChNFs, providing the large surface for enhanced boron adsorption. The great performance of ChNFs in the increase in surface area of adsorbent, the decrease in the use of reagents and the simple synthesis process offered the promising material for the development of an eco-friendly method for boron removal.

Chapter 6

Conclusions and outlook

This work can be divided into two separate parts. The first part of the study focused on the removal of phosphate from aqueous solution using natural dietary fibers and minerals. In the second part, green synthesis and characterization of the novel multi-hydroxyl functionalized chitosan and chitosan nanofibers for removal of boron were investigated. This chapter will discuss more detail in the principal outcomes, their applications and perspective for future study.

Removal of phosphate from aqueous solution using natural dietary fibers and minerals (Chapter 1 to 2)

In **chapter 1**, the general introduction of phosphorus and its removal processes was discussed. The excess of phosphate cause eutrophication that harms aquatic ecosystem functions and human health. In contrast, the decline in the reserve of phosphate ore and rock results in the shortage of fertilizer production and food supply in the future. The review of methods for phosphorus element removal and their advantages and disadvantages in the recovery the products for fertilizer production was presented.

In **chapter 2**, phosphate removal using calcium oxide (CaO) and calcium hydroxide $Ca(OH)_2$, the dominant compounds in calcined shells were investigated. The precipitates formed after the reaction between CaO or $Ca(OH)_2$ and phosphate solution at 50 mg/L could pass through the 2.7 μm filter paper by filtration. Due to the addition of flocculants of alginic acid: $NaHCO_3$: $CaCl_2.2H_2O$ with the weight ratio 1: 0.3: 0.02, the phosphate removal rate of samples filtered through 2.7 μm filter paper increased rapidly from 20 to 97%, and this removal rate was similar to the samples filtered via 0.2 μm membrane filter without flocculants which reach the highest level at 99%. The results suggest that the non-toxic flocculants of alginic, $NaHCO_3$ and $CaCl_2.2H_2O$ are effective for phosphate removal from 20 to 120 mg/L. Moreover, hydroxylapatite $Ca_{10}(PO4)_6(OH)_2$ generated after precipitation can be applied as the fertilizer for agricultural activities.

Further study is needed to investigate the capacity of the phosphate removal of using the real calcined shells from egg, crab or mussel with the addition of flocculants, and the phosphate solution can be collected from wastewater.

Green synthesis and characterization of the novel multi-hydroxyl functionalized chitosan and chitosan nanofibers for removal of boron (Chapter 3 to 5)

In **chapter 3**, the general introduction of boron and its removal processes was discussed. The commercial applications of boron and its compounds lead to the high boron concentration in wastewater. When boron amount is higher than the demand, boron toxicity on crops and human being have been recorded. The strong stable borate complexes are formed by the interaction of boric acid or borate ion with alcohols, polysaccharide and polyols containing multiple hydroxyl functional groups in the cis position (*vis*-diols). Commercial boron-selective adsorbents and their improvement versions have been reported by the numerous previous researches. The review of boron removal by various boron-selective adsorbents and their strengths and drawbacks was discussed.

In **chapter 4**, GChs were successfully modified by the functionalization of chitosan with GL in the simple process to provide the adsorbents with boron-selective sections for boron removal. The maximum boron adsorption capacity of GChs amounted to 5.8 mg/g after 700 min. The adsorption isotherm data were well fitted to Langmuir model ($R^2 = 0.9993$). The adsorption kinetics of boron was following the pseudo-second order model. The adsorption process was not considerably affected by pH wide range from 5.6 to 8.9, implying the pH adjustment is not required for the treatment of wastewater contaminated by boron. This finding confirms the reduction in chemical use in the boron removal using GChs. Due to the slight increase in boron adsorption after the addition of NaCl, GChs could be applied for boron removal from saline water or sea water. The achieved results revealed that GChs could be the non-toxic and affordable adsorbents for the removal of boron from aqueous solution.

In **chapter 5**, the novel GChNFs were successfully synthesized with GL with the high content of *vis*-diols for enhanced boron removal. GChNFs sponge prepared in pressure condition at 115 ℃ for 12 h had the *DG*% determined by colloidal titration 3.5 times higher than GChs particles prepared from chitosan flake in reflux condition at 115 ℃ for 24 h. In the process of GChNFs synthesis, the disappearance of the acidic solution for protonating amino groups and sodium hydroxide for the formation of particles resulted in the less use of reagents. The SEM images showed the fiber structure in

GChNFs which provided the large surface for enhancing the mass transfer in boron adsorption. The excellent performance of ChNFs in the rise in the surface area of adsorbent, the decrease in the use of chemicals and the facile synthesis process offered the promising material for the development of an eco-friendly method for boron removal.

For the next research, the investigation of boron adsorption behaviour of GChNF is going to carry out to strongly confirm the outstanding characteristics of this adsorbent comparing to GChs.

Reference

[1] R. Shabnam, M.H. Tarek, M.T. Iqbal, Understanding phosphorus dynamics in wheat plant and growth response in a split-root system in acidic soil, Agriculture and Natural Resources 52 (2018) 259-265.

[2] B. Wang, M. Xin, Q. Wei, L. Xie, A historical overview of coastal eutrophication in the China Seas, Marine Pollution Bulletin 136 (2018) 394-400.

[3] A. Ménesguen, G. Lacroix, Modelling the marine eutrophication: A review, Science of The Total Environment 636 (2018) 339-354.

[4] S.P. Boeykens, M.N. Piol, L. Samudio Legal, A.B. Saralegui, C. Vázquez, Eutrophication decrease: Phosphate adsorption processes in presence of nitrates, Journal of Environmental Management 203 (2017) 888-895.

[5] R.B. Chowdhury, G.A. Moore, A.J. Weatherley, M. Arora, Key sustainability challenges for the global phosphorus resource, their implications for global food security, and options for mitigation, Journal of Cleaner Production 140 (2017) 945-963.

[6] Y.V. Nancharaiah, S. Venkata Mohan, P.N.L. Lens, Recent advances in nutrient removal and recovery in biological and bioelectrochemical systems, Bioresource Technology 215 (2016) 173-185.

[7] H. Hauduc, I. Takács, S. Smith, A. Szabo, S. Murthy, G.T. Daigger, M. Spérandio, A dynamic physicochemical model for chemical phosphorus removal, Water Research 73 (2015) 157-170.

[8] O. Nir, R. Sengpiel, M. Wessling, Closing the cycle: Phosphorus removal and recovery from diluted effluents using acid resistive membranes, Chemical Engineering Journal 346 (2018) 640-648.

[9] S.K. Panda, F. Baluska, H. Matsumoto, Aluminum stress signaling in plants, Plant signaling & behavior 4 (2009) 592-597.

[10] J. Kim, Q. Deng, M.M. Benjamin, Simultaneous removal of phosphorus and foulants in a hybrid coagulation/membrane filtration system, Water Research 42 (2008) 2017-2024.

[11] Y.K. Chai, H.C. Lam, C.H. Koo, W.J. Lau, S.O. Lai, A.F. Ismail, Performance evaluation of polyamide nanofiltration membranes for phosphorous removal process and their stability against strong acid/alkali solution, Chinese Journal of Chemical Engineering (2018).

[12] W. Luo, F.I. Hai, W.E. Price, W. Guo, H.H. Ngo, K. Yamamoto, L.D. Nghiem, Phosphorus and water recovery by a novel osmotic membrane bioreactor–reverse osmosis system, Bioresource Technology 200 (2016) 297-304.

[13] D. Franco, J. Lee, S. Arbelaez, N. Cohen, J.-Y. Kim, Removal of phosphate from surface and wastewater via electrocoagulation, Ecological Engineering 108 (2017) 589-596.

[14] K.S. Hashim, R. Al Khaddar, N. Jasim, A. Shaw, D. Phipps, P. Kot, M.O. Pedrola, A.W. Alattabi, M. Abdulredha, R. Alawsh, Electrocoagulation as a green technology for phosphate removal from river water, Separation and Purification Technology 210 (2019) 135-144.

[15] P. Song, Z. Yang, G. Zeng, X. Yang, H. Xu, L. Wang, R. Xu, W. Xiong, K. Ahmad, Electrocoagulation treatment of arsenic in wastewaters: A comprehensive review, Chemical Engineering Journal 317 (2017) 707-725.

[16] C. An, G. Huang, Y. Yao, S. Zhao, Emerging usage of electrocoagulation technology for oil removal from wastewater: A review, Science of The Total Environment 579 (2017) 537-556.

[17] G. Yang, D. Wang, Q. Yang, J. Zhao, Y. Liu, Q. Wang, G. Zeng, X. Li, H. Li, Effect of acetate to glycerol ratio on enhanced biological phosphorus removal, Chemosphere 196 (2018) 78-86.

[18] D. Luo, L. Yuan, L. Liu, Y. Wang, W. Fan, The mechanism of biological phosphorus removal under anoxic-aerobic alternation condition with starch as sole carbon source and its biochemical pathway, Biochemical Engineering Journal 132 (2018) 90-99.

[19] M. Wang, D.Q. Zhang, J.W. Dong, S.K. Tan, Constructed wetlands for wastewater treatment in cold climate — A review, Journal of Environmental Sciences 57 (2017) 293-311.

[20] T. Liu, S. Xu, S. Lu, P. Qin, B. Bi, H. Ding, Y. Liu, X. Guo, X. Liu, A review on removal of organophosphorus pesticides in constructed wetland: Performance, mechanism and influencing factors, Science of The Total Environment 651 (2019) 2247-2268.

[21] M.E. Pérez-López, A.E. Arreola-Ortiz, P. Malagón Zamora, Evaluation of detergent removal in artificial wetlands (biofilters), Ecological Engineering 122 (2018) 135-142.

[22] A. Hickey, J. Arnscheidt, E. Joyce, J. O'Toole, G. Galvin, M. O' Callaghan, K. Conroy, D. Killian, T. Shryane, F. Hughes, K. Walsh, E. Kavanagh, An assessment of the performance of municipal constructed wetlands in Ireland, Journal of Environmental Management 210 (2018) 263-272.

[23] L.W. Gill, P. Ring, B. Casey, N.M.P. Higgins, P.M. Johnston, Long term heavy metal removal by a constructed wetland treating rainfall runoff from a motorway, Science of The Total Environment 601-602 (2017) 32-44.

[24] S. Arden, X. Ma, Constructed wetlands for greywater recycle and reuse: A review, Science of The Total Environment 630 (2018) 587-599.

[25] E.J. Dunne, M.F. Coveney, V.R. Hoge, R. Conrow, R. Naleway, E.F. Lowe, L.E. Battoe, Y. Wang, Phosphorus removal performance of a large-scale constructed treatment wetland receiving eutrophic lake water, Ecological Engineering 79 (2015) 132-142.

[26] T. Avellán, P. Gremillion, Constructed wetlands for resource recovery in developing countries, Renewable and Sustainable Energy Reviews 99 (2019) 42-57.

[27] Z. Ge, D. Wei, J. Zhang, J. Hu, Z. Liu, R. Li, Natural pyrite to enhance simultaneous long-term nitrogen and phosphorus removal in constructed wetland: Three years of pilot study, Water Research 148 (2019) 153-161.

[28] M. Walaszek, P. Bois, J. Laurent, E. Lenormand, A. Wanko, Urban stormwater treatment by a constructed wetland: Seasonality impacts on hydraulic efficiency, physico-chemical behavior and heavy metal occurrence, Science of The Total Environment 637-638 (2018) 443-454.

[29] R. Liu, L. Chi, X. Wang, Y. Sui, Y. Wang, H. Arandiyan, Review of metal (hydr)oxide and other adsorptive materials for phosphate removal from water, Journal of Environmental Chemical Engineering 6 (2018) 5269-5286.

[30] Y. Liu, X. Sheng, Y. Dong, Y. Ma, Removal of high-concentration phosphate by calcite: Effect of sulfate and pH, Desalination 289 (2012) 66-71.

[31] N. Bellier, F. Chazarenc, Y. Comeau, Phosphorus removal from wastewater by mineral apatite, Water Research 40 (2006) 2965-2971.

[32] B.-W. Gu, S.-H. Hong, C.-G. Lee, S.-J. Park, The feasibility of using bentonite, illite, and zeolite as capping materials to stabilize nutrients and interrupt their release from contaminated lake sediments, Chemosphere 219 (2019) 217-226.

[33] C. Jiang, L. Jia, Y. He, B. Zhang, G. Kirumba, J. Xie, Adsorptive removal of phosphorus from aqueous solution using sponge iron and zeolite, Journal of Colloid and Interface Science 402 (2013) 246-252.

[34] H. Yin, Y. Yun, Y. Zhang, C. Fan, Phosphate removal from wastewaters by a naturally occurring, calcium-rich sepiolite, Journal of Hazardous Materials 198 (2011) 362-369.

[35] R. Li, C. Kelly, R. Keegan, L. Xiao, L. Morrison, X. Zhan, Phosphorus removal from wastewater using natural pyrrhotite, Colloids and Surfaces A: Physicochemical and Engineering Aspects 427 (2013) 13-18.

[36] J.B. Xiong, Q. Mahmood, Adsorptive removal of phosphate from aqueous media by peat, Desalination 259 (2010) 59-64.

[37] C. Jiang, L. Jia, B. Zhang, Y. He, G. Kirumba, Comparison of quartz sand, anthracite, shale and biological ceramsite for adsorptive removal of phosphorus from aqueous solution, Journal of Environmental Sciences 26 (2014) 466-477.

[38] E.M. Seftel, R.G. Ciocarlan, B. Michielsen, V. Meynen, S. Mullens, P. Cool, Insights into phosphate adsorption behavior on structurally modified ZnAl layered double hydroxides, Applied Clay Science 165 (2018) 234-246.

[39] M. Everaert, K. Slenders, K. Dox, S. Smolders, D. De Vos, E. Smolders, The isotopic exchangeability of phosphate in Mg-Al layered double hydroxides, Journal of Colloid and Interface Science 520 (2018) 25-32.

[40] W. Huang, Y. Zhang, D. Li, Adsorptive removal of phosphate from water using mesoporous materials: A review, Journal of Environmental Management 193 (2017) 470-482.

[41] J. Yu, W. Liang, L. Wang, F. Li, Y. Zou, H. Wang, Phosphate removal from domestic wastewater using thermally modified steel slag, Journal of Environmental Sciences 31 (2015) 81-88.

[42] R.A. Pepper, S.J. Couperthwaite, G.J. Millar, Re-use of waste red mud: Production of a functional iron oxide adsorbent for removal of phosphorous, Journal of Water Process Engineering 25 (2018) 138-148.

[43] M. Hermassi, C. Valderrama, N. Moreno, O. Font, X. Querol, N.H. Batis, J.L. Cortina, Fly ash as reactive sorbent for phosphate removal from treated waste water as a potential slow release fertilizer, Journal of Environmental Chemical Engineering 5 (2017) 160-169.

[44] J. Xiong, Y. Qin, E. Islam, M. Yue, W. Wang, Phosphate removal from solution using powdered freshwater mussel shells, Desalination 276 (2011) 317-321.

[45] D.J. Jeon, S.H. Yeom, Recycling wasted biomaterial, crab shells, as an adsorbent for the removal of high concentration of phosphate, Bioresource Technology 100 (2009) 2646-2649.

[46] S.H. Yeom, K.-Y. Jung, Recycling wasted scallop shell as an adsorbent for the removal of phosphate, Journal of Industrial and Engineering Chemistry 15 (2009) 40-44.

[47] M.C. Martins, E.B.H. Santos, C.R. Marques, First study on oyster-shell-based phosphorous removal in saltwater — A proxy to effluent bioremediation of marine aquaculture, Science of The Total Environment 574 (2017) 605-615.

[48] Y. Yu, R. Wu, M. Clark, Phosphate removal by hydrothermally modified fumed silica and pulverized oyster shell, Journal of Colloid and Interface Science 350 (2010) 538-543.

[49] P. Lopez-Sanchez, N. Fredriksson, A. Larsson, A. Altskär, A. Ström, High sugar content impacts microstructure, mechanics and release of calcium-alginate gels, Food Hydrocolloids 84 (2018) 26-33.

[50] A. Maureira, B.L. Rivas, Metal ions recovery with alginic acid coupled to ultrafiltration membrane, European Polymer Journal 45 (2009) 573-581.

[51] M. Kube, A. Mohseni, L. Fan, F. Roddick, Impact of alginate selection for wastewater treatment by immobilised Chlorella vulgaris, Chemical Engineering Journal 358 (2019) 1601-1609.

[52] T. Ramdhan, S.H. Ching, S. Prakash, B. Bhandari, Time dependent gelling properties of cuboid alginate gels made by external gelation method: Effects of alginate-CaCl2 solution ratios and pH, Food Hydrocolloids (2018).

[53] N.M. Sanchez-Ballester, I. Soulairol, B. Bataille, T. Sharkawi, Flexible heteroionic calcium-magnesium alginate beads for controlled drug release, Carbohydrate Polymers 207 (2019) 224-229.

[54] K.A. Bowman, O.A. Aarstad, M. Nakamura, B.T. Stokke, G. Skjåk-Bræk, A.N. Round, Single molecule investigation of the onset and minimum size of the calcium-mediated junction zone in alginate, Carbohydrate Polymers 148 (2016) 52-60.

[55] T. Nesme, G.S. Metson, E.M. Bennett, Global phosphorus flows through agricultural trade, Global Environmental Change 50 (2018) 133-141.

[56] J. Wang, Z. Fu, H. Qiao, F. Liu, Assessment of eutrophication and water quality in the estuarine area of Lake Wuli, Lake Taihu, China, Science of The Total Environment 650 (2019) 1392-1402.

[57] Environmental Quality Standard for Water Pollution, Japan's regulation and environmental law.

[58] M. El Wali, S.R. Golruodbary, A. Kraslawski, Impact of recycling improvement on the life cycle of phosphorus, Chinese Journal of Chemical Engineering (2018).

[59] W. Shi, Y. Fu, W. Jiang, Y. Ye, J. Kang, D. Liu, Y. Ren, D. Li, C. Luo, Z. Xu, Enhanced phosphate removal by zeolite loaded with Mg–Al–La ternary (hydr)oxides from aqueous solutions: Performance and mechanism, Chemical Engineering Journal 357 (2019) 33-44.

[60] H.N. Bhatti, J. Hayat, M. Iqbal, S. Noreen, S. Nawaz, Biocomposite application for the phosphate ions removal in aqueous medium, Journal of Materials Research and Technology 7 (2018) 300-307.

[61] B. An, S. Lee, H.-G. Kim, D. Zhao, J.-A. Park, J.-W. Choi, Organic/inorganic hybrid adsorbent for efficient phosphate removal from a reservoir affected by algae bloom, Journal of Industrial and Engineering Chemistry 69 (2019) 211-216.

[62] K. Zhou, B. Wu, L. Su, W. Xin, X. Chai, Enhanced phosphate removal using nanostructured hydrated ferric-zirconium binary oxide confined in a polymeric anion exchanger, Chemical Engineering Journal 345 (2018) 640-647.

[63] S. Shan, H. Tang, Y. Zhao, W. Wang, F. Cui, Highly porous zirconium-crosslinked graphene oxide/alginate aerogel beads for enhanced phosphate removal, Chemical Engineering Journal 359 (2019) 779-789.

[64] C. Barca, C. Gérente, D. Meyer, F. Chazarenc, Y. Andrès, Phosphate removal from synthetic and real wastewater using steel slags produced in Europe, Water Research 46 (2012) 2376-2384.

[65] E. Panagiotou, N. Kafa, L. Koutsokeras, P. Kouis, P. Nikolaou, G. Constantinides, I. Vyrides, Turning calcined waste egg shells and wastewater to Brushite: Phosphorus adsorption from aqua media and anaerobic sludge leach water, Journal of Cleaner Production 178 (2018) 419-428.

[66] P.O. Vargas, N.R. Pereira, A.O. Guimarães, W.R. Waldman, V.R. Pereira, Shrinkage and deformation during convective drying of calcium alginate, LWT 97 (2018) 213-222.

[67] S. Thakur, B. Sharma, A. Verma, J. Chaudhary, S. Tamulevicius, V.K. Thakur, Recent progress in sodium alginate based sustainable hydrogels for environmental applications, Journal of Cleaner Production 198 (2018) 143-159.

[68] H. Liao, W. Ai, K. Zhang, M. Nakauma, T. Funami, Y. Fang, K. Nishinari, K.I. Draget, G.O. Phillips, Mechanisms of oligoguluronate modulating the calcium-induced gelation of alginate, Polymer 74 (2015) 166-175.

[69] P. Lee, M.A. Rogers, Effect of calcium source and exposure-time on basic caviar spherification using sodium alginate, International Journal of Gastronomy and Food Science 1 (2012) 96-100.

[70] Standard methods for the examination of water and wastewater, American Public Health Association 18th edition (1992).

[71] P.E. Warmadewanthi W., Herumurti W., Bagastyo A., Misbachul M., Phosphate Recovery from Wastewater of Fertiliser Industries by Using Gypsum Waste, Chemical Engineering Transactions 56 (2017) 1765-1770.

[72] S. Stößlein, I. Grunwald, J. Stelten, A. Hartwig, In-situ determination of time-dependent alginate-hydrogel formation by mechanical texture analysis, Carbohydrate Polymers 205 (2019) 287-294.

[73] L. Caballero Aguilar, P.R. Stoddart, S.L. McArthur, S.E. Moulton, Polycaprolactone porous template facilitates modulated release of molecules from alginate hydrogels, Reactive and Functional Polymers 133 (2018) 29-36.

[74] K.L. Tu, L.D. Nghiem, A.R. Chivas, Boron removal by reverse osmosis membranes in seawater desalination applications, Separation and Purification Technology 75 (2010) 87-101.

[75] L. Bolaños, K. Lukaszewski, I. Bonilla, D. Blevins, Why boron?, Plant Physiology and Biochemistry 42 (2004) 907-912.

[76] B. Albert, H. Hillebrecht, Boron: Elementary Challenge for Experimenters and Theoreticians, Angewandte Chemie International Edition 48 (2009) 8640-8668.

[77] N. Kabay, M. Bryjak, N. Hilal, Boron Separation Processes, Elsevier2015.

[78] P.P. Power, W.G. Woods, The chemistry of boron and its speciation in plants, Plant and Soil 193 (1997) 1-13.

[79] R.B. Kistler, C. Helvaci, Boron and borates, Industrial minerals and rocks 6 (1994) 171-186.

[80] J.A. Ober, Mineral commodity summaries 2018, US Geological Survey, 2018.

[81] P. Argust, Distribution of boron in the environment, Biological Trace Element Research 66 (1998) 131-143.

[82] P. Haewon, S.W. H., Global biogeochemical cycle of boron, Global Biogeochemical Cycles 16 (2002) 20-21-20-11.

[83] R. Herrmann, On processes controlling the distribution and fluxes of boron in natural waters and air along transects across the South Island of New Zealand, CATENA 44 (2001) 263-284.

[84] J.D. Mather, N.C. Porteous, The geochemistry of boron and its isotopes in groundwaters from marine and non-marine sandstone aquifers, Applied Geochemistry 16 (2001) 821-834.

[85] J. Wolska, M. Bryjak, Methods for boron removal from aqueous solutions — A review, Desalination 310 (2013) 18-24.

[86] K.L. Tu, L.D. Nghiem, A.R. Chivas, Coupling effects of feed solution pH and ionic strength on the rejection of boron by NF/RO membranes, Chemical Engineering Journal 168 (2011) 700-706.

[87] Z. Guan, J. Lv, P. Bai, X. Guo, Boron removal from aqueous solutions by adsorption — A review, Desalination 383 (2016) 29-37.

[88] V. Kochkodan, N.B. Darwish, N. Hilal, The chemistry of boron in water, Elsevier: Amsterdam2015.

[89] J. Schott, J. Kretzschmar, M. Acker, S. Eidner, M.U. Kumke, B. Drobot, A. Barkleit, S. Taut, V. Brendler, T. Stumpf, Formation of a Eu(iii) borate solid species from a weak Eu(iii) borate complex in aqueous solution, Dalton Transactions 43 (2014) 11516-11528.

[90] J. Simon, R. Smith, Borate raw materials, Glass technology 41 (2000) 169-173.

[91] M.C.C. Azevedo, A.M.V. Cavaleiro, The Acid–Base Titration of a Very Weak Acid: Boric Acid, Journal of Chemical Education 89 (2012) 767-770.

[92] V.M. Dembitsky, R. Smoum, A.A. Al-Quntar, H.A. Ali, I. Pergament, M. Srebnik, Natural occurrence of boron-containing compounds in plants, algae and microorganisms, Plant Science 163 (2002) 931-942.

[93] K.L. Tu, A.R. Chivas, L.D. Nghiem, Enhanced boron rejection by NF/RO membranes by complexation with polyols: Measurement and mechanisms, Desalination 310 (2013) 115-121.

[94] Y.P. Tang, L. Luo, Z. Thong, T.S. Chung, Recent advances in membrane materials and technologies for boron removal, Journal of Membrane Science 541 (2017) 434-446.

[95] J.A. Ober, Mineral commodity summaries 2018, Mineral Commodity SummariesReston, VA, 2018, pp. 204.

[96] B.H. Robinson, S.R. Green, B. Chancerel, T.M. Mills, B.E. Clothier, Poplar for the phytomanagement of boron contaminated sites, Environmental Pollution 150 (2007) 225-233.

[97] C.F. Heidrich, Hans-Joachim; Weir, Anne, Coal combustion products. A global perspective, VGB PowerTech 45 (2013) 46-52.

[98] American Coal Ash Association's Coal Combustion Product Production & Use Survey Report, (2014).

[99] M. Izquierdo, X. Querol, Leaching behaviour of elements from coal combustion fly ash: An overview, International Journal of Coal Geology 94 (2012) 54-66.

[100] Hazardous and Solid Waste Management System; Disposal of Coal Combustion Residuals From Electric Utilities: Final rule, United State Environmental Protection Agency: Washington, DC (2015) 21301-21501.

[101] L.B. Williams, R.L. Hervig, Boron isotope composition of coals: a potential tracer of organic contaminated fluids, Applied Geochemistry 19 (2004) 1625-1636.

[102] L.S. Ruhl, G.S. Dwyer, H. Hsu-Kim, J.C. Hower, A. Vengosh, Boron and Strontium Isotopic Characterization of Coal Combustion Residuals: Validation of New Environmental Tracers, Environmental Science & Technology 48 (2014) 14790-14798.

[103] J.S. Harkness, B. Sulkin, A. Vengosh, Evidence for Coal Ash Ponds Leaking in the Southeastern United States, Environmental Science & Technology 50 (2016) 6583-6592.

[104] http://www.uky.edu/KGS/coal/coal-for-elec.php.

[105] http://www.etiproducts.com/.

[106] C.C.J. J., R. Jesús, G.F. Agustín, Boron in Plants: Deficiency and Toxicity, Journal of Integrative Plant Biology 50 (2008) 1247-1255.

[107] M.M. Shaaban, Role of boron in plant nutrition and human health, American Journal of Plant Physiology 5 (2010) 224-240.

[108] I. Uluisik, H.C. Karakaya, A. Koc, The importance of boron in biological systems, Journal of Trace Elements in Medicine and Biology 45 (2018) 156-162.

[109] W. Sang, Z.-R. Huang, Y.-P. Qi, L.-T. Yang, P. Guo, L.-S. Chen, An investigation of boron-toxicity in leaves of two citrus species differing in boron-tolerance using comparative proteomics, Journal of Proteomics 123 (2015) 128-146.

[110] K. Yıldırım, Transcriptomic and hormonal control of boron uptake, accumulation and toxicity tolerance in poplar, Environmental and Experimental Botany 141 (2017) 60-73.

[111] R.O. Nable, G.S. Bañuelos, J.G. Paull, Boron toxicity, Plant and Soil 193 (1997) 181-198.

[112] J. Takano, K. Miwa, T. Fujiwara, Boron transport mechanisms: collaboration of channels and transporters, Trends in Plant Science 13 (2008) 451-457.

[113] R.S. Ayers, D.W. Westcot, Water quality for agriculture, FAO irrigation and drainage paper (1994).

[114] F.H. Nielsen, Update on human health effects of boron, Journal of Trace Elements in Medicine and Biology 28 (2014) 383-387.

[115] S. Bakirdere, S. Orenay, M. Korkmaz, Effect of Boron on Human Health, The Open Mineral Processing Journal 3 (2010) 54-59.

[116] Dietary Reference Intakes for Vitamin A, Vitamin K, Arsenic, Boron, Chromium, Copper, Iodine, Iron, Manganese, Molybdenum, Nickel, Silicon, Vanadium, and Zinc, Institute of Medicine (US) Panel on Micronutrients, Washington (DC): National Academies Press (US) (2001).

[117] Opinion of the Scientific Panel on Dietetic Products, Nutrition and Allergies

on a request from the Commission related to the Tolerable Upper Intake

Level of Boron (Sodium Borate and Boric Acid) The EFSA Journal 80 (2004) 1-22.

[118] Environmental health criteria 204 boron, International programme on chemical safety, World Health Organization, Geneva (1998).

[119] Boron as a Medicinal Ingredient in Oral Natural Health Products, Natural Health Products Directorate, Health Canada (2007).

[120] N. Başaran, Y. Duydu, H.M. Bolt, Reproductive toxicity in boron exposed workers in Bandirma, Turkey, Journal of Trace Elements in Medicine and Biology 26 (2012) 165-167.

[121] A. Şimşek, D. Korkmaz, Y.S. Velioğlu, O.Y. Ataman, Determination of boron in hazelnut (Corylus avellana L.) varieties by inductively coupled plasma optical emission spectrometry and spectrophotometry, Food Chemistry 83 (2003) 293-296.

[122] Guidelines for Drinking-water Quality, World Health Organization 4th Edition (2011).

[123] N. Hilal, G.J. Kim, C. Somerfield, Boron removal from saline water: A comprehensive review, Desalination 273 (2011) 23-35.

[124] M.M. Nasef, M. Nallappan, Z. Ujang, Polymer-based chelating adsorbents for the selective removal of boron from water and wastewater: A review, Reactive and Functional Polymers 85 (2014) 54-68.

[125] E. Güler, C. Kaya, N. Kabay, M. Arda, Boron removal from seawater: State-of-the-art review, Desalination 356 (2015) 85-93.

[126] H. Zhao, R. Gao, P. Bai, Advances in Boron Isotope Separation by Ion Exchange Chromatography, Asian Journal of Chemistry 26 (2014) 2187-2190.

[127] A. Sabarudin, K. Oshita, M. Oshima, S. Motomizu, Synthesis of cross-linked chitosan possessing N-methyl-d-glucamine moiety (CCTS-NMDG) for adsorption/concentration of boron in water samples and its accurate measurement by ICP-MS and ICP-AES, Talanta 66 (2005) 136-144.

[128] B. Wang, X. Guo, P. Bai, Removal technology of boron dissolved in aqueous solutions – A review, Colloids and Surfaces A: Physicochemical and Engineering Aspects 444 (2014) 338-344.

[129] S. Nishihama, Y. Sumiyoshi, T. Ookubo, K. Yoshizuka, Adsorption of boron using glucamine-based chelate adsorbents, Desalination 310 (2013) 81-86.

[130] H. Parschová, E. Mištová, Z. Matějka, L. Jelínek, N. Kabay, P. Kauppinen, Comparison of several polymeric sorbents for selective boron removal from reverse osmosis permeate, Reactive and Functional Polymers 67 (2007) 1622-1627.

[131] I. Yilmaz Ipek, R. Holdich, N. Kabay, M. Bryjak, M. Yuksel, Kinetic behaviour of boron selective resins for boron removal using seeded microfiltration system, Reactive and Functional Polymers 67 (2007) 1628-1634.

[132] N. Kabay, S. Sarp, M. Yuksel, Ö. Arar, M. Bryjak, Removal of boron from seawater by selective ion exchange resins, Reactive and Functional Polymers 67 (2007) 1643-1650.

[133] T.E. Köse, N. Öztürk, Boron removal from aqueous solutions by ion-exchange resin: Column sorption–elution studies, Journal of Hazardous Materials 152 (2008) 744-749.

[134] K.W. Baek, S.H. Song, S.H. Kang, Y.W. Rhee, C.S. Lee, B.J. Lee, S. Hudson, T.S. Hwang, Adsorption Kinetics of Boron by Anion Exchange Resin in Packed Column Bed, Journal of Industrial and Engineering Chemistry 13 (2007) 452-456.

[135] K. Ikeda, D. Umeno, K. Saito, F. Koide, E. Miyata, T. Sugo, Removal of Boron Using Nylon-Based Chelating Fibers, Industrial & Engineering Chemistry Research 50 (2011) 5727-5732.

[136] H. Hoshina, N. Seko, Y. Ueki, M. Tamada, Synthesis of Graft Adsorbent with N-Methyl-D-glucamine for Boron Adsorption, Journal of Ion Exchange 18 (2007) 236-239.

[137] T.M. Ting, M.M. Nasef, Modification of polyethylene-polypropylene fibers by emulsion and solvent radiation grafting systems for boron removal, Fibers and Polymers 18 (2017) 1048-1055.

[138] N. Biçak, N. Bulutçu, B.F. Şenkal, M. Gazi, Modification of crosslinked glycidyl methacrylate-based polymers for boron-specific column extraction, Reactive and Functional Polymers 47 (2001) 175-184.

[139] B.F. Senkal, N. Bicak, Polymer supported iminodipropylene glycol functions for removal of boron, Reactive and Functional Polymers 55 (2003) 27-33.

[140] H. Mishra, C. Yu, D.P. Chen, W.A. Goddard, N.F. Dalleska, M.R. Hoffmann, M.S. Diallo, Branched Polymeric Media: Boron-Chelating Resins from Hyperbranched Polyethylenimine, Environmental Science & Technology 46 (2012) 8998-9004.

[141] M.S. Moorthy, D.-J. Seo, H.-J. Song, S.S. Park, C.-S. Ha, Magnetic mesoporous silica hybrid nanoparticles for highly selective boron adsorption, Journal of Materials Chemistry A 1 (2013) 12485-12496.

[142] Y. Inukai, Y. Tanaka, T. Matsuda, N. Mihara, K. Yamada, N. Nambu, O. Itoh, T. Doi, Y. Kaida, S. Yasuda, Removal of boron(III) by N-methylglucamine-type cellulose derivatives with higher adsorption rate, Analytica Chimica Acta 511 (2004) 261-265.

[143] S. Liu, M. Xu, T. Yu, D. Han, J. Peng, J. Li, M. Zhai, Radiation synthesis and performance of novel cellulose-based microsphere adsorbents for efficient removal of boron (III), Carbohydrate Polymers 174 (2017) 273-281.

[144] M. Matsumoto, T. Matsui, K. Kondo, Adsorption Mechanism of Boric Acid on Chitosan Resin Modified by Saccharides, Journal of Chemical Engineering of Japan 32 (1999) 190-196.

[145] H. Demey-Cedeño, M. Ruiz, J.A. Barron-Zambrano, A.M. Sastre, Boron removal from aqueous solutions using alginate gel beads in fixed-bed systems, Journal of Chemical Technology and Biotechnology 89 (2014) 934-940.

[146] S. Morisada, T. Rin, T. Ogata, Y.-H. Kim, Y. Nakano, Adsorption removal of boron in aqueous solutions by amine-modified tannin gel, Water Research 45 (2011) 4028-4034.

[147] H. Demey, T. Vincent, M. Ruiz, A.M. Sastre, E. Guibal, Development of a new chitosan/Ni(OH)2-based sorbent for boron removal, Chemical Engineering Journal 244 (2014) 576-586.

[148] A.A. Oladipo, M. Gazi, Hydroxyl-enhanced magnetic chitosan microbeads for boron adsorption: Parameter optimization and selectivity in saline water, Reactive and Functional Polymers 109 (2016) 23-32.

[149] K. Yıldırım, G.Ç. Kasım, Phytoremediation potential of poplar and willow species in small scale constructed wetland for boron removal, Chemosphere 194 (2018) 722-736.

[150] S. Wang, Y. Zhou, C. Gao, Novel high boron removal polyamide reverse osmosis membranes, Journal of Membrane Science 554 (2018) 244-252.

[151] C. Yan, W. Yi, P. Ma, X. Deng, F. Li, Removal of boron from refined brine by using selective ion exchange resins, Journal of Hazardous Materials 154 (2008) 564-571.

[152] A.E. Yilmaz, R. Boncukcuoğlu, S. Bayar, B.A. Fil, M.M. Kocakerim, Boron removal by means of chemical precipitation with calcium hydroxide and calcium borate formation, Korean Journal of Chemical Engineering 29 (2012) 1382-1387.

[153] D. Chorghe, M.A. Sari, S. Chellam, Boron removal from hydraulic fracturing wastewater by aluminum and iron coagulation: Mechanisms and limitations, Water Research 126 (2017) 481-487.

[154] M. Dolati, A.A. Aghapour, H. Khorsandi, S. Karimzade, Boron removal from aqueous solutions by electrocoagulation at low concentrations, Journal of Environmental Chemical Engineering 5 (2017) 5150-5156.

[155] N. Kabay, O. Arar, F. Acar, A. Ghazal, U. Yuksel, M. Yuksel, Removal of boron from water by electrodialysis: effect of feed characteristics and interfering ions, Desalination 223 (2008) 63-72.

[156] M. Bryjak, I. Duraj, Anion-exchange membranes for separation of borates by Donnan dialysis, Desalination 310 (2013) 39-42.

[157] N. Kabay, P. Köseoğlu, E. Yavuz, Ü. Yüksel, M. Yüksel, An innovative integrated system for boron removal from geothermal water using RO process and ion exchange-ultrafiltration hybrid method, Desalination 316 (2013) 1-7.

[158] M. Bryjak, J. Wolska, N. Kabay, Removal of boron from seawater by adsorption–membrane hybrid process: implementation and challenges, Desalination 223 (2008) 57-62.

[159] M. Dumont, R. Villet, M. Guirand, A. Montembault, T. Delair, S. Lack, M. Barikosky, A. Crepet, P. Alcouffe, F. Laurent, L. David, Processing and antibacterial properties of chitosan-coated alginate fibers, Carbohydrate Polymers 190 (2018) 31-42.

[160] A. Muxika, A. Etxabide, J. Uranga, P. Guerrero, K. de la Caba, Chitosan as a bioactive polymer: Processing, properties and applications, International Journal of Biological Macromolecules 105 (2017) 1358-1368.

[161] S. Islam, M.A.R. Bhuiyan, M.N. Islam, Chitin and Chitosan: Structure, Properties and Applications in Biomedical Engineering, Journal of Polymers and the Environment 25 (2017) 854-866.

[162] W.S. Wan Ngah, L.C. Teong, M.A.K.M. Hanafiah, Adsorption of dyes and heavy metal ions by chitosan composites: A review, Carbohydrate Polymers 83 (2011) 1446-1456.

[163] V. Zargar, M. Asghari, A. Dashti, A Review on Chitin and Chitosan Polymers: Structure, Chemistry, Solubility, Derivatives, and Applications, ChemBioEng Reviews 2 (2015) 204-226.

[164] X. Liu, C. He, X. Yu, Y. Bai, L. Ye, B. Wang, L. Zhang, Net-like porous activated carbon materials from shrimp shell by solution-processed carbonization and H3PO4 activation for methylene blue adsorption, Powder Technology 326 (2018) 181-189.

[165] T. Maruthiah, A. Palavesam, Characterization of haloalkalophilic organic solvent tolerant protease for chitin extraction from shrimp shell waste, International Journal of Biological Macromolecules 97 (2017) 552-560.

[166] R.N. Sah, P.H. Brown, Boron Determination—A Review of Analytical Methods, Microchemical Journal 56 (1997) 285-304.

[167] M. Endo, E. Yoshikawa, S. Nemoto, Y. Takahashi, K. Sakai, H. Mizuguchi, A. Sasaki, K. Sugawara, K. Sato, T. Ihara, Simple and Rapid Determination of Boron in the Wastewater with Azomethine H Using Accelerating Effect of Ammonium Ion, Journal of Water and Environment Technology 11 (2013) 355-365.

[168] D.L. Harp, Modifications to the azomethine-H method for determining boron in water, Analytica Chimica Acta 346 (1997) 373-379.

[169] Y.G. Abou El-Reash, Magnetic chitosan modified with cysteine-glutaraldehyde as adsorbent for removal of heavy metals from water, Journal of Environmental Chemical Engineering 4 (2016) 3835-3847.

[170] S. Lagergren, Zur theorie der sogenannten adsorption geloster stoffe, Kungliga Svenska Vetenskapsakademiens. Handlingar 24 (1898) 1-39.

[171] G. Blanchard, M. Maunaye, G. Martin, Removal of heavy metals from waters by means of natural zeolites, Water Research 18 (1984) 1501-1507.

[172] Ö. Kaftan, M. Açıkel, A.E. Eroğlu, T. Shahwan, L. Artok, C. Ni, Synthesis, characterization and application of a novel sorbent, glucamine-modified MCM-41, for the removal/preconcentration of boron from waters, Analytica Chimica Acta 547 (2005) 31-41.

[173] E. Salehi, P. Daraei, A. Arabi Shamsabadi, A review on chitosan-based adsorptive membranes, Carbohydrate Polymers 152 (2016) 419-432.

[174] K.M. Kim, J.H. Son, S.-K. Kim, C.L. Weller, M.A. Hanna, Properties of Chitosan Films as a Function of pH and Solvent Type, Journal of Food Science 71 (2006) E119-E124.

[175] H. Hamedi, S. Moradi, S.M. Hudson, A.E. Tonelli, Chitosan based hydrogels and their applications for drug delivery in wound dressings: A review, Carbohydrate Polymers 199 (2018) 445-460.

[176] S. Shenvi, A.F. Ismail, A.M. Isloor, Preparation and characterization study of PPEES/chitosan composite membrane crosslinked with tripolyphosphate, Desalination 344 (2014) 90-96.

[177] A. Homez-Jara, L.D. Daza, D.M. Aguirre, J.A. Muñoz, J.F. Solanilla, H.A. Váquiro, Characterization of chitosan edible films obtained with various polymer concentrations and drying temperatures, International Journal of Biological Macromolecules 113 (2018) 1233-1240.

[178] Z.A. Sutirman, M.M. Sanagi, K.J. Abd Karim, W.A. Wan Ibrahim, B.H. Jume, Equilibrium, kinetic and mechanism studies of Cu(II) and Cd(II) ions adsorption by modified chitosan beads, International Journal of Biological Macromolecules 116 (2018) 255-263.

[179] J. Becerra, G. Sudre, I. Royaud, R. Montserret, B. Verrier, C. Rochas, T. Delair, L. David, Tuning the Hydrophilic/Hydrophobic Balance to Control the Structure of Chitosan Films and Their Protein Release Behavior, AAPS PharmSciTech 18 (2017) 1070-1083.

[180] M.L. Monte, M.L. Moreno, J. Senna, L.S. Arrieche, L.A.A. Pinto, Moisture sorption isotherms of chitosan-glycerol films: Thermodynamic properties and microstructure, Food Bioscience 22 (2018) 170-177.

[181] S. Ramakrishna, K. Fujihara, W.-E. Teo, T. Yong, Z. Ma, R. Ramaseshan, Electrospun nanofibers: solving global issues, Materials Today 9 (2006) 40-50.

[182] L. Lin, L. Xue, S. Duraiarasan, C. Haiying, Preparation of ε-polylysine/chitosan nanofibers for food packaging against Salmonella on chicken, Food Packaging and Shelf Life 17 (2018) 134-141.

[183] B.S. de Farias, T.R. Sant'Anna Cadaval Junior, L.A. de Almeida Pinto, Chitosan-functionalized nanofibers: A comprehensive review on challenges and prospects for food applications, International Journal of Biological Macromolecules 123 (2019) 210-220.

[184] E. Shekarforoush, F. Ajalloueian, G. Zeng, A.C. Mendes, I.S. Chronakis, Electrospun xanthan gum-chitosan nanofibers as delivery carrier of hydrophobic bioactives, Materials Letters 228 (2018) 322-326.

[185] H. Toshiaki, K. Kazuhito, K. Masanao, I. Masato, M. Youichi, Colloidal Titration of Chitosan and Critical Unit of Chitosan to the Potentiometric Colloidal Titration with Poly(vinyl sulfate) Using Toluidine Blue as Indicator, Bulletin of the Chemical Society of Japan 72 (1999) 37-41.

[186] M.X. Weinhold, J.C.M. Sauvageau, N. Keddig, M. Matzke, B. Tartsch, I. Grunwald, C. Kübel, B. Jastorff, J. Thöming, Strategy to improve the characterization of chitosan for sustainable biomedical applications: SAR guided multi-dimensional analysis, Green Chemistry 11 (2009) 498-509.

[187] A.G.B. Pereira, E.C. Muniz, Y.-L. Hsieh, 1H NMR and 1H–13C HSQC surface characterization of chitosan–chitin sheath-core nanowhiskers, Carbohydrate Polymers 123 (2015) 46-52.

[188] Y. Xiao, Z.T. Lin, Y. Chen, H. Wang, Y.L. Deng, D.E. Le, J. Bin, M. Li, Y. Liao, Y. Liu, G. Jiang, J. Bin, High molecular weight chitosan derivative polymeric micelles encapsulating superparamagnetic iron oxide for tumor-targeted magnetic resonance imaging, International journal of nanomedicine 10 (2015) 1155-1172.

[189] E. Audebeau, E.K. Oikonomou, S. Norvez, I. Iliopoulos, One-pot synthesis and gelation by borax of glycopolymers in water, Polymer Chemistry 5 (2014) 2273-2281.

[190] C. Zhao, Q. Shi, J. Hou, Z. Xin, J. Jin, C. Li, S.-C. Wong, J. Yin, Capturing red blood cells from the blood by lectin recognition on a glycopolymer-patterned surface, Journal of Materials Chemistry B 4 (2016) 4130-4137.

[191] T. Chivangkul, S. Pengprecha, P. Padungros, K. Siraleartmukul, S. Prasongsuk, N. Muangsin, Enhanced water-solubility and mucoadhesion of N,N,N-trimethyl-N-gluconate-N-homocysteine thiolactone chitosan, Carbohydrate Polymers 108 (2014) 224-231.

[192] H.B. Cardoso, P.A. Wierenga, H. Gruppen, H.A. Schols, Maillard induced aggregation of individual milk proteins and interactions involved, Food Chemistry 276 (2019) 652-661.

[193] M. Patrignani, G.J. Rinaldi, J.Á. Rufián-Henares, C.E. Lupano, Antioxidant capacity of Maillard reaction products in the digestive tract: An in vitro and in vivo study, Food Chemistry 276 (2019) 443-450.